이학박사 학위논문

Coordinated integrations of light growth regulator cues enhance plant morphogenic adaptation to environmental changes

통합적인 생장조절 신호들의 환경변화에 대한 식물 형태 적응에 끼치는 영향에 대한 연구

2022년 2월

서울대학교 대학원

화학부

김 재 영

Coordinated integrations of light growth regulator cues enhance plant morphogenic adaptation to environmental changes

통합적인 생장조절 신호들의 환경변화에 대한 식물 형태 적응에 끼치는 영향에 대한 연구

지도교수 박 충 모

이 논문을 이학박사 학위논문으로 제출함
2022년 1월

서울대학교 대학원
화학부
김 재 영

김재영의 이학박사 학위논문을 인준함
2022년 1월

위 원 장 서 필 준 (인)

부위원장 박 충 모 (인)

위 원 이 형 호 (인)

위 원 이 현 우 (인)

위 원 정 재 훈 (인)

ABSTRACT

Plants in early developmental stages, from soil emergence to seedling establishment, experience dramatic changes in surrounding environments. Seedlings are particularly sensitive to changes imposed by environmental stimuli, such as light and temperature, and undergo morphological changes to achieve the best fitness. Alterations in plant body are elaborately shaped by coordination of diverse endogenous signaling pathways with external signals. Thus, studies on signaling crosstalks between endogenous and external signaling pathways are essential for understanding physiological responses of seedlings to fluctuating environments. However, not yet unexplored molecular and genetic linkages between endogenous signaling pathway and environmental cues still exist. In this study, I investigated molecular and genetic mechanisms underlying morphogenic adaptation of hypocotyls regulated by endogenous signaling pathways under varying light and temperature environments.

In Chapter 1, I discuss the effects of a plant hormone ethylene on hypocotyl thermomorphogenesis in the light. The gaseous phytohormone ethylene plays vital roles in diverse developmental and environmental adaptation processes, such as fruit ripening, seedling establishment, mechanical stress tolerance and submergence escape. It is also known that in the light, ethylene promotes hypocotyl growth by stimulating the expression of PHYTOCHROME-INTERACTING FACTOR 3 (PIF3) transcription factor, which triggers microtubule reorganization during hypocotyl cell elongation. In particular, ethylene has been implicated in plant responses to warm temperatures in recent years. However, it is currently

unclear how ethylene signals are functionally associated with hypocotyl thermomorphogenesis at the molecular level. Here, I show that ETHYLENE-INSENSITIVE 3 (EIN3)-mediated ethylene signals attenuate hypocotyl thermomorphogenesis by suppressing auxin responses. At warm temperatures, when the activity of the PIF4 thermomorphogenesis promoter is prominently high, the ethylene-activated EIN3 transcription factor directly induces the transcription of *ARABIDOPSIS PP2C CLADE D7* (*APD7*) gene encoding a protein phosphatase that inactivates the plasma membrane (PM) H^+-ATPase proton pumps. In conjunction with the promotive role of the PM H^+-ATPases in hypocotyl cell elongation, these observations strongly support that the EIN3-directed induction of *APD7* gene is linked with the suppression of auxin-induced cell expansion, leading to the reduction in thermomorphogenic hypocotyl growth. These data demonstrate that APD7 acts as a molecular hub that integrates ethylene and auxin signals into hypocotyl thermomorphogenesis. I propose that the ethylene–auxin signaling crosstalks via the EIN3-APD7 module facilitate the fine-tuning of hypocotyl thermomorphogenesis under natural environments, which often fluctuate in a complex manner.

In Chapter 2, studies on molecular crosstalks between karrikin (KAR) and GA (gibberellic acid)/DELLA signaling pathways in the hypocotyl deetiolation process are described. Morphogenic adaptation of young seedlings to light environments is a critical developmental process that ensures plant survival and propagation, as they emerge from the soil. The photomorphogenic responses are facilitated by a network of light and growth hormonal signals, such as auxin and GA. KARs, a group of small butenolide compounds that is produced from burning plant materials in wildfires, are known to stimulate seed germination in fire-prone

plant species. Notably, recent studies strongly support that they also facilitate seedling establishment, while underlying molecular mechanisms have been unexplored yet. Here, I demonstrate that SUPPRESSOR OF MAX2 1 (SMAX1), a negative regulator of KAR signaling, integrates light and KAR signals into GA-DELLA pathways that regulate hypocotyl growth during seedling photomorphogenesis and establishment. SMAX1-deficient *Arabidopsis* mutants exhibited a reduced hypocotyl elongation, and the short hypocotyl phenotypes were efficiently rescued by exogenous GA application and mutations in *DELLA* genes, such as *REPRESSOR OF ga1-3* (*RGA*) and *GIBBERELLIC ACID INSENSITIVE* (*GAI*). Consistently, I found that SMAX1 facilitates the degradation of DELLA proteins in the hypocotyls in the light. Interestingly, light induces the accumulation of SMAX1 proteins, and the SMAX1-mediated degradation of DELLA is elevated in seedling establishment during the dark-to-light transition. These observations indicate that the SMAX1-mediated integration of light and KAR signals into GA pathways elaborately modulates seedling establishment. I propose that SMAX1 serves as a safeguard that ensures an optimized photomorphogenesis upon exposure to KARs, which is indicative of clear growth environments, as encountered following wildfires in nature.

Keyword : EIN3, ethylene, hypocotyl thermomorphogenesis, SMAX1, karrikins, seedling establishment

Student Number : 2018-21999

CONTENTS

LIST OF FIGURES

LIST OF TABLES

ABBREVIATION

ACC	1-aminocyclopropane-1-carboxylic acid
AFBs	AUXIN SIGNALING F-BOX PROTEINs
AHA	ARABIDOPSIS H^+-ATPASE
APD7	ARABIDOPSIS PP2C CLADE D7
At	Arabidopsis thaliana
BBX	B-BOX DOMAIN PROTEIN
BL	Brassinolide
BOPs	BLADE-ON-PETIOLEs
BR	Brassinosteroid
CaMV	Cauliflower mosaic virus
ChIP	Chromatin Immunoprecipitation
CK	Cytokinin
COP1	CONSTITUTIVE PHOTOMORPHOGENIC 1
Co-IP	Coimmunoprecipitation
CTR1	CONSTITUTIVE TRIPLE RESPONSE 1
D14	DWARF14
EBF1/2	EIN3 BINDING F-BOX 1/2
EBS	EIN3-binding sequence
EIL1	ETHYLENE-INSENSITIVE3-LIKE 1
EIN2	ETHYLENE-INSENSITIVE 2
EIN3	ETHYLENE-INSENSITIVE 3
KLs	Endogenous KAI2 ligand
ELF3	EARLY FLOWERING 3

ELF4	EARLY FLOWERING 4
ERF1	ETHYLENE RESPONSE FACTOR 1
ETR1	ETHYLENE RESPONSE 1
GA	Gibberellic acid
GA3ox1	GIBBERELLIN 3-OXIDASE 1
GA3ox2	GIBBERELLIN 3-OXIDASE 2
GA2ox2	GIBBERELLIN 2-OXIDASE 2
GAI	GIBBERELLIC ACID INSENSITIVE
GID1s	GIBBERELLIN-INSENSITIVE DWARF 1s
H3	Histone 3
HY5	ELONGATED HYPOCOTYL 5
IAA19	INDOLE-3-ACETIC ACID INDUCIBLE 19
KAI2	KARRIKIN-INSENSITIVE 2
KAR	Karrikin
LDs	Long days
LUX	LUX ARRHYTHMO
MAX2	MORE AXILLARY GROWTH 2
MS	Murashige and Skoog
NPA	Naphthylphthalamic acid
NLS	Nuclear localization signal
ORA59	OCTADECANOID-RESPONSIVE ARABIDOPSIS AP2/ERF 59
PAC	Paclobutrazol
PCR	Polymerase chain reaction
PHYB	PHYTOCHROME B

PIC	Picloram
PIF	PHYTOCHROME-INTERACTING FACTOR
PM	Plasma membrane
PP2C	protein phosphatase type 2C
RGA	REPRESSOR OF *ga1-3*
RGB	RED, GREEN, BLUE
RGLs	RGA-LIKEs
RT-qPCR	Reverse transcription-mediated quantitative PCR
SAURs	SMALL AUXIN UP-RNAs
SAS	Shade avoidance syndrome
SDs	Short days
SL	Strigolactone
SLY1	SLEEPY 1
SMAX1	SUPPRESSOR OF MAX2 1
SMXL2	SMAX1-LIKE 2
TCPs	TEOSINTE BRANCHED 1/CYCLOIDEA/PCFs
TIR1	TRANSPORT INHIBITOR RESPONSE 1
VAN	Vanadate
WDL5	WAVE-DAMPENED 5
YUC8	YUCCA 8
ZT	Zeitgeber time

CHAPTER 1

EIN3-mediated ethylene signals attenuate auxin response during hypocotyl thermomorphogenesis

INTRODUCTION

Versatile roles of ethylene have been described in a variety of plant growth and developmental processes, such as hypocotyl growth, fruit ripening, and leaf senescence (Grbić et al., 1995; Zhong et al., 2012; Liu et al., 2015), and plant adaptive responses to environmental stresses, including mechanical disturbance and submergence (Zhong et al., 2014; Wang et al., 2019). Ethylene is perceived by the endoplasmic reticulum membrane-localized ETHYLENE RESPONSE 1 (ETR1) receptor (Chen et al., 2002; Chen et al., 2005). The ETR1 receptor deactivates the serine/threonine protein kinase CONSTITUTIVE TRIPLE RESPONSE 1 (CTR1) by modifying its protein conformation (Kieber et al., 1993; Chen et al., 2005), which eventually leads to a proteolytic cleavage in the C-terminal domain of EIN2. The C-terminal segment of EIN2 suppresses the translation of *EIN3 BINDING F-BOX 1/2* (*EBF1/2*) mRNAs, whose encoded EBF1/2 proteins direct the degradation of EIN3 transcription factor, a master regulator of ethylene signaling (Potuschak et al., 2003; Shi et al., 2016).

Ethylene signaling events towards shaping hypocotyl morphogenesis have been characterized in detail. *Arabidopsis* seedlings germinating in the presence of ethylene under dark conditions exhibit shortening and thickening of hypocotyls, exaggeration of apical hooks, and shortening of the roots, which are termed the triple response (Guzman and Ecker, 1990). A set of genes, including *ETHYLENE RESPONSE FACTOR 1* (*ERF1*), *WAVE-DAMPENED 5* (*WDL5*), and *OCTADECANOID-RESPONSIVE ARABIDOPSIS AP2/ERF 59* (*ORA59*), mediates the triple response (Zhong et al., 2014; Sun et al., 2015; Kim et al., 2018). On the other hand, ethylene promotes hypocotyl growth in the light by inducing the

transcription of *PIF3* gene via EIN3 (Zhong et al., 2012; Zhong et al., 2014). Of particular interests is that warm temperatures suppress the ethylene-induced exaggeration of apical hooks in etiolated seedlings (Jin et al., 2018), raising a possibility that ethylene is also involved in plant responses to warm temperatures.

Warm ambient temperatures, while not stressful, broadly influence plant growth and architecture, which includes elongation of hypocotyls and leaf petioles, increased leaf hyponasty, and formation of small, thin leaves (Gray et al., 1998; Franklin et al., 2011; Park et al., 2019). These thermomorphogenic traits have been suggested to protect the heat-labile shoot apical meristems from hot soil surface and facilitate evaporative leaf cooling (Crawford et al., 2012; Kim et al., 2019; Park et al., 2019).

The representative thermosensor phytochrome B (phyB) and its interacting partner PIF4 play a central role in plant thermomorphogenesis (Franklin et al., 2011; Jung et al., 2016; Legris et al., 2016). The thermally activated PIF4 transcription factor induces the transcription of *YUCCA 8* (*YUC8*) gene encoding an auxin biosynthetic enzyme, resulting in auxin accumulation (Gray et al., 1998; Franklin et al., 2011; Crawford et al., 2012). Auxin is perceived by a small group of receptors, including TRANSPORT INHIBITOR RESPONSE 1 (TIR1) and its related F-box proteins, AUXIN SIGNALING F BOX PROTEINs (AFBs) (Dharmasiri et al., 2005). The auxin-stimulated receptors trigger the proteasomal degradation of Aux/IAA transcriptional repressors, thereby activating AUXIN RESPONSE FACTOR transcription factors that regulate the expression of downstream genes, such as those encoding SMALL AUXIN UP-RNAs (SAURs) (Dharmasiri et al., 2005).

Notably, PIF4 also activates the transcription of *SAUR* genes under warm

environments (Franklin et al., 2011). The SAUR proteins inhibit the action of clade D members of the protein phosphatase type 2C (PP2C) family, such as APD7, which inhibits the PM H^+-ATPases through protein dephosphorylation (Spartz et al., 2014). The SAUR-mediated activation of the PM H^+-ATPase proton pumps accelerates the acidification of apoplasts owing to proton efflux, which helps plants to uptake water and nutrients, culminating in cell expansion (Spartz et al., 2014). The underlying biochemical mechanisms of auxin action during cell expansion have given rise to the auxin-acid growth theory (Takahashi et al., 2012; Spartz et al., 2014).

In this work, I demonstrated that ethylene constitutes a dual regulatory signaling circuit that contributes to fine-tuning hypocotyl growth under fluctuating temperature environments. At normal temperatures, the ethylene-stimulated EIN3 transcription factor activates the expression of PIF3, which modulates cellular microtubule networks, leading to a moderate hypocotyl elongation (Zhong et al., 2012). Meanwhile, these data indicate that at warm temperatures, when auxin responses are highly enhanced by the PIF4 thermomorphogenesis pathway, EIN3 directly activates the transcription of *APD7* gene, thus attenuating auxin responses. The ethylene-directed attenuation of warm temperature-responsive auxin responses would facilitate an optimized adaptation to fluctuating environments in nature, where multiple climate changes, such as those in temperature and light, often occur simultaneously with diverse environmental stresses.

MATERIALS AND METHODS

Plant materials

All *Arabidopsis thaliana* lines used were in Columbia (Col-0) background, unless specified otherwise. The *ctr1-1* (CS8057), *phyB-9* (CS6217), *pif3-7* (CS66042), *pif4-2* (CS66043), *pif3-7 pif4-2* (CS66045), *wdl5-1* (CS436432), and *wdl5-2* (CS434701) mutants were obtained from a pool of T-DNA insertional lines deposited in the Arabidopsis Biological Resource Center (ABRC, Ohio State University, OH). The *pif4-101* (Garlic-114-G06) has been described previously (Lorrain et al., 2008). The *phyB-9 ein3 eil1* triple mutant has been described previously (Shi et al., 2016). The *tir1-1 afb1-1 afb2-1 afb3-1* quadruple mutant has been described previously (Dharmasiri et al., 2005). The *ora59-1* mutant and 35S:*ORA59* transgenic plants were obtained from Ohkmae K. Park. The *ein3-1 eil1-3* mutant was obtained from Sang-Dong Yoo. The *DR5*:*GUS* transgenic plant has been described previously (Lee et al., 2010). The p*PIF4*:*PIF4-FLAG* transgenic plants have been described previously (Lee et al., 2014). The 35S:*ERF1* transgenic plants (N6142) were obtained from the Nottingham Arabidopsis Stock Center (NASC, University of Nottingham, Nottingham, UK).

The p*PIF4*:*PIF4-FLAG ctr1-1* plants were generated by genetic cross between p*PIF4*:*PIF4-FLAG* transgenic plants and *ctr1-1* mutant. The p*PIF4*:*PIF4-FLAG ein3 eil1* plants were generated by genetic cross between p*PIF4*:*PIF4-FLAG* transgenic plants and *ein3 eil1* double mutant. The *phyB-9 ctr1-1* double mutant was generated by genetic cross between *phyB-9* and *ctr1-1* mutants. To generate 35S:*MYC-EIN3* p*PIF4*:*PIF4-FLAG* plants, the myc-pBA vector harboring an EIN3-coding sequence was transformed into p*PIF4*:*PIF4-FLAG* transgenic plants.

To generate p*EIN3*:*EIN3-MYC* transgenic plants, a 1.3-kb sequence region from the translational start site of *EIN3* gene was fused to the 5' end of an EIN3-coding sequence, and the fusion construct was subcloned into the pBA002a-6MYC (Type II) vector.

Plant growth conditions

Arabidopsis seeds were sterilized in 70% ethanol prior to cold imbibition for 3 d and allowed to germinate on 1/2 X Murashige and Skoog agar (hereafter, referred to as MS-agar) plates under long days (LDs, 16-h light and 8-h dark) with white light illumination (120 μmol $m^{-2}s^{-1}$) provided by fluorescent FLR40D/A tubes (Osram, Seoul, Korea) in a controlled growth chamber set at either 22°C or 28°C. For hypocotyl growth phenotype assays, two-day-old seedlings grown at 22°C were further grown for 5 d at either 22°C or 28°C under LDs. For the preparation of total RNA and protein samples, five-day-old seedlings grown at 22°C under LDs were further grown for 1 d at either 22°C or 28°C before harvesting whole seedlings. For 1-aminocyclopropane-1-carboxylic acid (ACC) treatments, ACC was included in growth media at the final concentration of 10 μM.

Gene expression analysis

Total RNA samples were extracted from appropriate plant materials using the Trizol reagent-based purification system (Invitrogen, Carlsbad, CA) and treated extensively with RNase-free DNase to eliminate contaminating genomic DNA before use. Synthesis of primary cDNA by reverse transcriptase was performed, as described previously (Park et al., 2017). Transcript levels were analyzed by reverse transcription-mediated quantitative PCR (RT-qPCR) using the primary cDNA

samples as substrates. PCR runs were carried out in 384-well blocks with the QuantStudio 6 Flex thermal cycler (Applied Biosystems, Foster City, CA) using the SYBR Green I master mix (KAPA Biosystems, Wilmington, MA) in a volume of 10 μl. The PCR primers used were listed in Supplemental Table S1. The *Arabidopsis eIF4A* gene (AT3G13920) was used as internal control in individual PCR reactions to normalize the variations in the amounts of primary cDNA samples used. Biological triplicates, each consisting of 15 seedlings grown under identical conditions, were averaged and statistically analyzed.

Confocal microscopy

Confocal microscopic analysis was performed, as described previously (Park et al., 2019). Two-day-old seedlings grown on MS-agar plates with or without ACC at 22^{o}C were further grown at either 22^{o}C or 28^{o}C for 5 d. The temperature-treated seedlings were then mounted on microscopy slides soaked in liquid growth medium containing 2 μM propidium iodide (Sigma-Aldrich, St Louis, MO) for 5 min. The seedling samples were covered with a coverslip and subjected to confocal microscopy using a Leica SP8 X confocal laser scanning microscope (Wetzlar, Germany) with the following laser and filter setup: 543 nm for excitation and 580 to 595 nm for emission.

Immunological assay

Five-day-old seedlings grown at 22^{o}C under LDs were further grown for 1 d at either 22^{o}C or 28^{o}C, and whole seedlings were harvested at appropriate time points. Total protein extraction was performed using appropriate plant materials, as described previously (Lee et al., 2014). Anti-FLAG (Sigma-Aldrich, F7425), anti-

PIF4 (Abiocode, Agoura Hills, CA, Cat No. R2534-4), anti-MYC (Millipore, Burlington, MA, 05-724; RRID:AB-11211891), and anti-H3 (Abcam, Cambridge, UK, Ab1791; RRID: SCR_012931) antibodies were used for the immunological detection of FLAG, PIF4, MYC, and H3 proteins, respectively. An anti-rabbit IgG-peroxidase antibody (Millipore, AP132P) was used as the secondary antibody for the immunoblot assays with the anti-MYC primary antibody. An anti-mouse IgG-peroxidase antibody (Millipore, AP124P) was used as the secondary antibody for the immunoblot assays with anti-FLAG, anti-PIF4, and anti-H3 primary antibodies.

GUS staining

For the histochemical detection of GUS activity, the *DR5*:*GUS* plants were fixed in 90% acetone for 20 min on ice and washed twice with rinsing solution (50 mM sodium phosphate, pH 7.2, 0.5 mM $K_3Fe(CN)_6$, and 0.5 mM $K_4Fe(CN)_6$), each for 20 min. The plant materials were subsequently incubated at 37°C for 3 h in fresh rinsing solution containing 2 mM 5-bromo-4-chloro-3-indolyl-β-D-glucuronide (Gold Biotechnology, St Louis, MO, G1281C1). They were then dehydrated by soaking in a series of ethanol dilutions, ranging from 15 - 80%, mounted on slide glasses, and visualized using a fluorescence microscope (Olympus, Tokyo, Japan, BX53F).

ChIP assay

ChIP assays were performed, essentially as described previously (Lee et al., 2014). Seedlings grown on MS-agar plates for 9 d at 22°C under LDs were transferred to 28°C for 1 d, and whole seedlings were harvested and soaked in 1% (v/v) formaldehyde by vacuum infiltration for cross-linking. After quenching the cross-

linking process by adding glycine, the vacuum-infiltrated samples were ground in liquid nitrogen. The powder of plant materials was resuspended in 30 ml of nuclear extraction buffer (1.7 M sucrose, 10 mM Tris-Cl, pH 7.5, 2 mM $MgCl_2$, 0.15% Triton-X-100, 5 mM β-mercaptoethanol, 0.1 mM PMSF) containing a mixture of protease inhibitors (Sigma-Aldrich) and centrifuged at 16,000 X g for 45 min at 4^{o}C to obtain nuclear fraction. The nuclear fraction was lysed with lysis buffer (50 mM Tris-Cl, pH 8.0, 0.5 M EDTA, 1% SDS, and a mixture of protease inhibitors) to extract chromatin. The extracted chromatin was sonicated into approximately 0.4 - 0.7-kb fragments. Five μg of an anti-MYC antibody (Millipore, 05-724; RRID:AB_11211891) was added to the chromatin solution, which was precleared with salmon sperm DNA/Protein G magnetic beads (Bio-Rad, Cat No. 161-4023). The precipitates were eluted from the beads. Cross-links were reversed, and residual proteins were removed by incubation with proteinase K (Invitrogen). DNA was recovered using a spin column (Promega, Madison, WI). Quantitative PCR was used to determine the amounts of genomic DNA enriched in the chromatin preparations, and the values were normalized to the amount of input in each sample. The primers used and sequence elements assayed were listed in Table 1 and Figure 1, respectively.

Yeast two-hybrid assay

I employed the BD Matchmaker system (Takara, Shiga, Japan) to examine protein-protein interactions in yeast cells. The pGADT7 vector was used for the GAL4 activation domain, and the pGBKT7 vector was used for the GAL4 DNA-binding domain. The PIF4-coding sequence was subcloned into the pGBKT7 vector. The EIN3-coding sequence was subcloned into the pGADT7 vector. The yeast strain

Primers	Sequences	Usage
eIF4A-F	5′-TGACCACACAGTCTCTGCAA	RT-qPCR
eIF4A-R	5′-ACCAGGGAGACTTGTTGGAC	"
PIF3-F	5′-AGTTCCAAGTCTCGGGGATG	"
PIF3-R	5′-CTCTAGTCGAGCCATTGCCA	"
PIF4-F	5′-AGATCATCTCCGACCGGTTT	"
PIF4-R	5′-CGCCGGTGAACTAAATCTCA	"
YUC8-F	5′-GACTGCTCGGTTCGATGAGA	"
YUC8-R	5′-TGAATCACCTCACCGGAAAA	"
IAA19-F	5′-CGACCACGAAAGTGGGGTTA	"
IAA19-R	5′-TCTTTCAAGGCCACACCGAT	"
SAUR22-F	5′-GACAAATAGAGAATTATAAATGGCTCTG	"
SAUR22-R	5′-ATGAATTAAGTCTATATCTAACTCGGAAA	"
pAPD7A-F	5′-GTAGGGGTTAAGACAGCTAAGAG	"
pAPD7A-R	5′-CTTTTGTTTGCAAAGTGGTAATTTG	"
pAPD7B-F	5′-GGATCTGTTTTCTTATATATCGG	"
pAPD7B-R	5′-ATCGACACTGTCTCTAATTTGAA	"
pAPD7C-F	5′-TCATGTATATGAGCATTGGTTT	"
pAPD7C-R	5′-CGAATATAGAAAGCTCAAAAATG	"
pPIF3-F	5′-CGTTCTTCAGTGTGATTAAACAATTGGTT	"
pPIF3-R	5′-GACGAATTAGGCCAAGAAAAACTTGC	"
WDL5-F	5′-ATCTCCAAAACTCGGGCGAA	"
WDL5-R	5′-AAGGCGAGGGGTTTGAGTTT	"
ELF3-F	5′-CAGGTCAAGGCGAATGCAAG	"
ELF3-R	5′-AGTTTTGCCACCATCTCGGT	"
LUX-F	5′-GGAGCTGGTGGAAATGGTTCT	"
LUX-R	5′-TGCAATTTGGGACTTTGCGG	"
ELF4-F	5′-AGTTTCTCGTCGGGCTTTCA	"
ELF4-R	5′-TAAGCTCTAGTTCCGGCAGC	"
TCP5-F	5′-GGGTTTAACACCAATCATCAACAA	"
TCP5-R	5′-CGACAGTAACGTTATTACCAGATT	"
TCP13-F	5′-CTGGTTCAGGGACTATGGAGACATT	"
TCP13-R	5′-AAATGTTTTGGGAAGACGAAGATGA	"
TCP17-F	5′-GGTAACGTCACTGTCGCATTTTCTAA	"
TCP17-R	5′-GAAACGAAGGGTACCTTGTTGGGA	"
BOP1-F	5′-ATCGCCAAATCCGGTCTTCC	"
BOP1-R	5′-GAGGCATTGAAGATTTGAGACGG	"
BOP2-F	5′-TCTTGTTCAAGGGGGCAGTT	"
BOP2-R	5′-CGAGATATCACCATTGCAGCG	"
SAUR19-F	5′-CTTCAAGAGCTTCATAATAATTCAAACTT	"
SAUR19-R	5′-GAAGGAAAAAATGTTGGATCATCTT	"
AHA1-F	5′-TCTCATGGCCATTGCTTTGG	"
AHA1-R	5′-GCATTTCCGGCGTTGTTTTC	"
AHA2-F	5′-CCCCCAAGACATGACAGTGC	"
AHA2-R	5′-AATGGATGCGAGGTTTGCGT	"
APD7-F	5′-GGGCAGATCTGAGAGAGGTG	"
APD7-R	5′-CCGCACTAAGGATTGGCTTA	"
TIR1-F	5′-GAGCTGCCCTGTTGAGAGAG	"
TIR1-R	5′-ATGTTCCAGACGAAGCCAGG	"
EIN3-F	5′-CCGATTGGACCGACTCCTCATAC	"
EIN3-R	5′-ATAGCAAGCCAGGTAGCACTCTC	"
GUS-F	5′-GAATTGATCAGCGTTGGTGG	"
GUS-R	5′-ATCGAAACGCAGCACGATAC	"

Table 1. Primers used in Chapter 1.

The PCR primers were designed according to the NCBI Primer-BLAST software (https://www.ncbi.nlm.nih.gov/tools/primer-blast/) in a way that the calculated melting temperatures of the primers are in a temperature range of 50 - 65^{o}C. F denotes forward primer. R denotes reverse primer.

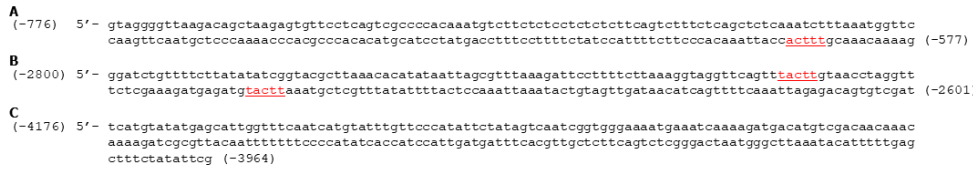

Figure 1. Nucleotide sequences of *EIN3* promoter elements used in ChIP assays.

The nucleotide sequences were extracted from the *Arabidopsis* Information Resource (TAIR) database (https://www.arabidopsis.org). The putative EIN3-binding sequence (EBS) motifs were underlined in red color. Note that the sequence region C does not contain any EBS elements.

used was AH109 (Leu-, Trp-, Ade-, His-), which contains chromosomally integrated reporter genes encoding β-galactosidase (lacZ) and HIS3 enzyme under the control of the GAL1 promoter. Transformation of yeast cells was performed according to the manufacturer's instruction. Colonies obtained were restreaked on a selective medium lacking Leu, Trp, Ade, and His. To eliminate nonspecific growth of yeast cells, 3-amino-1,2,4-triazole was included in the media at the final concentration of 10-30 mM.

Media acidification

Four-day-old seedlings grown on MS-agar plates at 22^{o}C under LDs were transferred to fresh MS-agar plates containing a pH indicator bromocresol purple. ACC was used at the final concentration of 10 μM. The pH indicator plates were incubated for 24 h at either 22^{o}C or 28^{o}C before taking photographs.

Color quantitation was performed using the images. Twenty points were randomly selected around the root tip regions, where media acidification was most progressed. The RGB values of the selected points were used in the following calculation. The R, G, and B values were considered as coordinates of a 3-D space (X. Y. Z). The acidification degrees were calculated as relative distances ranging in-between the pH 5.7-selected point and the pH 5.0-selected point. Positive values indicate that the distances are more close to yellow color (pH 5.0), and negative values indicate that the distances are more close to brown color (pH 5.7). Two standard media having pH 5.0 and 5.7 were also photographed. The pH 5.7 media has a RGB value of (180. 130. 94), and the pH 5.0 media has a RGB value of (255. 231. 91). The relative degrees of acidification of the randomly selected points were calculated according to the following formula. I subtracted 1 from each calculation

value to make the differences more clear.

$$Relative\ acidification = \frac{\sqrt{(180-X)^2+(130-Y)^2+(94-Z)^2}}{\sqrt{(180-X)^2+(130-Y)^2+(94-Z)^2}+\sqrt{(255-X)^2+(231-Y)^2+(91-Z)^2}} - 1$$

Statistical analysis

The statistical significance between two means of measurements was determined using a two-sided Student's *t*-test with *P* values of < 0.01 or < 0.05. To determine statistical significance for more than two populations, one-way analysis of variance (ANOVA) with *post hoc* Tukey test ($P < 0.01$) was used. Statistical analyses were performed using the IBM Statistical Package for the Social Sciences (SPSS) Statistics 25 software (www.ibm.com/products/spss-statistics).

RESULTS

Ethylene suppresses hypocotyl growth at warm temperatures

Considering the antagonistic modes of ethylene action on hypocotyl growth in the light and darkness (Zhong et al., 2012; Zhong et al., 2014) and the suppressive effects of warm temperatures on the ethylene-induced exaggeration of apical hooks in etiolated seedlings (Jin et al., 2018), I hypothesized that ethylene is involved in plant thermomorphogenesis.

To obtain clues as to whether ethylene influences the thermal responses of hypocotyl growth, I examined the thermomorphogenic hypocotyl growth of the *Arabidopsis ctr1-1* mutant in the light, which exhibits a constitutive ethylene response (Kieber et al., 1993). While the mutant seedlings exhibited elongated hypocotyls at normal temperatures (22^{o}C), they displayed shorter hypocotyls compared to those of wild-type Col-0 seedlings at warm temperatures (28^{o}C) (Figure 2A). In agreement with the thermomorphogenic hypocotyl growth phenotypes of the *ctr1-1* seedlings, treatments of Col-0 seedlings with an ethylene precursor ACC, promoted hypocotyl growth at 22^{o}C, but the promotive effects of ACC were completely reversed at 28^{o}C (Figure 2B). Measurements of hypocotyl growth at varying temperatures showed that the promotive effects of ACC on hypocotyl growth steadily decline and eventually are reversed as temperatures go up to 28^{o}C (Figure 3), supporting the temperature-responsive effects of ethylene on hypocotyl growth.

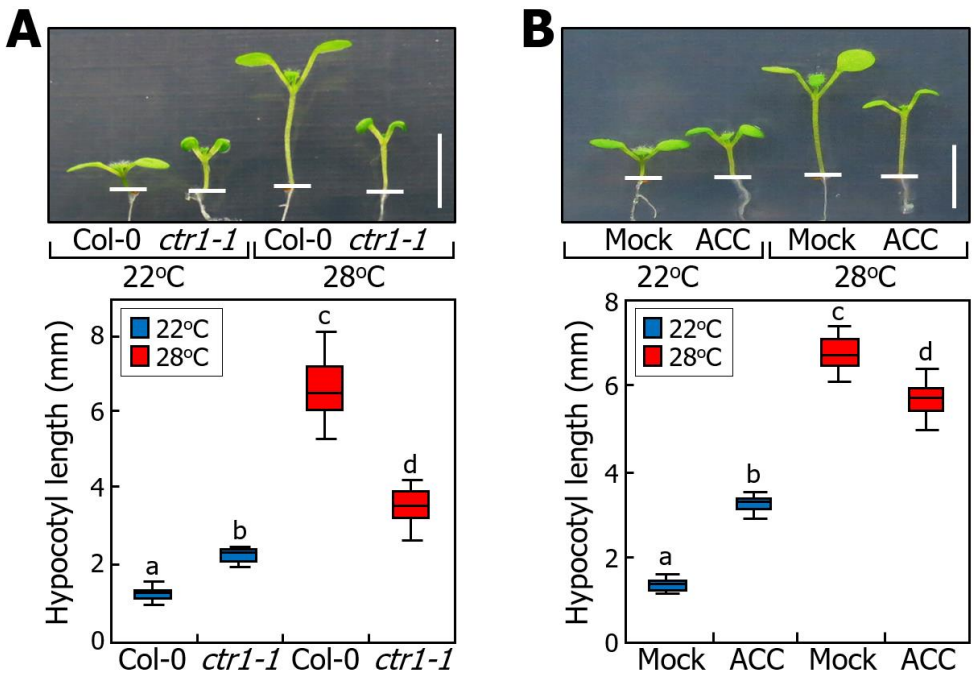

Figure 2. Ethylene promotion of hypocotyl growth is reversed at warm temperatures in the light.

Two-day-old *Arabidopsis* seedlings grown on MS-agar plates at 22°C were exposed to 28°C for 5 d under long days (LDs, 16-h light and 8-h dark). ACC was used at the final concentration of 10 μM. Three independent measurements, each consisting of 15 seedlings, were statistically analyzed. Different letters represent significant differences ($P < 0.01$) determined by one-way analysis of variance (ANOVA) with *post hoc* Tukey test.

(A) Thermomorphogenic hypocotyl growth phenotypes of *ctr1-1* mutant. The root-hypocotyl junctions are marked with horizontal white bars. Scale bar, 5 mm.

(B) Effects of ethylene on thermomorphogenic hypocotyl growth. Col-0 seedlings were grown on MS-agar plates supplemented with ACC. Scale bar, 5 mm.

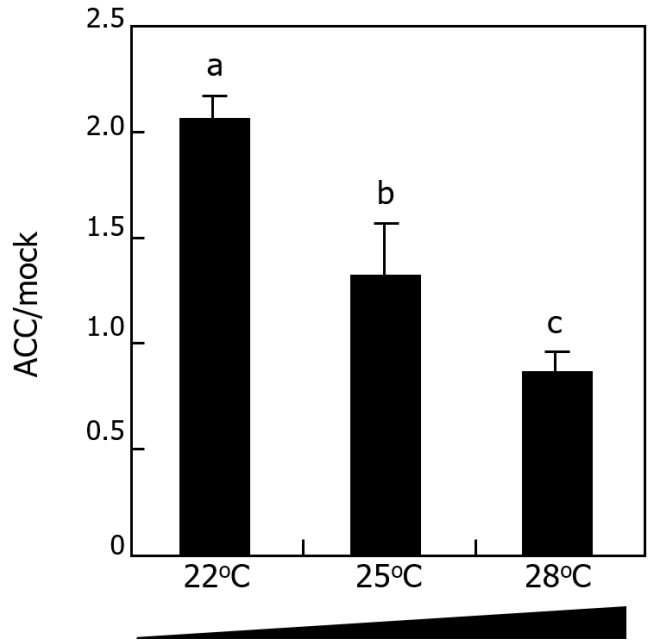

Figure 3. Effects of ethylene on hypocotyl growth at varying temperatures.

Col-0 seedlings were exposed to varying temperatures in the presence of ACC. ACC/mock indicates the ratio of the hypocotyl length of ACC-treated seedlings relative to that of mock-treated seedlings. Five independent measurements were statistically analyzed.

Staining of hypocotyls with a fluorescent dye propidium iodide revealed that the epidermal hypocotyl cells are relatively longer at 22°C but shorter at 28°C in ACC-treated Col-0 seedlings compared to those in mock-treated seedlings (Figure 4A and 4B), indicating that the ethylene action on hypocotyl growth is exerted primarily by modulating cell lengths rather than cell numbers, as reported previously (Ma et al., 2018). Meanwhile, leaf span was reduced by ACC treatments to a similar degree at both 22°C and 28°C (Figure 5A). In addition, leaf hyponasty, representing an upward bending of the leaves (Kim et al., 2019; Park et al., 2019), was increased in the presence of ACC at both 22°C and 28°C (Figure 5B), indicating that ethylene affects mainly hypocotyl growth among different thermomorphogenic traits.

Kinetic measurements of thermomorphogenic hypocotyl growth revealed that the patterns of hypocotyl growth were gradually reversed in the presence of ACC in the time course of warm temperature treatments (Figure 6), indicating that ethylene suppresses the stimulating effects of warm temperatures on hypocotyl growth.

Thermoresponsive action of ethylene on hypocotyl growth is independent of PIF3

The ethylene signaling mediator EIN3 enhances hypocotyl growth by inducing the transcription of *PIF3* gene in the light (Zhong et al., 2012; Zhong et al., 2014). Consistent with the previous reports, the hypocotyl growth of the PIF3-dficient *pif3-7* mutant seedlings was insensitive to ACC at 22°C (Figure 7A).

A question was whether PIF3 is involved in the ethylene-mediated attenuation of hypocotyl thermomorphogenesis. At 28°C, the hypocotyls of both

Col-0 wild-type and *pif3-7* mutant seedlings were elongated to a similar degree (Figure 7A). In the presence of ACC, the thermomorphogenic hypocotyl growth was reduced in both Col-0 and *pif3-7* seedlings, suggesting that the ethylene action in hypocotyl thermomorphogenesis does not depend on PIF3. The more prominent reduction of hypocotyl growth in the *pif3-7* seedlings at 28^{o}C is because PIF3 promotes hypocotyl growth in response to ethylene, regardless of temperatures (Figure 7A, 7B and 7C). These observations suggest that PIF3 is not directly involved in the ethylene-mediated attenuation of hypocotyl thermomorphogenesis.

Gene expression assays revealed that the *PIF3* transcription was not discernibly affected by warm temperature in Col-0 seedlings (Figure 7B). The *PIF3* transcription was 2 to 3 fold higher in the *ctr1-1* mutant seedlings at both 22^{o}C and 28^{o}C, consistent with the warm temperature-independent role of PIF3 in promoting hypocotyl growth (Figure 7A). Similarly, the *PIF3* transcription was elevated to a similar degree by ACC at both 22^{o}C and 28^{o}C (Figure 7C). Together, these observations demonstrate that PIF3 is largely independent of the ethylene action in attenuating hypocotyl thermomorphogenesis.

Ethylene function in hypocotyl thermomorphogenesis is distinct from the triple response

The triple response of ethylene-treated etiolated *Arabidopsis* seedlings is illustrated by thickening and shortening of hypocotyls and roots and pronounced curvature of apical hooks, which are robust and readily countable in ethylene-related studies (Guzman and Ecker, 1990). In a morphological point of view, the ethylene-induced shortening of hypocotyls in etiolated seedlings resembles the ethylene-mediated suppression of hypocotyl growth at warm temperatures (Figure 2A and 2B).

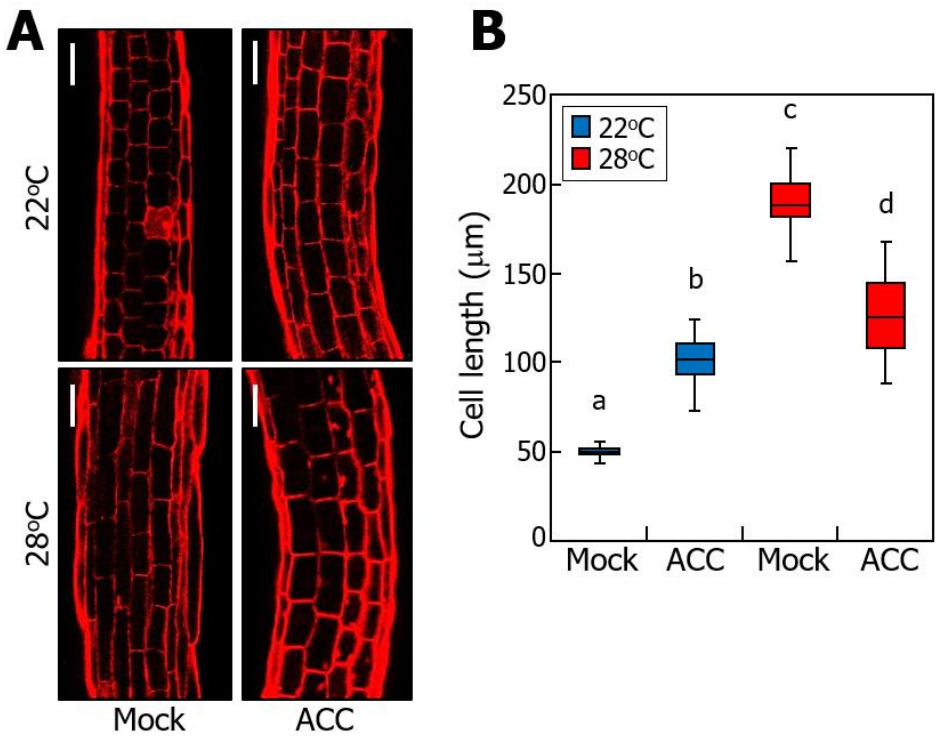

Figure 4. Effects of ethylene on hypocotyl epidermal cell elongation under warm temperatures.

Col-0 seedling growth and warm temperature treatments were performed, as described in Figure 2. Hypocotyls of seven-day-old seedlings were stained with a red fluorescence dye propidium iodide (A). Scale bars, 100 μm. Lengths of hypocotyl cells were measured and statistically analyzed (B).

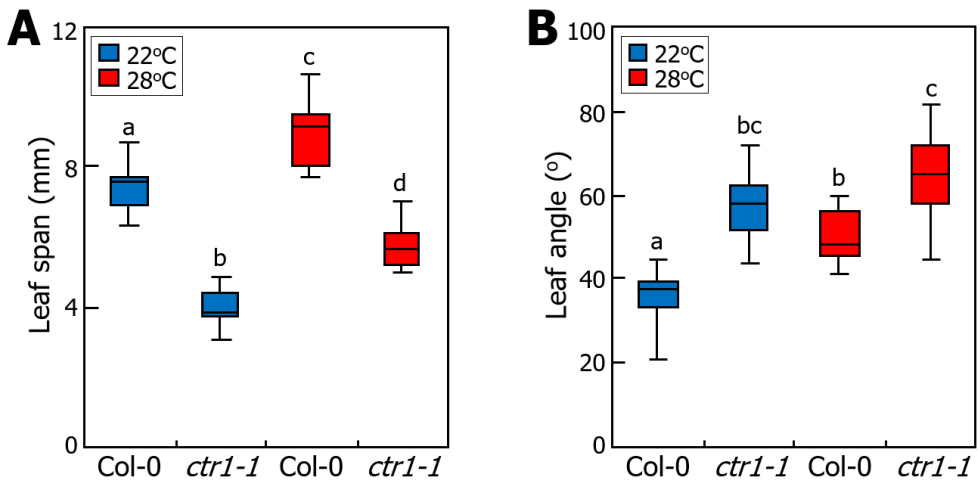

Figure 5. Leaf thermomorphogenic traits in *ctr1-1* mutant.

Two-day-old *Arabidopsis* seedlings grown on MS-agar plates at 22°C were exposed to 28°C for 5 d under LDs. Three independent measurements, each consisting of 15 seedlings, were statistically analyzed. Different letters represent significant differences ($P < 0.01$) determined by one-way analysis of variance ANOVA with *post hoc* Tukey test.

(A) Leaf span phenotypes. The tip-to-tip distances of cotyledon pairs were measured.

(B) Leaf hyponasty phenotypes. The angles of cotyledon petioles relative to the horizontal plane were measured.

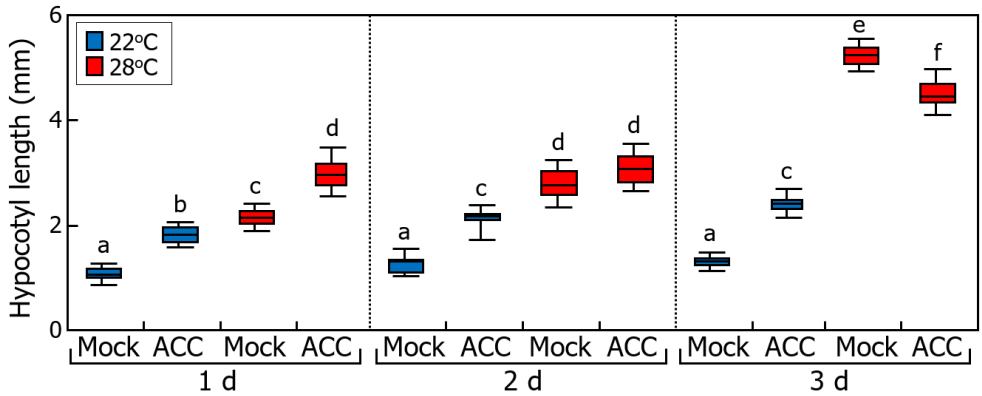

Figure 6. Kinetic effects of warm temperatures on ethylene-mediated hypocotyl growth.

Four-day-old Col-0 seedlings grown on MS-agar plates at 22°C were exposed to 28°C for the indicated days under LDs. Different letters represent significant differences ($P < 0.01$) determined by one-way analysis of variance ANOVA with *post hoc* Tukey test. d, day.

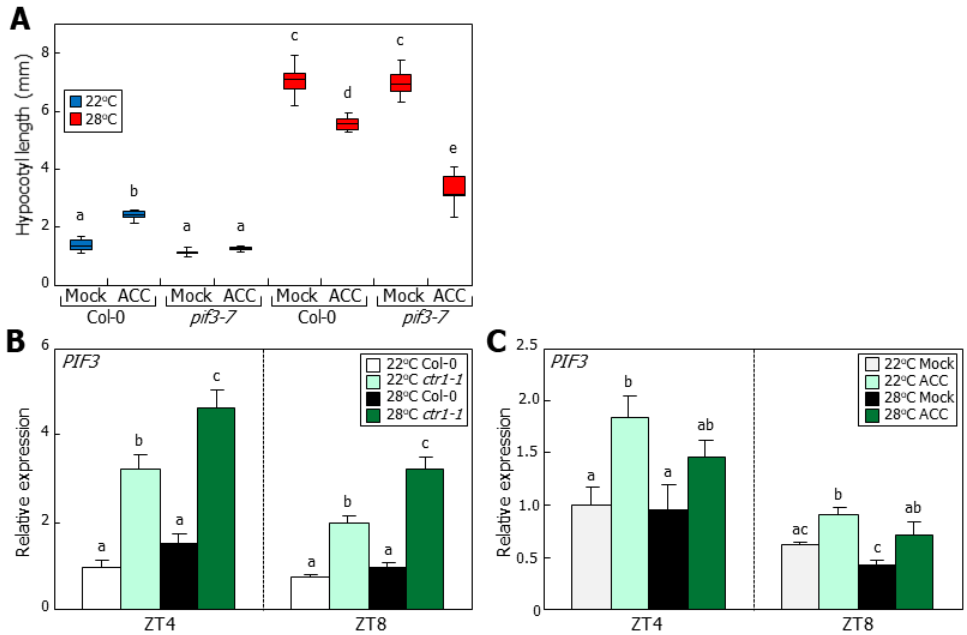

Figure 7. PIF3 is not linked with suppression of hypocotyl thermomorphogenesis by ethylene.

(A) Thermomorphogenic hypocotyl growth phenotypes of *pif3-7* mutant.

(B) Relative transcript levels of *PIF3* gene in *ctr1-1* mutant. Five-day-old Col-0 seedlings grown on MS-agar plates at 22°C were exposed to 28°C for 1 d. Seedlings were harvested at zeitgeber time (ZT) 4 and 8 for total RNA extraction. Transcript levels were analyzed by reverse transcription-mediated quantitative PCR (RT-qPCR). Biological triplicates, each consisting of 15 seedlings, were statistically analyzed. Different letters represent significant differences ($P < 0.05$) determined by one-way ANOVA with *post hoc* Tukey test. Error bars indicate standard error of the mean (SE).

(C) Effects of ethylene on *PIF3* transcription in the hypocotyls of Col-0 seedlings. Seedlings were grown in the presence of 10 μM ACC. RT-qPCR analysis was performed, as described above.

I therefore investigated whether the suppressive effects of ethylene on thermomorphogenic hypocotyl growth are related with the triple response. It is known that *ERF1*, *WDL5*, and *ORA59* genes mediate the triple response (Zhong et al., 2012; Zhong et al., 2014; Sun et al., 2015; Kim et al., 2018). I found that *ERF1*-overexpressing transgenic seedlings exhibited elongated hypocotyls at 28°C, like Col-0 seedlings (Figure 8A). In addition, the WDL5-deficient *wdl5* mutant exhibited a wild-type thermomorphogenic hypocotyl growth in the presence of ACC (Figure 8B), and the levels of *WDL5* transcripts were only slightly decreased in ACC-treated Col-0 seedlings under identical temperature conditions (Figure 8C). Similarly, the ORA59-deficient *ora59-1* mutant exhibited a wild-type hypocotyl growth phenotype at both 22°C and 28°C (Figure 8D). Moreover, overexpression of *ORA59* did not alter the thermoresponsive hypocotyl growth (Figure 8E). Together, these observations suggest that the thermoresponsive action of ethylene in hypocotyl elongation is functionally distinct from the triple response (see also the following section).

Thermoresponsive role of ethylene is functionally associated with PIF4

PIF4 plays a central role in hypocotyl thermomorphogenesis by activating auxin production and signaling (Gray et al., 1998; Franklin et al., 2011; Park et al., 2017). A question was whether PIF4 is associated with the ethylene action during hypocotyl thermomorphogenesis.

Hypocotyl growth assays revealed that ACC promoted hypocotyl elongation in the *pif4-101* mutant seedlings at 22°C, similar to what observed in Col-0 seedlings (Figure 9A). Notably, hypocotyls were much longer in ACC-treated mutant seedlings compared to those of mock-treated mutant seedlings at

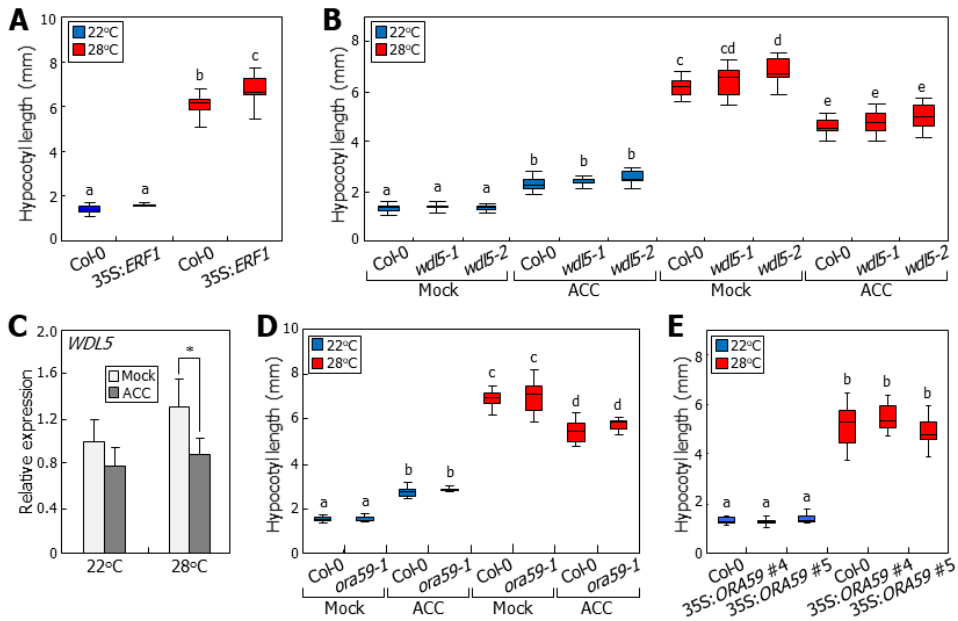

Figure 8. The triple response genes are not involved in the ethylene-mediated attenuation of hypocotyl thermomorphogenesis.

Two-day-old seedlings grown on MS-agar plates at 22°C were exposed to 28°C for 5 d under LDs. ACC was used at the final concentration of 10 μM. Three independent measurements, each consisting of 15 seedlings, were statistically analyzed. Different letters represent significant differences ($P < 0.01$) determined by one-way ANOVA with *post hoc* Tukey test.

(A) Thermomorphogenic hypocotyl growth phenotypes of 35S:*ERF1* transgenic plants. A full-size ERF1-coding sequence was overexpressed driven by the cauliflower mosaic virus (CaMV) 35S promoter in Col-0 background.

(B) Thermomorphogenic hypocotyl growth phenotypes of *wdl5* mutants.

(C) Effects of ethylene on the transcription of *WDL5* gene in hypocotyls. Six-day-old Col-0 seedlings grown on MS-agar plates supplemented with ACC at 22°C were exposed to 28°C for 1 d. Whole seedlings were harvested at ZT8 for total RNA extraction. RT-qPCR were performed, as described in Figure 7B. Biological

triplicates, each consisting of 20 seedlings, were statistically analyzed (*t*-test, $*P < 0.01$, difference from mock). Error bars indicate SE.

(D) Thermomorphogenic hypocotyl growth phenotypes of *ora59-1* mutant.

(E) Thermomorphogenic hypocotyl growth phenotypes of 35S:*ORA59* transgenic plants. A full-size ORA59-coding sequence was overexpressed driven by the CaMV 35S promoter in Col-0 background. Two independent transgenic lines, #4 and #5, were assayed.

28°C, which is in contrast to the thermomorphogenic hypocotyl growth of Col-0 seedlings. In addition, the *ctr1-1* mutation significantly reduced the hypocotyl growth of the p*PIF4*:*PIF4-FLAG* transgenic seedlings at both 22°C and 28°C (Figure 9B). ACC treatments also attenuated the hypocotyl growth of the p*PIF4*:*PIF4-FLAG* transgenic seedlings at both 22°C and 28°C (Figure 9C), similar to the suppressive effects of the *ctr1-1* mutation (Figure 9B). Meanwhile, the levels of *PIF4* transcripts in the p*PIF4*:*PIF4-FLAG* transgenic seedlings are higher by approximately 7-fold compared to those in Col-0 seedlings (Figure 10). These observations suggest that PIF4 is functionally associated with the ethylene-mediated suppression of hypocotyl growth at warm temperatures.

The *phyB-9* mutant seedlings exhibits elongated hypocotyls, which is morphologically similar to the thermomorphogenic elongation of hypocotyls, and PIF4 activity is elevated in the mutant (Jung et al., 2016; Legris et al., 2016). In harmony with the notion that PIF4 is associated with the ethylene-mediated suppression of hypocotyl thermomorphogenesis, the *phyB-9 ctr1-1* double mutant exhibited shorter hypocotyls than those of the *phyB-9* single mutant at both 22°C and 28°C (Figure 11A), similar to what observed in the p*PIF4*:*PIF4-FLAG ctr1-1* seedlings (Figure 9B). In addition, ACC treatments suppressed the hypocotyl growth of *phyB-9* mutant at both 22°C and 28°C (Figure 11B). These observations further support that the ethylene-mediated suppression of hypocotyl thermomorphogenesis is exerted via the PIF4 thermomorphogenesis pathway.

I next investigated whether PIF3 and PIF4 are functionally interrelated with each other in modulating the ethylene-mediated control of hypocotyl growth. In the *pif3-7* mutant seedlings, while the promotive effects of ACC on hypocotyl growth at 22°C completely disappeared, the suppressive effects of ACC on

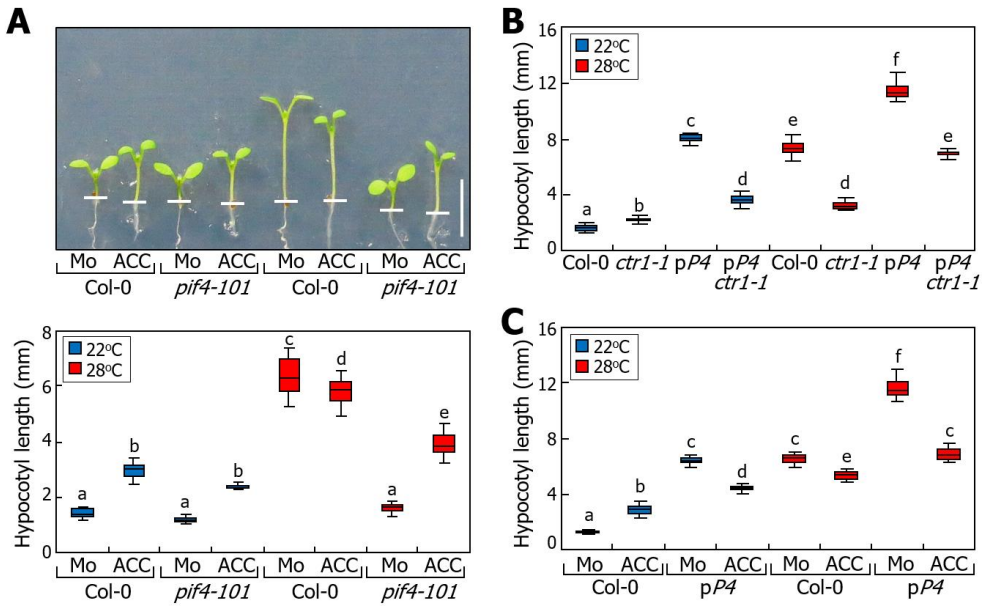

Figure 9. Ethylene-mediated suppression of hypocotyl thermomorphogenesis is associated with PIF4.

Seedling growth and warm temperature treatments were performed, as described in Figure 2. Three independent measurements, each consisting of 15 seedlings, were statistically analyzed. Different letters represent significant differences ($P < 0.01$) determined by one-way ANOVA with *post hoc* Tukey test. ACC was used at the final concentration of 10 μM. Mo, mock.

(A) Effects of ethylene on thermomorphogenic hypocotyl growth of *pif4-101* mutant. The root-hypocotyl junctions are marked with horizontal white bars. Scale bar, 5 mm.

(B) Thermomorphogenic hypocotyl growth phenotypes of p*PIF4*:*PIF4-FLAG* transgenic plants. The *PIF4-FLAG* gene fusion was expressed driven by an endogenous *PIF4* promoter, consisting of approximately 2.5 kbp sequence region from the translational start site, in Col-0 and *ctr1-1* backgrounds, resulting in p*P4* and p*P4 ctr1-1* plants, respectively.

(C) Effects of ethylene on thermomorphogenic hypocotyl growth of p*P4* transgenic plants.

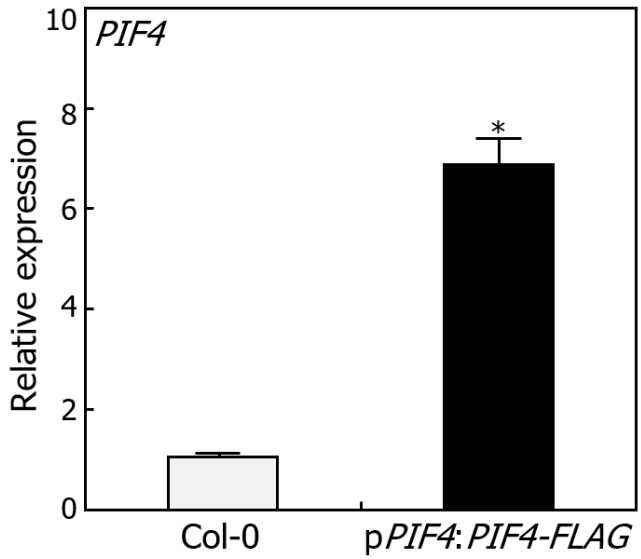

Figure 10. Relative levels of *PIF4* transcripts in p*PIF4*:*PIF4-FLAG* transgenic plants.

A *PIF4-FLAG* gene fusion, in which a FLAG-coding sequence was fused in-frame to the 3' end of the PIF4-coding sequence, was expressed driven by an endogenous *PIF4* promoter, consisting of approximately 2.5-kb sequence region from the translational start site, in Col-0 background. Five-day-old whole seedlings grown on MS-agar plates at 22^{o}C under LDs were harvested at ZT8 for total RNA extraction. Transcript levels were analyzed by RT-qPCR. Biological triplicates, each consisting of 15 seedlings, were statistically analyzed using Student *t*-test (*$P < 0.01$, difference from Col-0). Error bars indicate SE.

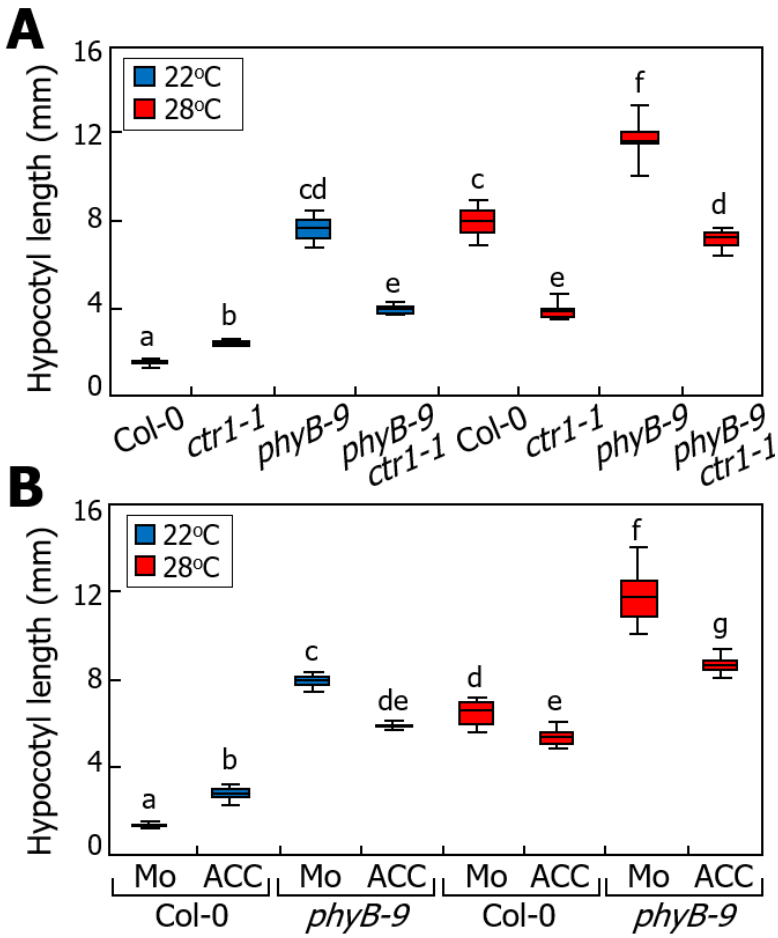

Figure 11. PhyB, an upstream regulator of PIF4, is related with suppressed hypocotyl thermomorphogenesis by ethylene.

Seedling growth was performed, as described in Figure 2. Different letters represent significant differences ($P < 0.01$) determined by one-way ANOVA with *post hoc* Tukey test.

(A) Thermomorphogenic hypocotyl growth phenotypes of *phyB-9 ctr1-1* double mutant.

(B) Effects of ethylene on thermomorphogenic hypocotyl growth of *phyB-9* mutant.

thermomorphogenic hypocotyl growth were evident (Figure 7A and Figure 12). Conversely, in the *pif4-2* mutant seedlings, while ACC promoted the hypocotyl growth at 22^{o}C, as observed in Col-0 seedlings, the suppressive effects of ACC on thermomorphogenic hypocotyl growth were reversed (Figure 9A and Figure 12). In addition, the *pif3-7 pif4-2* double mutant was insensitive to ACC at both 22^{o}C and 28^{o}C (Figure 12). Together, these observations indicate that the PIF3- and PIF4-mediated ethylene signaling events are mutually independent in modulating hypocotyl growth, consistent with the notion that PIF3 is functionally independent of hypocotyl thermomorphogenesis.

These data indicate that ethylene attenuates hypocotyl thermomorphogenesis by affecting the phyB-PIF4 thermomorphogenesis pathway, which is also associated with photomorphogenic responses in plants (Yan et al., 2020). I therefore compared the effects of ACC on the hypocotyl growth of *pif4* mutants in the light and darkness. The *pif4* mutants exhibited similar hypocotyl growth phenotypes to those observed in Col-0 seedlings at 22^{o}C, regardless of light conditions (Figure 13A). In addition, the skotomorphogenic hypocotyl growth of the *phyB-9* mutant was similar to that of Col-0 seedlings, unlike the *ctr1-1* mutant (Figure 13B). These observations further support that the ethylene-mediated suppression of hypocotyl thermomorphogenesis is distinct from the ethylene function in hypocotyl skotomorphogenesis, that is, the triple response.

EIN3 is involved in the ethylene-mediated attenuation of hypocotyl thermomorphogenesis

A next question was how ethylene signals suppress the PIF4-mediated hypocotyl thermomorphogenesis. It is known that the EIN3 and EIN3-like 1 (EIL1)

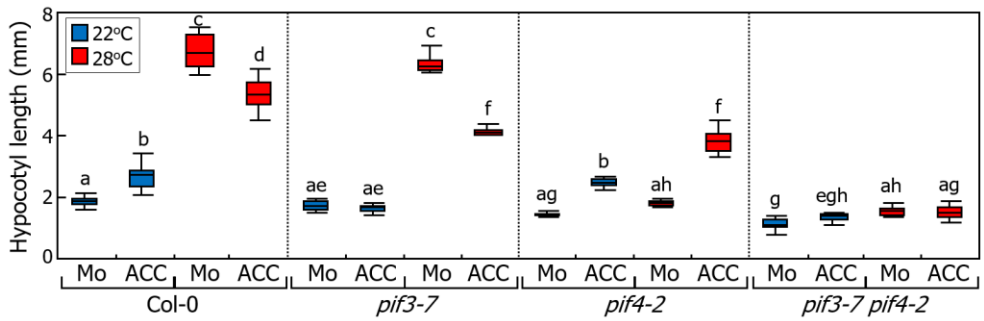

Figure 12. PIF4 and PIF3 is independent in ethylene-mediated suppression of hypocotyl thermomorphogenesis.

Thermomorphogenic hypocotyl growth phenotypes of *pif3-7 pif4-2* double mutant. Seedling growth and warm temperature treatments were performed, as described in Figure 2.

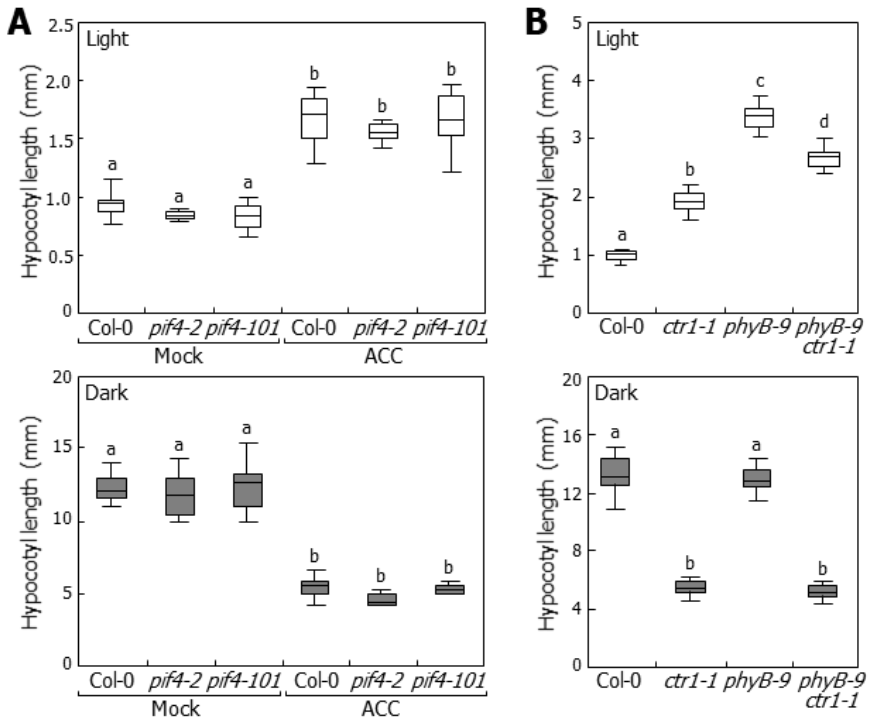

Figure 13. Attenuation of hypocotyl thermomorphogenesis by ethylene is distinct from the triple response.

Arabidopsis seedlings germinating in the presence of saturating concentrations of ethylene under dark conditions display distinct morphological phenotypes, collectively termed the triple response, which is featured by shortening and thickening of hypocotyls and overcurvature of apical hooks. Three independent measurements, each consisting of 15 seedlings grown either in the light or darkness, were statistically analyzed. Different letters represent significant differences ($P < 0.01$) determined by one-way ANOVA with *post hoc* Tukey test.

(A) Hypocotyl growth phenotypes of PIF4-deficient mutants in the light and darkness. Seedlings were grown on MS-agar plates supplemented with 10 μM ACC at 22^{o}C for either 5 d in the light or 4 d in darkness. Two mutant alleles, *pif4-2* and *pif4-101*, were included in the assays.

(B) Hypocotyl growth phenotypes of *phyB-9 ctr1-1* double mutant. Seedlings were grown on MS-agar plates at 22^{o}C for either 5 d in the light or 4 d in darkness.

transcription factors act as master regulators of ethylene signaling (Chao et al., 1997). In addition, EIN3 promotes ethylene-mediated photomorphogenic hypocotyl growth by directly activating *PIF3* gene (Zhong et al., 2012). It was therefore anticipated that the EIN3 transcription factor would also modulate the ethylene action during hypocotyl thermomorphogenesis.

As expected, both the ethylene-mediated promotion of hypocotyl elongation at 22^{o}C and the ethylene-mediated suppression of hypocotyl growth at 28^{o}C were compromised in the *ein3 eil1* mutant that lacks the two master regulators (Figure 14A). In addition, the *phyB-9 ein3 eil1* triple mutant also exhibited insensitive hypocotyl growth phenotypes to ACC at both 22^{o}C and 28^{o}C (Figure 14B). Furthermore, the *ein3 eil1* mutation in the p*PIF4*:*PIF4-FLAG* transgenic plants abolished ACC effects on hypocotyl growth at both 22^{o}C and 28^{o}C (Figure 14C). Notably, the p*PIF4*:*PIF4-FLAG* transgenic seedlings overexpressing *EIN3* gene exhibited shorter hypocotyls than those of the p*PIF4*:*PIF4-FLAG* seedlings in the presence of ACC at 22^{o}C and even shorter under mock treatments at 28^{o}C (Figure 15A and 15B). These observations demonstrate that EIN3 mediates ethylene signals in suppressing the PIF4-driven hypocotyl thermomorphogenesis pathway.

EIN3-mediated ethylene signals do not affect the PIF4 activity

A critical question was as to how EIN3 suppresses the PIF4-mediated hypocotyl thermomorphogenesis. I compared the expression patterns of *PIF4* and its target genes in Col-0 and *ctr1-1* seedlings at 22^{o}C and 28^{o}C. Gene expression assays using whole seedlings showed that the transcript levels of *PIF4* and *YUC8* genes were lowered in the *ctr1-1* mutant at both 22^{o}C and 28^{o}C (Figure 16A). Those of

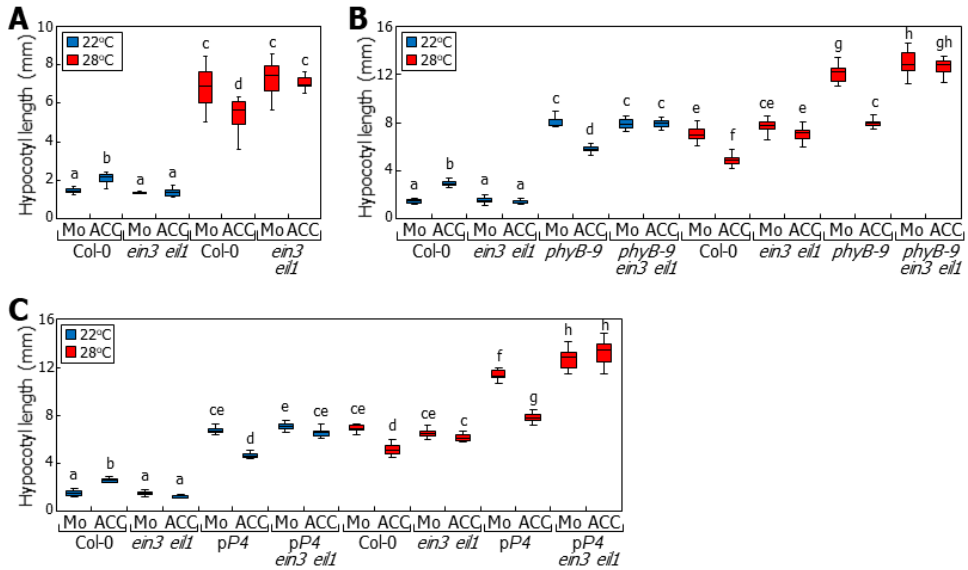

Figure 14. EIN3 mediates the suppressive effects of ethylene on PIF4 thermomorphogenesis pathway.

Seedling growth and warm temperature treatments were performed, as described in Figure 2. Three independent measurements, each consisting of 15 seedlings, were statistically analyzed. Different letters represent significant differences ($P < 0.01$) determined by one-way ANOVA with *post hoc* Tukey test. ACC was used at the final concentration of 10 μM. Mo, mock.

(A) Effects of ethylene on thermomorphogenic hypocotyl growth of *ein3 eil1* mutant.

(B) Effects of ethylene on thermomorphogenic hypocotyl growth of *phyB-9 ein3 eil1* triple mutant.

(C) Effects of ethylene on thermomorphogenic hypocotyl growth of p*P4* transgenic plants in *ein3 eil1* background. The *PIF4-FLAG* gene fusion was expressed driven by an endogenous *PIF4* promoter in *ein3 eil1* background, resulting in p*P4 ein3 eil1* plants.

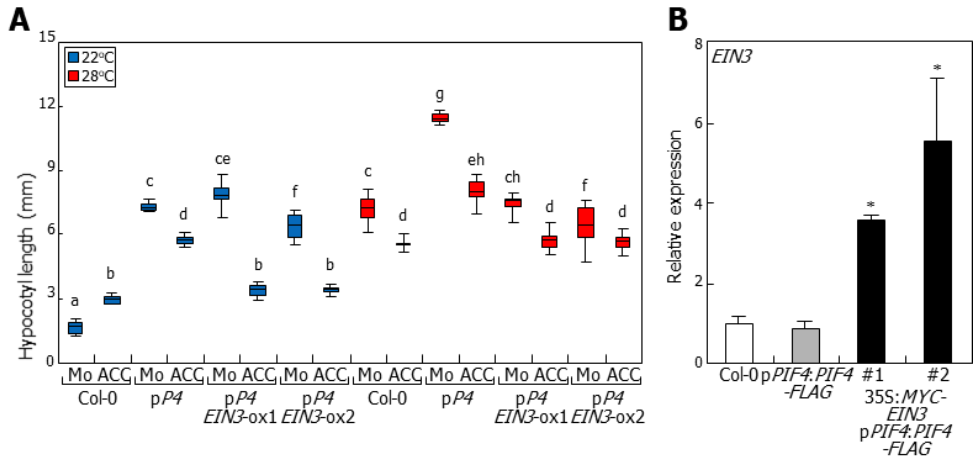

Figure 15. EIN3 mediates the suppressive effects of ethylene on hypocotyl thermomorphogenesis.

Seedling growth and warm temperature treatments were performed, as described in Figure 2. Three independent measurements, each consisting of 15 seedlings, were statistically analyzed. Different letters represent significant differences ($P < 0.01$) determined by one-way ANOVA with *post hoc* Tukey test.

(A) Effects of *EIN3* overexpression on thermomorphogenic hypocotyl growth of p*P4* transgenic plants. Two independent transgenic lines were assayed.

(B) Relative levels of *EIN3* transcripts in 35S:*MYC-EIN3* p*PIF4*:*PIF4-FLAG* plants.

The *MYC-EIN3* gene fusion was overexpressed driven by the CaMV 35S promoter in the p*PIF4:PIF4-FLAG* transgenic plants. Two independent transgenic lines were assayed. Seedling growth and RT-qPCR were performed, as described in Figure 7B. Biological triplicates, each consisting of 15 seedlings, were statistically analyzed (*t*-test, *$P < 0.01$, difference from Col-0). Error bars indicate SE.

IAA19 and *SAUR22* genes were also reduced in a similar pattern. Considering the polar auxin flow from the cotyledons to the hypocotyls, where cell elongation occurs during thermomorphogenic responses, I next examined the gene expression patterns separately in the cotyledons and hypocotyls of ACC-treated seedlings. It was found that while some variations were observed among the genes tested, ACC treatments did not discernibly affect the transcription of the *PIF4* and its target genes in the cotyledons at 28^{o}C, which were more evident at zeitgeber time (ZT) 8 (Figure 16B). On the other hand, under identical temperature conditions, the chemical treatments reduced the transcription of *PIF4*, *IAA19*, and *SAUR22* genes by approximately 2-fold in the hypocotyls at ZT8 (Figure 16C). In contrast, the *YUC8* transcription was unaltered when assayed under identical conditions. These gene expression data suggest that the transcriptional control of the *PIF4* and its target genes is not a major driving force for the ethylene-mediated suppression of hypocotyl thermomorphogenesis (see Discussion).

I next examined whether ethylene influences the protein abundance of PIF4. Immunological analysis revealed that the PIF4 protein abundance in whole seedlings was not significantly altered by ACC treatments at both 22^{o}C and 28^{o}C (Figure 17A and 17B). Consistent with the relatively small effects of ACC on the transcription of *PIF4* and its target genes in the cotyledons and the PIF4 protein abundance, ACC treatments did not alter the *GUS* expression in the *DR5*:*GUS* reporter plants at 22^{o}C and 28^{o}C (Figure 17C). Histochemical staining assays revealed that the pattern and intensity of GUS staining in the hypocotyls was not discernibly affected by ACC treatments and warm temperatures (Figure 17D), supporting the notion that the EIN3-mediated ethylene signals do not prominently affect PIF4 function during the suppression of hypocotyl thermomorphogenesis.

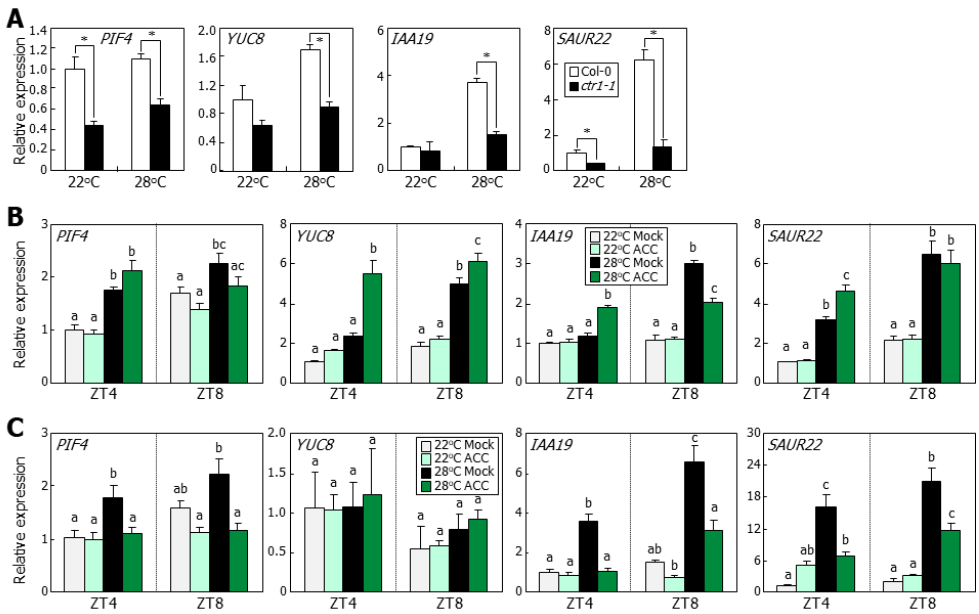

Figure 16. Effects of ethylene on the transcription of *PIF4* and auxin response genes.

Seedling growth, warm temperature treatments, and RT-qPCR were performed, as described in Figure 7B. Biological triplicates, each consisting of 15 seedlings, were statistically analyzed (*t*-test, $*P < 0.01$, difference from Col-0). Different letters represent significant differences ($P < 0.01$) determined by one-way ANOVA with *post hoc* Tukey test. Error bars indicate SE.

(A) Relative transcript levels of *PIF4* and its downstream genes in *ctr1-1* mutant. Seedlings were harvested at ZT8 for total RNA extraction.

(B) Effects of ethylene on the transcription of *PIF4* and its downstream genes in cotyledons. Seedlings were grown in the presence of 10 μM ACC.

(C) Effects of ethylene on the transcription of *PIF4* and its downstream genes in hypocotyls. Seedlings were grown in the presence of 10 μM ACC.

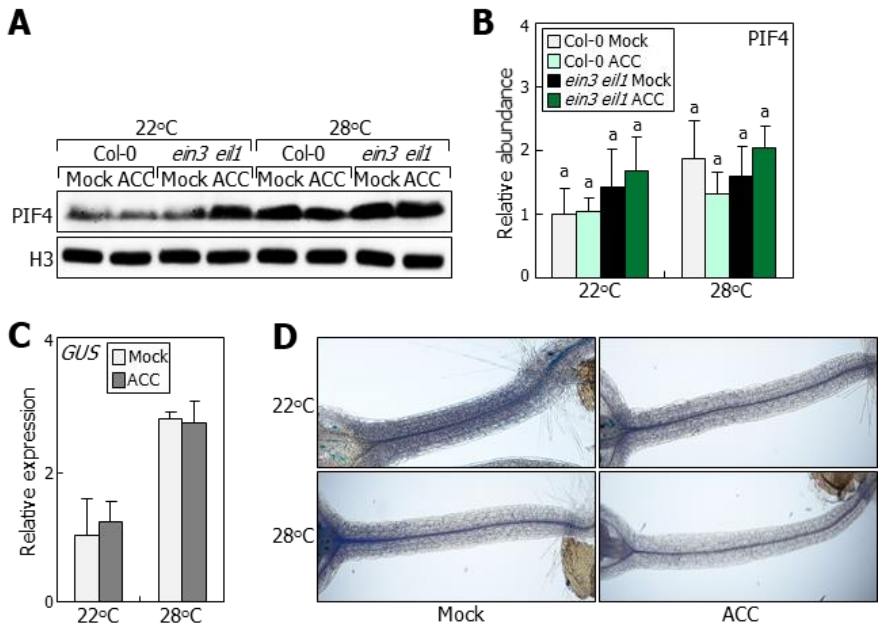

Figure 17. Effects of ethylene on PIF4 function.

Six-day-old seedlings grown on MS-agar plates at 22°C were exposed to 28°C for 1 d. Ten μM ACC was included in the growth media. Whole seedlings were harvested at ZT8 for total protein extraction.

(A) PIF4 protein abundance in *ein3 eil1* mutant. PIF4 proteins were immunologically detected using an anti-PIF4 antibody. Histone 3 (H3) proteins were also immunodetected in parallel for protein quality control.

(B) Quantitation of PIF4 protein abundance. Five independent measurements were statistically analyzed. Different letters represent significant differences ($P < 0.01$) determined by one-way ANOVA with *post hoc* Tukey test. Error bars indicate SE.

(C) Effects of ethylene on the transcription of *DR5*:*GUS* reporter. The *DR5*:*GUS* transgenic plants were grown in the presence of 10 μM ACC. The relative levels of *GUS* transcripts were analyzed by RT-qPCR, as described in Figure 7B.

(D) GUS staining of *DR5*:*GUS* hypocotyls. The reporter seedlings were in the presence of 10μM ACC, as described in (C).

It is known that the *PIF4* gene transcription and its protein accumulation are regulated by upstream regulators, such as *EARLY FLOWERING 3* (*ELF3*), *LUX ARRHYTHMO* (*LUX*), *EARLY FLOWERING 4* (*ELF4*), *TEOSINTE BRANCHED 1/CYCLOIDEA/PCFs* (*TCP*s), and *BLADE-ON-PETIOLEs* (*BOP*s), during various growth and photomorphogenic processes (Nusinow et al., 2011; Zhang et al., 2017; Han et al., 2019). Gene expression analysis using the hypocotyls showed that ACC treatments did not significantly affect the transcription of the upstream genes (Figure 18). Even the slight modifications of gene expression patterns at warm temperatures were not in harmony with the patterns of thermomorphogenic hypocotyl growth. Furthermore, PIF4 did not directly interact with EIN3 (Figure 19). Collectively, these observations indicate that PIF4 itself and the PIF4-mediated thermal induction of auxin biosynthesis are not directly connected with the EIN3-mediated ethylene signaling during hypocotyl thermomorphogenesis.

EIN3 attenuates auxin response during hypocotyl thermomorphogenesis

Since PIF4 function is not directly linked with the EIN3-mediated attenuation of hypocotyl thermomorphogenesis, I hypothesized that downstream events, such as auxin response and signaling, in the PIF4 thermomorphogenesis pathway would be affected by the EIN3-mediated ethylene signals.

Notably, the ethylene-mediated attenuation of hypocotyl thermomorphogenesis was reversed in the *tir1-1 afb1-1 afb2-1 afb3-1* quadruple mutant that lacks four major auxin receptors (Figure 20A), as observed in the *pif4* mutant (Figure 9A). In the meantime, ACC treatments did not discernibly affect the transcription of *TIR1* gene at both 22^{o}C and 28^{o}C (Figure 20B), suggesting that the EIN3-mediated ethylene signals target not auxin perception but auxin response and

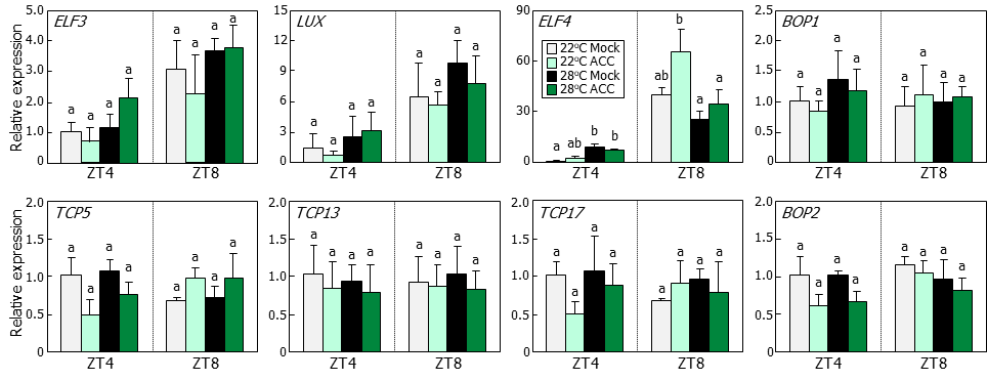

Figure 18. Effects of ethylene on the transcription of PIF4 upstream regulator genes.

Seedling growth, warm temperature treatments, and RT-qPCR were performed, as described in Figure 7B. Ten μM ACC was included in the growth media. Hypocotyls were used for total RNA extraction. Different letters represent significant differences ($P < 0.01$) determined by one-way ANOVA with *post hoc* Tukey test.

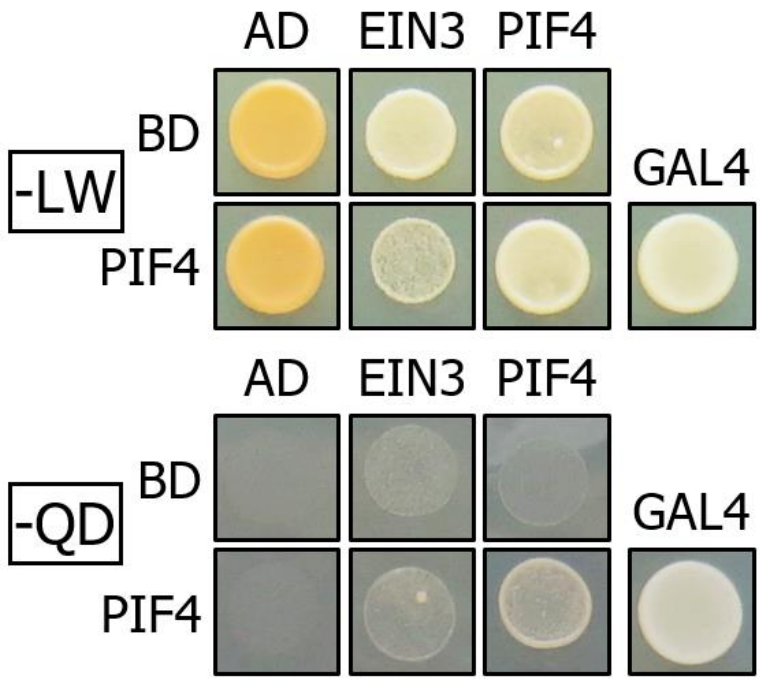

Figure 19. Lack of EIN3-PIF4 interactions in yeast cells.

-LW marks Leu and Trp dropout plates. -QD marks Leu, Trp, His, and Ade dropout plates. Ten mM of 3-amino-1,2,4-triazole was included in the growth media to suppress the potential autocatalytic activity of PIF4 and EIN3 proteins. PIF4 was included as positive control of PIF4 binding.

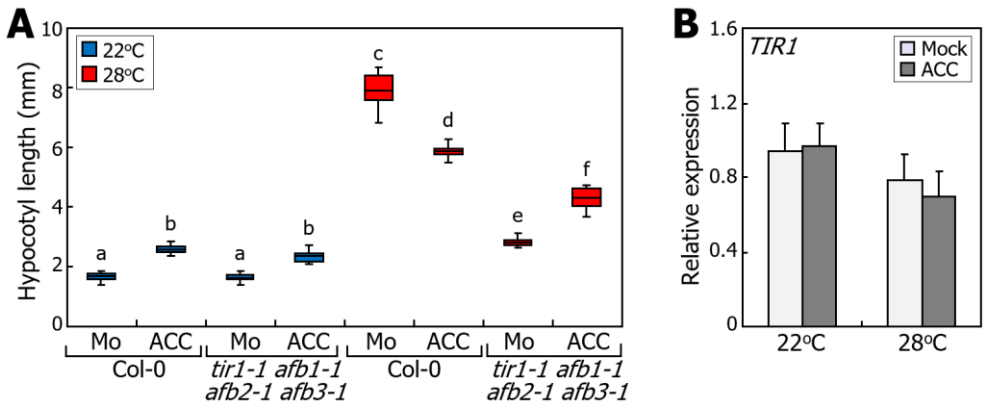

Figure 20. Lack of auxin perception is essential for suppressive effects on hypocotyl thermomorphogenesis.

Seedling growth and warm temperature treatments were performed, as described in Figure 2. Three independent measurements, each consisting of 15 seedlings, were statistically analyzed. Different letters represent significant differences ($P < 0.01$) determined by one-way ANOVA with *post hoc* Tukey test. ACC was used at the final concentration of 10 μM. Mo, mock.

(A) Effects of ethylene on thermomorphogenic hypocotyl growth of auxin receptor-deficient mutants.

(B) Effects of ethylene on the transcription of *TIR1* gene. Six-day-old Col-0 seedlings grown on MS-agar plates at 22°C were exposed to 28°C for 1 d. Hypocotyls of the seedlings were harvested at ZT8 for total RNA extraction. Transcript levels were analyzed by RT-qPCR. Biological triplicates, each consisting of 20 seedlings, were statistically analyzed (*t*-test, $*P < 0.01$, difference from mock). Error bars indicate SE.

signaling steps during hypocotyl thermomorphogenesis.

To further investigate the linkage between ethylene and auxin action during hypocotyl thermomorphogenesis, I employed the auxin transport inhibitor, naphthylphthalamic acid (NPA). It was found that the ACC-promoted hypocotyl growth of Col-0 seedlings was markedly reduced in the presence of NPA at 22^{o}C (Figure 21). In addition, the thermomorphogenic hypocotyl elongation of the *ein3 eil1* seedlings was also reduced significantly in the presence of NPA, regardless of ACC. Interestingly, the ACC-mediated attenuation of hypocotyl thermomorphogenesis was eliminated in NPA-treated Col-0 seedlings. Together, these observations support that polar auxin transport, and perhaps auxin action as well, is required for the ethylene-mediated attenuation of hypocotyl thermomorphogenesis.

I also employed the synthetic auxin, picloram (PIC), to further examine the linkage between ethylene and auxin actions during hypocotyl thermomorphogenesis. In the presence of PIC at 22^{o}C, while mock-treated Col-0 seedlings exhibited a greatly enhanced hypocotyl growth, ACC-treated Col-0 seedlings did not exhibit discernible changes in hypocotyl growth (Figure 22A), which is because the promotive effects of auxin on hypocotyl growth is attenuated by ACC treatments. These patterns of hypocotyl growth are similar to what observed in warm temperature-exposed Col-0 seedlings grown in the presence of ACC (Figure 2B). On the other hand, treatments of *ein3 eil1* seedlings with PIC promoted hypocotyl growth to a similar level in mock-treated and ACC-treated mutant seedlings, in which auxin action is not attenuated by ethylene (Figure 22A). These observations indicate that EIN3-mediated ethylene signals suppress auxin response during thermomorphogenic hypocotyl growth.

Meanwhile, PIC treatments promoted the hypocotyl growth of the *pif4-101* mutant seedlings, but the hypocotyls were shorter than those of PIC-treated Col-0 seedlings (Figure 22B), suggesting that the PIF4-directed thermal responses require additional signaling routes other than auxin signaling (Franklin et al., 2011). The hypocotyls of the *pif4-101* mutant seedlings were further elongated in the presence of both PIC and ACC, probably because of the EIN3-mediated induction of *PIF3* gene. In conjunction with the lack of ethylene effects on PIF4 activity and auxin production (Figure 17), these observations unequivocally demonstrate that the EIN3-mediated ethylene signals repress auxin response and signaling steps during hypocotyl thermomorphogenesis.

EIN3 directly activates the PP2C-encoding APD7 gene

These data indicate that the EIN3-mediated ethylene signals attenuate auxin action during hypocotyl thermomorphogenesis, raising a possibility that EIN3 targets far-downstream auxin signaling steps, which are rather directly involved in hypocotyl cell elongation in the PIF4 thermomorphogenesis pathway.

The auxin acid-growth model illustrates that auxin signals induce proton efflux into the apoplasts and the apoplastic acidification causes cell wall loosening, which helps plant cells to efficiently uptake water and solute, leading to cell expansion (Takahashi et al., 2012; Spartz et al., 2014). Molecular genetic studies have established a regulatory mechanism underlying the auxin acid-growth phenomenon, in which auxin-activated SAUR19 inhibits the APD7 enzyme to activate the PM H^+-ATPase proton pumps (Takahashi et al., 2012; Spartz et al., 2014). Therefore, I asked whether EIN3 affects the regulatory machinery of the PM H^+-ATPase proton pumps.

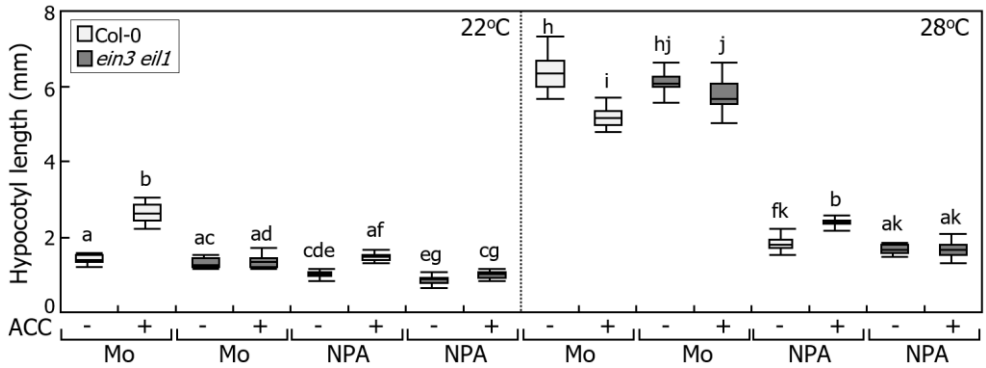

Figure 21. Auxin transport is required for ethylene action on suppression of hypocotyl thermomorphogenesis.

Seedling growth and warm temperature treatments were performed, as described in Figure 2. Three independent measurements, each consisting of 15 seedlings, were statistically analyzed. Different letters represent significant differences ($P < 0.01$) determined by one-way ANOVA with *post hoc* Tukey test. ACC was used at the final concentration of 10 μM. Mo, mock. Effects of auxin transport inhibitors on thermomorphogenic hypocotyl growth of *ein3 eil1* mutant. NPA was used at the final concentration of 10 μM.

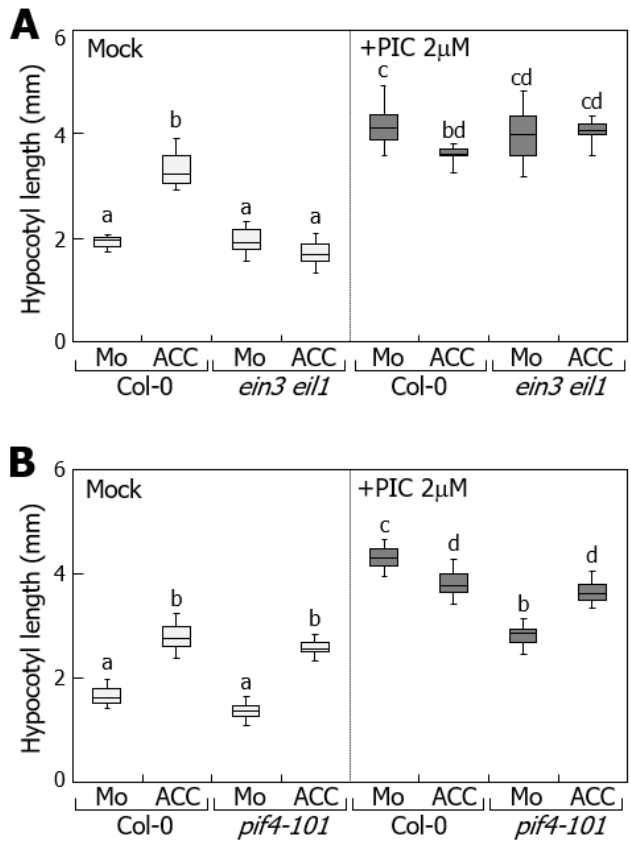

Figure 22. EIN3 attenuates PIF4-mediated auxin response during hypocotyl thermomorphogenesis.

Different letters represent significant differences ($P < 0.01$) determined by one-way ANOVA with *post hoc* Tukey test. ACC was used at the final concentration of 10 μM. Mo, mock.

(A) Effects of auxin on hypocotyl growth of *ein3 eil1* mutant. Seedlings were grown on MS-agar plates supplemented with 2 μM picloram (PIC) at 22°C for 7 d under LDs.

(B) Effects of auxin on hypocotyl growth of *pif4-101* mutant. Seedlings were grown, as described in (A).

Gene expression analysis showed that while the transcription of *ARABIDOPSIS H^+-ATPASE* (*AHA*) genes encoding the PM H^+-ATPases was slightly induced by ACC treatments at both 22°C and 28°C, that of *SAUR19* gene was unaltered under identical conditions (Figure 23). However, these gene expression patterns were not in accordance with the ethylene-mediated attenuation of auxin responses. Interestingly, the transcription of *APD7* gene encoding the protein phosphatase PP2C-D7 was upregulated by more than 2-fold in the presence of ACC at 22°C and further elevated by more than 4-fold at 28°C (Figure 24). In addition, the ACC-mediated induction of the *APD7* gene disappeared in the *ein3 eil1* mutant, suggesting that EIN3 mediates the transcription of the *APD7* gene, possibly by directly binding to the gene promoter.

Nucleotide sequence analysis identified a couple of potential EIN3-binding sequences (EBSs) within the *APD7* promoter (Figure 1 and Figure 25A). As inferred from the promoter sequence analysis, chromatin immunoprecipitation (ChIP) assays using the p*EIN3*:*EIN3-MYC* transgenic plants (Figure 25B) showed that the EIN3 proteins efficiently bind to the predicted EBS elements in the *APD7* promoter (Sequence elements A and B in Figure 25C). Furthermore, the DNA binding of EIN3 was significantly elevated in the presence of ACC at 28°C, demonstrating that the EIN3/EIL1 transcription factors activate the transcription of *APD7* gene by directly binding to the gene promoter.

EIN3-mediated ethylene signals inhibit the progression of apoplastic acidification

The APD7 protein phosphatase inactivates the PM H^+-ATPases via protein dephosphorylation (Spartz et al., 2014). I therefore anticipated that the EIN3-

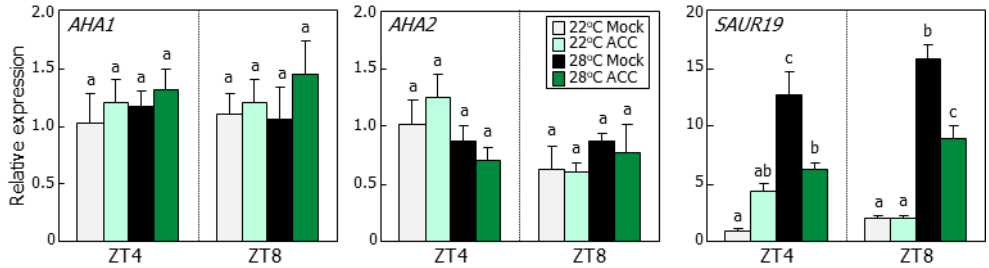

Figure 23. Effects of ethylene on the transcription of *SAUR19* and proton pump component genes.

Seedling growth, warm temperature treatments, and RT-qPCR were performed, as described in Figure 7B. Ten μM ACC was included in the growth media. Hypocotyls were used for total RNA extraction. Biological triplicates, each consisting of 15 seedlings, were statistically. Different letters represent significant differences ($P < 0.01$) determined by one-way ANOVA with *post hoc* Tukey test. Error bars indicate SE.

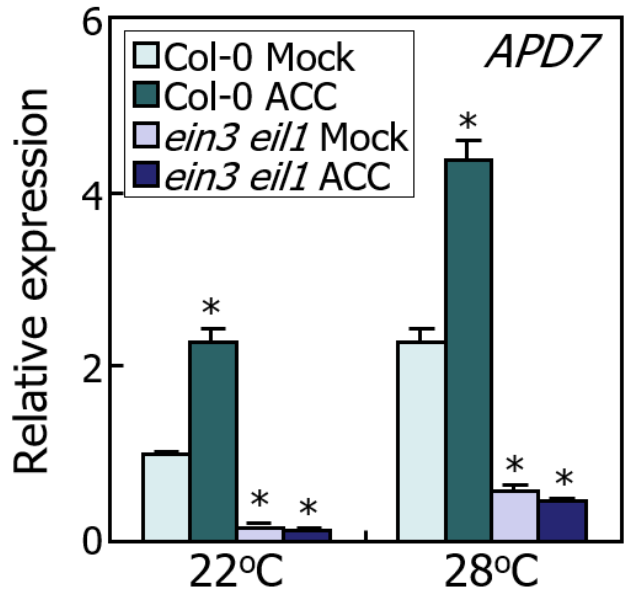

Figure 24. EIN3 induces the transcription of *APD7* gene.

Transcription of *APD7* gene in *ein3 eil1* mutant. Seedling growth in the presence of 10 μM ACC and RT-qPCR were performed, as described in Figure 7B. Biological triplicates, each consisting of 20 seedlings, were statistically analyzed (*t*-test, **P* < 0.01, difference from Col-0 Mock). Error bars indicate SE.

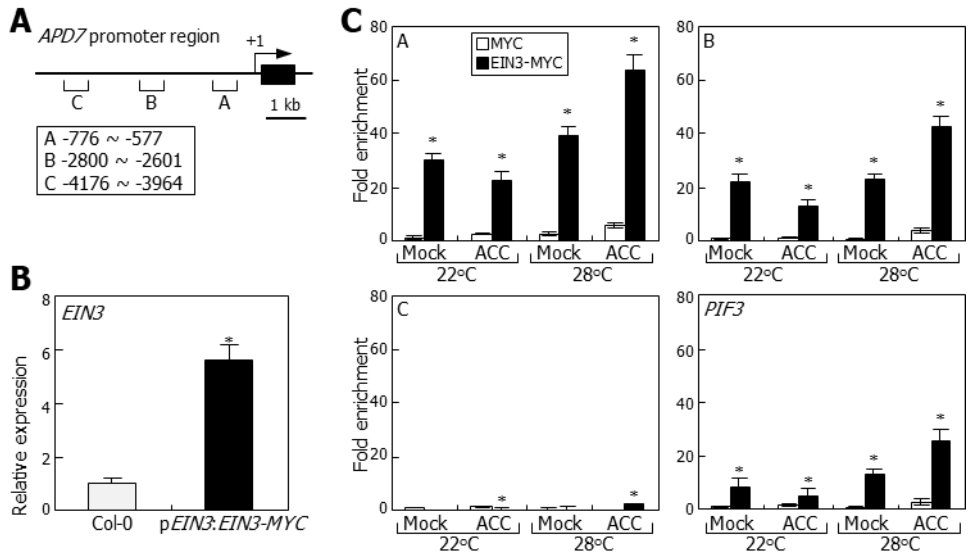

Figure 25. EIN3 directly activates the transcription of *APD7* gene.

(A) Sequence elements in *APD7* promoter. The A to C sequence elements were chosen for ChIP assays. The transcriptional start site is marked as (+1). bp, base pair.

(B) An *EIN3-MYC* gene fusion, in which a MYC-coding sequence was fused in-frame to the 3' end of the EIN3-coding sequence, was expressed driven by an endogenous *EIN3* promoter, consisting of an approximately 1.3-kb sequence region from the translational start site, in Col-0 background. Seedling growth and RT-qPCR were performed, as described in Figure 7B. Biological triplicates, each consisting of 15 seedlings, were statistically analyzed (*t*-test, $*P < 0.01$, difference from Col-0). Error bars indicate SE.

(C) ChIP assays on the binding of EIN3 to *APD7* promoter. The p*EIN3*:*EIN3-MYC* and 35S:*MYC* transgenic seedlings grown at 22^{o}C for 9 d were subsequently exposed to 28^{o}C for 1 d before harvesting whole seedlings. The A to C sequence elements described in (A) were used. Three independent measurements were

statistically analyzed (*t*-test, $*P < 0.01$, difference from MYC alone). Error bars indicate SE. A *PIF3* promoter sequence element was included as positive control in the assays.

mediated induction of *APD7* gene would lead to the inactivation of the PM H^+-ATPase proton pumps.

I first investigated whether the EIN3-mediated induction of *APD7* gene is correlated with the inactivation of the PM H^+-ATPases. Vanadate is a transition-state analog of phosphate and frequently used as an inhibitor of P-type ATPases, including the H^+-ATPases, in the field (Møller et al., 1996). It was found that vanadate treatments discernibly reduced the thermomorphogenic hypocotyl growth of Col-0 seedlings (Figure 26). It also attenuated more prominently hypocotyl thermomorphogenesis in the p*PIF4*:*PIF4-FLAG* transgenic seedlings and the *phyB-9* mutant seedlings that exhibit an elongated hypocotyl growth at warm temperatures, suggesting that the attenuation of hypocotyl thermomorphogenesis by ethylene is correlated with the reduction of the PM H^+-ATPase activity. These observations are also consistent with the thermal induction of the *SAUR19* gene (Figure 23), whose gene product acts as a negative regulator of the APD7 protein phosphatase.

To examine more directly whether the EIN3-mediated ethylene signals repress the proton pump activity, I performed media acidification assays using a pH indicator bromocresol purple, which is colored from yellow (<pH 5.2) to violet (>pH 6.8). Image color quantitation of the media area surrounding seedlings showed that ACC treatments detectably decrease the media acidification by Col-0 seedlings at 28^{o}C (Figure 27A and 27B), which represents a reduction of the PM H^+-ATPase proton pump activity. On the other hand, the media acidification was not discernibly altered by ACC treatments in the *ein3 eil1* mutant seedlings at 28^{o}C, which would be associated with the ACC-insensitive thermomorphogenic hypocotyl growth of the mutant (Figure 14A). Altogether, these observations

support the notion that EIN3 attenuates hypocotyl thermomorphogenesis by activating the expression of the APD7 protein phosphatase that inactivates the PM H^+-ATPase proton pumps during cell expansion. Media acidification assay systems having a better resolution than the bromocresol purple-based method will clarify the functional linkage between EIN3 and auxin response during hypocotyl thermomorphogenesis.

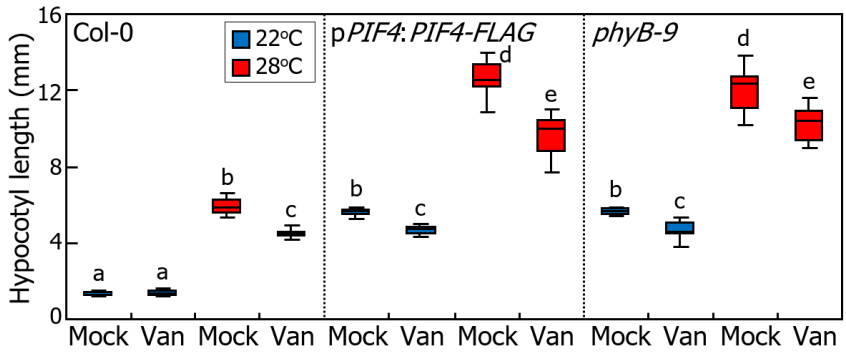

Figure 26. Effects of proton pump inhibitor on thermomorphogenic hypocotyl growth.

Seedling growth, warm temperature treatments, and statistical analysis were performed, as described in Figure 2. Vanadate (Van) was used at the final concentration of 100 μM. Different letters represent significant differences (P < 0.01) determined by one-way analysis of variance ANOVA with *post hoc* Tukey test.

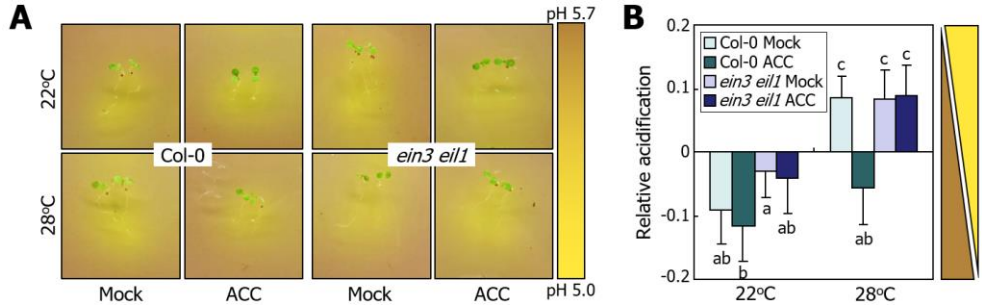

Figure 27. EIN3-mediated ethylene responses inhibit media acidification induced by warm temperature stimuli.

(A) Media acidification by *ein3 eil1* mutant seedlings. Seedlings grown on MS-agar plates for 4 d were transferred to fresh MS-agar plates containing a pH indicator bromocresol purple for 24 h before taking photographs.

(B) Quantitation of media acidification. In the images taken in (A), twenty points were randomly selected around the root tip regions, where media acidification was most prominent. Relative acidification indicates the relative position of each selected point compared to standard pH (pH 5.0 and 5.7). The detailed quantitation method is described in Materials and Methods section.

DISCUSSION

Recent molecular genetic and biochemical studies have established a network of thermomorphogenic signaling pathways that governs plant responses to warm ambient temperatures, in which the PIF4 master regulator of plant thermomorphogenesis and its downstream auxin signaling events have been extensively studied (Casal and Balasubramanian, 2019; Quint et al., 2017). Here, I identified a distinct, temperature-responsive ethylene signaling scheme that differentially regulates hypocotyl growth, depending on temperature conditions. At normal temperatures, the ethylene-activated EIN3 transcription factor moderately promotes hypocotyl elongation by inducing the transcription of *PIF3* gene. When PIF4 activity is greatly elevated at 28^{o}C, EIN3 activates the expression of *APD7* gene and thus counteracts the inhibitory effects of SAUR19 on APD7 activity that suppresses the function of the PM H^{+}-ATPase proton pumps. While these data strongly support that EIN3 attenuates hypocotyl thermomorphogenesis primarily by directly activating the *APD7* transcription, it is also possible that the EIN3-mediated ethylene signals affect the PIF4 function either at the transcriptional level or at the protein level. Alternatively, the moderate reduction of the transcription of *PIF4* and its target genes by ACC would be simply due to an as-yet unidentified feedback control by the suppression of hypocotyl thermomorphogenesis.

There is a growing impact on plant responses to warm temperatures in recent years because of its climatic association with global warming (Hatfield and Prueger, 2015). It is widely perceived that plant thermomorphogenic responses provide an adaptive strategy that facilitates heat dissipation from the plant body and evaporative leaf cooling, thus enhancing the chance of survival under

fluctuating climates (Gray et al., 1998; Franklin et al., 2011; Crawford et al., 2012). While such thermomorphogenic responses are essential for plant survival and optimal growth, exposure of plants to a prolonged period of warm temperatures would elicit hypocotyl overgrowth, potentially causing falling down of the plant body by itself or caused by external mechanical stimuli, such as wind and raindrop. Plants have evolved versatile adaptation mechanisms to deal with such physical problems imposed by stem overgrowth. It has been reported that a plant-specific RNA-binding protein FCA is activated at warm temperatures to attenuate thermomorphogenic hypocotyl growth by inhibiting the binding of PIF4 to *YUC8* promoter (Lee et al., 2014). It is envisioned that hypocotyl thermomorphogenesis should be tightly controlled, especially under fluctuating environments in a complex manner, to achieve optimal growth. These observations illustrate such an elaborate thermoadaptive mechanism in plants, in which the ethylene-activated EIN3 transcription factor fine-tunes hypocotyl thermomorphogenesis by attenuating auxin-induced cell expansion during hypocotyl thermomorphogenesis. Assuming that both FCA and EIN3 act as warm temperature signaling attenuators, it will be interesting to investigate whether they interact with each other physically or functionally during plant thermomorphogenesis.

It is interesting that while the EIN3 transcription factor promotes hypocotyl growth, regardless of temperatures, it suppresses hypocotyl growth by attenuating auxin response in the PIF4 thermomorphogenesis pathway. Accumulating evidence in recent years depict that hypocotyl thermomorphogenesis is not simply regulated by on-off switches that are operated by promotive or repressive signals. Instead, it is coordinately modulated by a complex network of extensive hormonal signaling crosstalks, including auxin, abscisic acid, and

ethylene. In particular, the auxin-ethylene signaling crosstalk during hypocotyl thermomorphogenesis is distinctive from others in that the EIN3-mediated ethylene signals do not directly target the central thermomorphogenesis regulator PIF4, unlike the FCA-mediated attenuation of PIF4 activity, but instead modulate auxin responses during cell elongation.

These data show that EIN3 provides a temperature-dependent, bifunctional control mechanism for hypocotyl growth: while it activates the transcription of *PIF3* gene to promote hypocotyl growth at normal temperatures, it activates the transcription of *APD7* gene to suppress hypocotyl growth at warm temperatures (Figure 28). It is known that the EIN3-activated PIF3 transcription factor promotes hypocotyl cell elongation by destabilizing the organization of cortical microtubules (Ma et al., 2018). On the other hand, the APD7-mediated suppression of cell expansion occurs through the inactivation of the PM H^+-ATPase proton pumps, which promote the progression of apoplastic acidification during hypocotyl cell elongation (Takahashi et al., 2012; Spartz et al., 2014). A dual mode of control for cellular and molecular activities is frequently observed in plant adaptation strategies to environmental and developmental cues, in which plants optimize an environmental adaptive capacity, while sustaining growth and performance (Grégory et al., 2003; Yoo et al., 2008).

A critical issue is as to the physiological relevance of the ethylene-mediated attenuation of thermomorphogenic hypocotyl growth in plants. While ethylene is known to regulate a variety of plant developmental activities, such as fruit ripening, flower opening, and leaf abscission (Ogawara et al., 2003; Liu et al., 2015; Botton and Ruperti, 2019), it is also considered to be a versatile combatant for environmental stresses, including high salinity, water deficit, wounding by

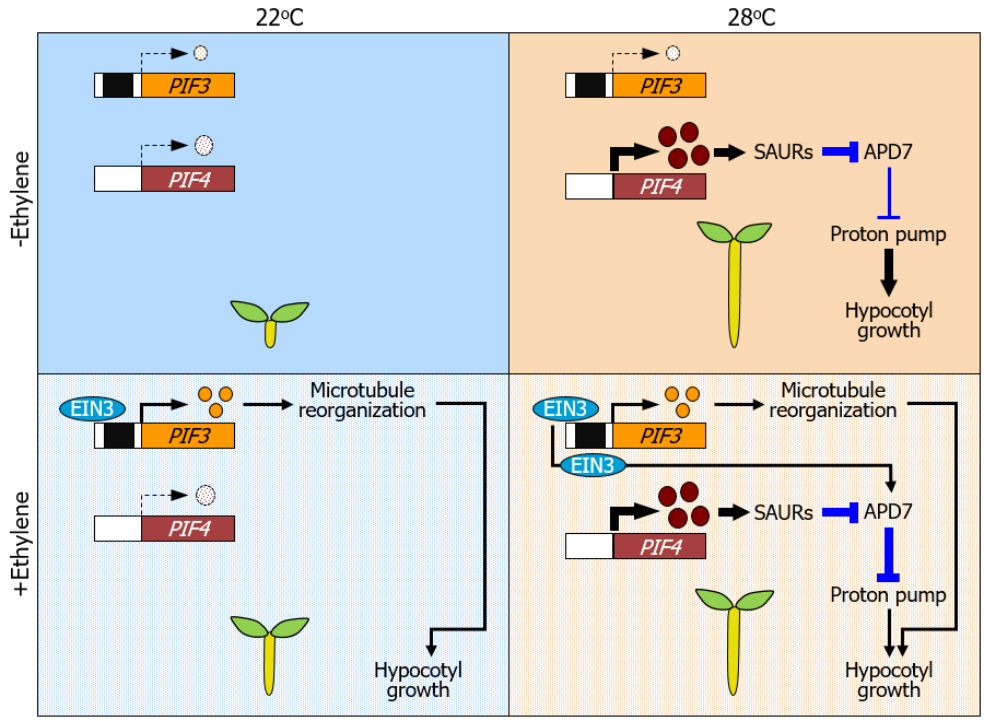

Figure 28. A molecular framework of the EIN3-mediated attenuation of hypocotyl thermomorphogenesis.

The ethylene-activated EIN3 transcription factor induces the expression of PIF3, which triggers microtubule reorganization, leading to a moderate promotion of hypocotyl growth (Zhong et al. 2014, Ma et al. 2018). Under warm temperatures, where PIF4 is highly activated, EIN3 induces the expression of APD7 but inhibits the expression of PIF4 in the hypocotyls, resulting in the attenuation of hypocotyl thermomorphogenesis. In this signaling scheme, APD7 acts as a molecular hub that integrates the EIN3-mediated ethylene signals and the PIF4-mediated auxin signals into hypocotyl thermomorphogenesis, which is likely to be driven by the apoplastic pH shift that underlies auxin-induced hypocotyl cell expansion. The EIN3-driven modulation of thermomorphogenic hypocotyl growth would help plants to precisely adapt to complex environmental stimuli. Black arrows indicate transcriptional controls, and blue arrows indicate phosphorylation-dependent

protein activity controls. The thickness of arrows represents the relative strength of each signaling step.

insects and animals, and mechanical disturbance by wind, touch, and submergence (Morgan and Drew, 1997). Notably, ethylene signaling is intimately associated with the early responses of plants to flooding (Sasidharan and Voesenek, 2015). It is possible that the ethylene-mediated attenuating system would contribute to plant adaptation to flooding stress, under which hypocotyl overgrowth is certainly a disadvantageous phenotype. The attenuation of hypocotyl growth would also help plants to sustain viability and biological activities under other stress conditions. It is well known that tolerance to abiotic stresses is a high energy-requiring process (Munns et al., 2020). Reduction of hypocotyl growth would be desired for the reallocation of metabolites and energy saving to establishing stress-tolerant physiological states. It is particularly interesting that EIN3 directly activates the expression of APD7 protein phosphatase, which belongs to the PP2C clade. It is known that plant PP2C enzymes function as key regulators of signal transduction pathways governing plant adaptation to developmental status and environmental stresses (Schweighofer et al., 2004). In natural environments, multiple climate factors, such as light and temperature, fluctuate in a complex manner. Various stressful conditions also frequently accompany the climate changes. The temperature-dependent antagonistic modes of ethylene actions on hypocotyl growth would contribute to optimizing thermomorphogenic hypocotyl growth, which will harmonize the reprogramming of metabolic allocation and the mechanical sustainability.

These findings elucidate a network of extensive signaling integrations among light, temperature, and ethylene signals, which culminate in the optimal reshaping of hypocotyl thermomorphogenesis. A previous study has shown that hypocotyl photomorphogenesis is regulated by ethylene (Zhong et al., 2012; Zhong

et al., 2014). Conversely, ethylene signaling is turned off by the phyB-mediated degradation of EIN3, thus terminating EIN3-mediated skotomorphogenesis (Shi et al., 2016). Meanwhile, it has been reported that root hair growth is promoted by both light and ethylene signals (De Simone et al., 2000; Feng et al., 2017). Similarly, the onset of flowering is regulated by both temperature and ethylene signals (Ogawara et al., 2003; Song et al., 2013). It will be worthy of investigating how ethylene signaling is integrated with multiple signaling events during these developmental processes.

ACKNOWLEDGMENTS

I thank Ohkmae K. Park for providing *ora59-1* mutant and transgenic plants overexpressing *ORA59*, Sang-Dong Yoo for providing *ein3 eil1* mutant, Shangwei Zhong for providing *phyB-9 ein3 eil1* mutant, Hyung-Taeg Cho for providing *DR5*:*GUS* transgenic plant, and Martin Van Rongen for providing *tir1-1 afb1-1 afb2-1 afb3-1* mutant.

CHAPTER 2

SMAX1 integrates karrikin and light signals into GA-mediated hypocotyl growth during seedling establishment

INTRODUCTION

Developing young seedlings actively monitor fluctuations in surrounding environments, such as daily and seasonal changes in light and temperature, to optimize their growth and morphogenesis. These morphogenic adaptation behaviors are particularly important for the acquisition of photosynthetic capacity, as they emerge from the soil layer. It has been well documented that morphogenic and physiological adaptation of young seedlings to light environments is coordinately regulated by an elaborate network of light and growth hormonal signaling pathways (Arsovski et al., 2012), among which the regulatory roles of auxin and GA have been most extensively studied through molecular genetic and global-scale gene expression approaches (Achard et al., 2007; Alabadí et al., 2008; Halliday et al., 2009; Cheminant et al., 2011).

Developing seedlings emerging from the soil undergo a number of morphological changes to achieve proper seedling establishment, such as suppression of hypocotyl growth, formation of true leaves, and development of photosynthetic apparatus (Chory et al., 1996; Symons et al., 2008). It is known that phytochrome-perceived light signaling cues are coordinated through growth hormonal signaling pathways, such as GA, brassinosteroid (BR), and cytokinin (CK), to optimize morphogenic development (Szekeres et al., 1996; Achard et al., 2007; Symons et al., 2008; Cortleven and Schmülling 2015). Upon exposure to light, the endogenous levels of bioactive GAs are decreased, leading to an accumulation of the GA signaling repressors DELLAs (Achard et al., 2007). While the DELLA members repress seedling growth, they facilitate the synthesis of chlorophylls and carotenoids in conjunction with light and BR signaling regulators

(Cheminant et al., 2011; Liu et al., 2017). CKs also contribute to seedling deetiolation by accelerating chlorophyll biosynthesis and development of chloroplasts (Cortleven and Schmülling 2015).

KARs, a small group of butenolide chemicals, have been identified from burning smokes of plant materials during wildfires (Flematti et al., 2004). They have been verified to be the chemical constituents of smoke waters that stimulate seed germination in a wide array of plants as well as fire-prone plants (Nelson et al., 2009). There are six major types of KAR compounds identified in *Arabidopsis*, among which KAR_2 is most effective on stimulating seed germination (Nelson et al., 2009). Accumulating evidence in recent years strongly support that KARs exhibit profound effects on an array of plant early developmental traits ranging from seed germination to seedling establishment, such as seedling growth, cotyledon expansion, and chlorophyll biosynthesis (Nelson et al., 2009; Nelson et al., 2010; Waters et al., 2014). It is widely perceived that the presence of KARs in nature informs seeds buried in the soil that there are open terrain circumstances and the probability of competition for optimal emergence is not high on the aboveground (Nelson et al., 2012).

KAR molecules are perceived by the α/β hydrolase receptor KARRIKIN-INSENSITIVE 2 (KAI2) and act through the F-box protein MORE AXILLARY GROWTH 2 (MAX2) (Nelson et al., 2011; Guo et al., 2013). The KAR-KAI2-MAX2 complexes then recruit the KAR signaling repressors SMAX1 and SMAX1-LIKE 2 (SMXL2) through direct interactions with the KAI2 receptor (Stanga et al., 2013; Khosla et al., 2020). Upon perception by the receptor-ligand complexes, the SMAX1 and SMXL2 proteins are degraded, promoting KAR-mediated responses, such as seed germination (Khosla et al., 2020; Figure 29).

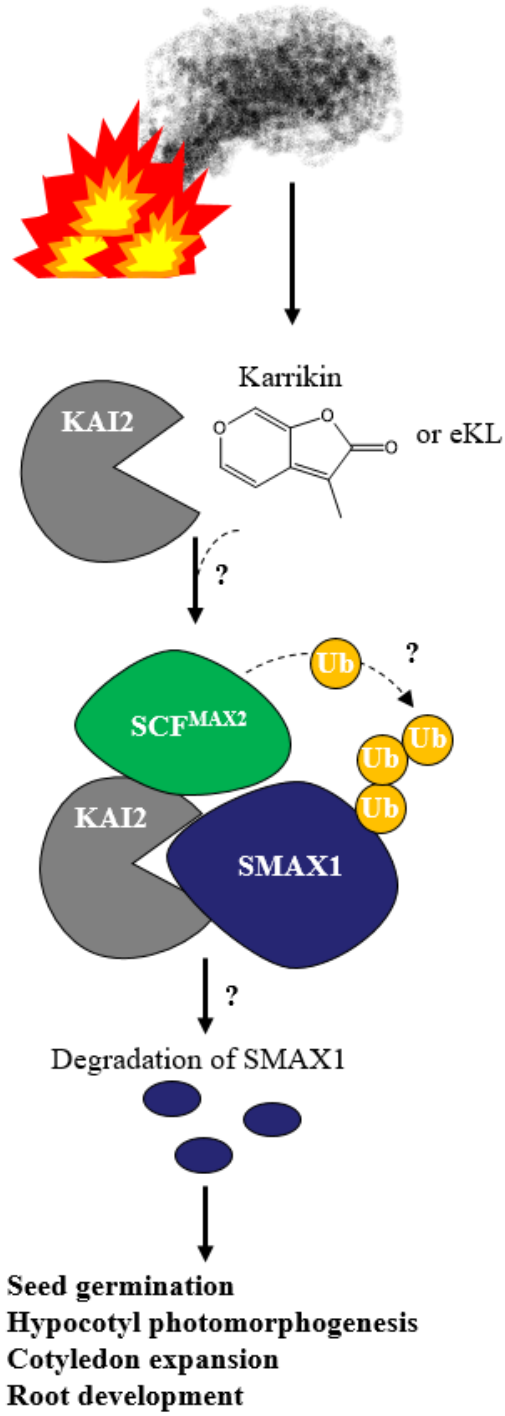

Figure 29. Overview of karrikin signaling pathway.

Karrikins (KARs) are synthesized from burning plant body, when a wildfire occurs. KARs or endogenous KAI2 ligands (KLs) are captured by their receptor protein KAI2, triggering KAR signaling. The ligand-bound KAI2 recruits a KAR signaling repressor SMAX1 and an F-box protein MAX2. The complex of KAI2-MAX2-SMAX1 promotes degradation of SMAX1, resulting in activation of KAR signaling and thus regulation of growth and developments. The image used in this figure referred to the schematic diagram in the previously published paper (Morffy et al., 2016).

On the other hand, previous studies have reported that the KAI2 signaling pathways play pleiotropic roles in early developmental stages, even when KARs are not present (Li et al., 2017; Villaécija-Aguilar et al., 2019; Shah et al., 2021). It seems that KARs share the endogenous KAI2 signaling pathways that are originally regulated by as-yet unidentified signaling compounds, which are termed endogenous KAI2 ligands (KLs; Figure 29). The molecular identity of KLs remains to be determined.

Notably, the KAR-mediated responses are influenced by light stimuli: KARs enhance light responses in plants, such as seed germination and hypocotyl photomorphogenesis (Nelson et al., 2009; Nelson et al., 2010). It has been reported that KAR_1 treatments markedly improve seed germination even under low light fluence conditions, under which seed germination is not prominent (Nelson et al., 2009; Nelson et al., 2010). In addition, it has been shown that a central light signaling regulator ELONGATED HYPOCOTYL 5 (HY5) acts as a downstream modulator of KAR signaling (Bursch et al., 2021). A recent study has demonstrated HY5 and its interacting partner B-BOX DOMAIN PROTEIN (BBX) transcription factor mediate KAR-responsive gene expression in promoting hypocotyl photomorphogenesis and anthocyanin biosynthesis (Bursch et al., 2021). It is anticipated that the KAR-light signaling interactions coordinate successful developmental adaptation of young seedlings to changing light environments during the developmental transition from seed germination to seedling establishment following soil emergence.

In addition to the signaling linkage of the KAI2 signaling responses with light signaling, they are also associated with growth hormone signaling events during plant growth and development and adaptive environmental fitness (Nelson

et al., 2009; Nelson et al., 2010; Wang et al., 2018). It is known that KAR-mediated promotion of seed germination requires GA biosynthesis, while there are no detectable increases of bioactive GA levels after KAR treatments (Nelson et al., 2009; Nelson et al., 2010). It is also proven that auxin is linked with KAR-mediated regulation of hypocotyl growth (Nelson et al., 2010). Notably, KAI2-mediated signals induce abscisic acid catabolism and its responses under drought stress (Li et al., 2017; Wang et al., 2018). Together, these reports suggest that coordinated signaling crosstalks between KAR and endogenous growth hormones contribute to successful seedling establishment under fluctuating environments, including occurrence of wildfires. However, molecular mechanisms underlying the intricate signaling interactions are not fully understood in most cases, in particular during seedling establishment.

In this work, I demonstrate that the negative regulator of KAR signaling, SMAX1, serves as a molecular hub that coordinately integrates KAR and light signals into GA/DELLA-mediated regulation of hypocotyl growth to optimize seedling establishment. Under light environments, light-stabilized DELLA proteins accelerate the seedling deetiolation process that contributes to plant photomorphogenesis (Achard et al., 2007). On the other hand, when KARs are detected in surrounding soil environments, as detected from wildfire smokes, the KAR signals trigger the degradation of SMAX1, which represses DELLA accumulation, thus further enhancing photomorphogenic hypocotyl growth. These observations indicate that the integration of light and KAR signals by SMAX1 into hypocotyl photomorphogenesis would guarantee the optimization of hypocotyl photomorphogenesis that ensures seedling establishment in natural environments.

MATERIALS AND METHODS

Plant materials

All *Arabidopsis thaliana* lines used were generated in Col-0 background. The *smax1-3* (SALK-097346), *max2-1* (CS9565), and *smxl2-1* (SAIL-596-E08) mutants were obtained from a pool of mutant lines deposited in the ABRC (Ohio State University, OH). The *kai2-1* mutant in Col-0 background, which has been produced by backcrossing the original one in Landsberg *erecta* background to Col-0 for multiple generations (Soundappan et al., 2015; Wang et al., 2018), was obtained from Ottoline Leyser and Mark Waters. The *smax1-3 smxl2-1* double mutant was generated by genetic cross between *smax1-3* and *smxl2-1* single mutants. The *rga-28 gai-t6* double mutant was obtained from Giltsu Choi. The *smax1-3 rga-28 gai-t6* triple mutant was generated by genetic cross between *smax1-3* single and *rga-28 gai-t6* double mutants. The p*RGA*:*GFP-RGA* transgenic plants, which overexpress a *GFP-RGA* gene fusion that has been previously described (Silverstone et al., 2001), were obtained from a seed stock deposited in the NASC (University of Nottingham, Sutton Bonington Campus, UK), and the transgenic plants were used to produce p*RGA*:*GFP-RGA smax1-3 smxl2-1* plants by genetic cross with *smax1-3 smxl2-1* double mutant.

To generate 35S:*FLAG-KAI2* transgenic plants, a full-size KAI2-coding cDNA was fused in-frame to the 3’ end of the FLAG-coding sequence in the pEarleyGate 202 vector, and the expression construct was transformed into Col-0 plants. To generate 35S:*MYC-MAX2* transgenic plants, a full-size MAX2-coding cDNA was fused in-frame to the 3’ end of the MYC-coding sequence in the MYC-pBA vector, and the expression construct was transformed into Col-0 plants. In

order to generate 35S:*SMAX1-GFP*, 35S:*SMAX1ΔN-GFP*, and 35S:*SMAX1ΔD2*-GFP transgenic plants in the *smax1-3* backgrounds, the full-size or truncated SMAX1-coding transgenes were overexpressed driven by the CaMV 35S promoter in the mutant. The truncated SMAX1-coding cDNAs used were those encoding SMAX1ΔN, which lacks the N-terminal residues 1-162, and SMAX1ΔD2, which lacks the C-terminal residues 604-990. They were fused in-frame to the 5' end of the GFP-coding sequence in the JJ461 vector.

To generate 35S:*MYC-RGA* transgenic plants, a full-size RGA-coding cDNA was fused in-frame to the 3' end of the MYC-coding sequence in the MYC-pBA vector, and the expression construct was transformed into Col-0 plants. The 35S:*MYC-RGA* 35S:*SMAX1-GFP* transgenic plants in the *smax1-3* mutant background is generated by genetic cross between 35S:*MYC-RGA* and 35S:*SMAX1-GFP smax1-3* transgenic plants. To generate 35S:*MYC-RGAΔ17* transgenic plants, a RGAΔ17-coding cDNA, which harbors a deletion of 51 base pairs in the DELLA motif of *RGA* gene (Dill et al., 2001), was fused in-frame to the 3' end of the MYC-coding sequence in the MYC-pBA vector, and the expression constructs were transformed into *kai2-1* and *max2-1* mutants.

Plant growth conditions

Arabidopsis seeds were sterilized in 70% ethanol prior to cold imbibition for 3 d and allowed to germinate on ½ X Murashige and Skoog agar (hereafter, referred to as MS-agar) plates with white light illumination (120 μmol $m^{-2}s^{-1}$) provided by fluorescent FLR40D/A tubes (Osram, Seoul, Korea) under short day (SD) conditions (8-h light and 16-h dark, respectively) at 22°C. For hypocotyl

phenotyping and preparation of total RNA and protein samples, seedlings were grown at 22°C for 7 d under SDs. For treatments with different light wavelengths, seedlings were grown on MS-agar plates with white light (50 μmol m^{-2} s^{-1}), red (40 μmol m^{-2} s^{-1}), far-red (15 μmol m^{-2} s^{-1}), or blue (35 μmol m^{-2} s^{-1}) light illumination. For hormone and chemical treatments, GA with a final concentrations of 1-50 μM (Sigma-Aldrich, St. Louis, MO; G7645), KAR_2 of 1 μM (Toronto Research Chemicals, North York, Canada; F864800), PIC of 2 μM (Sigma-Aldrich; P5575), ACC of 10 μM (Sigma-Aldrich; A3903), brassinolide (BL) of 100 nM (Sigma-Aldrich; B1439), and paclobutrazol (PAC) of 0.2 μM (Sigma-Aldrich; 46046) were included in growth media.

Gene expression assays

Trizol reagent-based RNA purification kit (Invitrogen, Carlsbad, CA) was used to extract total RNA samples from appropriate plant materials. Extracted RNA samples were subjected to primary cDNA synthesis, as described previously (Park et al., 2017). Using the primary cDNA samples, RT-qPCR was performed to measure relative transcript levels. PCR runs were carried out in 384-well blocks with the QuantStudio 6 Flex thermal cycler (Applied Biosystems, Waltham, MA) using the SYBR Green I master mix (KAPA Biosystems, Wilmington, MA) in a volume of 10 μl. The PCR primers used were listed in Table 2. The *Arabidopsis eIF4A* gene was used as internal control in individual PCR reactions to normalize the variations in the amounts of primary cDNA samples used.

Yeast two-hybrid assays

Primers	Sequences	Usage
eIF4A-F	5′-TGACCACACAGTCTCTGCAA	RT-qPCR
eIF4A-R	5′-ACCAGGGAGACTTGTTGGAC	"
GA3ox1-F	5′-GGGTTAACCAAACCAGAGCC	"
GA3ox1-R	5′-CGATTCAACGGGACTAACCA	"
GA3ox2-F	5′-GGAGCGTTCCAGATCACCAA	"
GA3ox2-R	5′-TACGGGAAGCCGGAAAAGAC	"
GA2ox2-F	5′-GGTTGCCGAAGAACTAGGGA	"
GA2ox2-R	5′-CCGCCGGATAATGGTTTAGT	"
RGA-F	5′-CTCGCGACGGATACTGTTCA	"
RGA-R	5′-TAGAACTCGCCGGAAGAGGA	"
GAI-F	5′-TGGCTTGTGATGGACCTGAC	"
GAI-R	5′-AATATGTGCAGCCGCAAACC	"
RGL1-F	5′-CGCGCTATTAGCTTGTGCTG	"
RGL1-R	5′-GCTTGAGAGGACGCGAGTAA	"
RGL2-F	5′-GCCGCTGAGAGTTTATCGGA	"
RGL2-R	5′-CGGTGGAGCTCAAATACCGA	"
RGL3-F	5′-GTTAGACTCGTTCAGGCGCT	"
RGL3-R	5′-TGAGAAGCCGCGAGTAATCC	"
KAI2-F	5′-AGCTCACAACGTGAAGGTGA	"
KAI2-R	5′-GTACCGGCTCCCATGTTGTC	"
MAX2-F	5′-CCCTACCGGTGGCGATTTT	"
MAX2-R	5′-TCTAACCGTGTAAGCCTCGC	"
SMAX1-F	5′-CGGGTCGGGTTATTCGTGAG	"
SMAX1-R	5′-GGGTCTGAAGCAACCCATCT	"

Table 2. Primers used in Chapter 2.

The PCR primers were designed along with the NCBI Primer-BLAST software (https://www.ncbi.nlm.nih.gov/tools/primer-blast/) in a way that the calculated melting temperatures of

the primers are in a range of 50 - 65^{o}C. F denotes forward primer. R denotes reverse primer.

The BD Matchmaker system (Takara, Shiga, Japan) was used for screening protein-protein interactions in yeast cells. For the GAL4 activation domain, pGADT7 vector was used. A set of cDNAs encoding RGA, GAI, RGL1, RGL2, RGL3, GID1A, GID1B, GID1C, SLY1, or COP1 was subcloned into the vector. For the GAL4 DNA-binding domain, pGBKT7 vector was used. A set of cDNAs encoding SMAX1 and SMXL2 was subcloned into the vector. The yeast strain AH109 (Leu-, Trp-, Ade-, His-) was transformed with the vector constructs according to the manufacturer's instruction. Selection of transformed colonies was performed by restreaking colonies on a selective medium lacking Leu, Trp, Ade, and His.

Coimmunoprecipitation assays

I employed the fast *Agrobacterium*-based seedling transformation method (Li et al., 2009), in which the *SMAX1* gene was transiently expressed in *Arabidopsis* seedlings with a few modifications. The full-size SMAX1-coding cDNA was subcloned into the JJ461 vector, and the vector construct transformed into *Agrobacterium tumefaciens* cells. The *Agrobacterium* cells harboring the *SMAX1* expression vector were used for the transformation of ten-day-old 35S:*MYC-RGA* transgenic seedling. The resultant seedlings were incubated for 36-40 h before harvesting whole seedling materials. The *Agrobacterium* cells harboring the empty JJ461 vector were also coincubated with the 35S:*MYC-RGA* transgenic seedlings for control reactions.

The seedling samples were ground in liquid nitrogen and resuspended in 30 ml of nuclear extraction buffer (1.7 M sucrose, 10 mM Tris-Cl pH 7.5, 2 mM $MgCl_2$, 0.15% Triton-X-100, 5 mM β-mercaptoethanol, 0.1 mM PMSF, and a mixture of protease inhibitors). The suspensions were centrifuged at 4,300 X g for

20 min at 4°C. The sucrose cushion method was performed to obtain nuclear fractions from the precipitants. The nuclear fractions were resuspended in co-IP buffer (1 mM EDTA, 10% glycerol, 75 mM NaCl, 0.1M Tris-Cl pH 7.5, 0.1% Triton X-100, and the mixture of protease inhibitors) and sonicated. The sonicated nuclear extracts were used for input control. The rest of the sonicated nuclear extracts were incubated with 7 μg of an anti-GFP antibody (Roche, Basel, CH; 11814460001) for 8 h at 4°C. The protein-antibody complexes were harvested using protein-G magnetic beads (Bio-Rad, Hercules, CA; 161-4023) for 3 h at 4°C. The beads were washed 4 times with fresh co-IP buffer, and an equal volume of 2X SDS-PAGE loading buffer (100 mM Tris-Cl pH 6.8, 4% sodium dodecyl sulfate, 20% glycerol, 1.4% β-mercaptoethanol, tiny amount of bromophenol blue dye) was added to the beads. The mixture was then heated for 5 min at 90°C. The amount of total coimmunoprecipitated samples was calibrated by western blotting analysis. To detect SMAX1-GFP protein complexes in the input and IP samples, I used an anti-GFP antibody (Santa Cruz, Dallas, TX; sc-8334). An anti-MYC antibody (Merck Millipore, Burlington, MA; 05-724MG) was used for the detection of MYC-RGA protein complexes.

Immunological analysis

Plant materials were ground in liquid nitrogen. An equal volume of 2X SDS-PAGE loading buffer was added into the powder. The sample mixture was heated for 10 min at 90°C and centrifuged at 16,000 X g for 5 min, and the supernatant was run on a 12% SDS-polyacrylamide gel. The proteins were blotted onto Immobilon-P PVDF membrane (Merck Millipore; IPVH00010) using a wet transfer system (Bio-Rad; 1703930).

Anti-GFP (Roche; 11814460001), anti-MYC (Merck Millipore; 05-724MG), anti-FLAG (Merck Millipore; F7425), and anti-H3 (Abcam, Cambridge, UK; Ab1791) antibodies were used for the primary detection of target proteins, such as SMAX1-GFP and GFP-RGA, MYC-MAX2, FLAG-KAI2, and H3 proteins, respectively. An anti-mouse IgG-peroxidase antibody (Merck Millipore; AP124P) was employed as the secondary antibody to capture the anti-GFP and anti-MYC primary antibodies. An anti-rabbit IgG-peroxidase antibody (Merck Millipore; AP132P) was used as the secondary antibody to capture the anti-FLAG and anti-H3 primary antibodies.

It has been previously reported that immunodetection of SMAX1 proteins is not efficient, perhaps due to a high turnover rate of the SMAX1 proteins (Khosla et al., 2020). To improve the detection efficiency of SMAX1-GFP proteins, I extended the incubation time with the primary anti-GFP antibody. Following a blocking step with 5% skim milk in TBST solution (0.2 mM Tris-base pH 7.5, 1.3 mM NaCl, 0.1% tween-20) for a relatively short period of 10 min, an anti-GFP antibody (diluted at a ratio of 1:1000 in TBST solution containing 5% skim milk) was added to the solution for at least 12 h. The membrane was washed 4 times with fresh TBST solution, each for 10 min. An anti-mouse (diluted at a ration of 1:5000 in TBST solution containing 5% skim milk) was added to the membrane-floating solution for 3 h. The membrane was washed thoroughly with fresh TBST solution. The SuperSignal™ West Femto Maximum Sensitivity Substrate (Thermo Scientific, Waltham, MA; 34096) was used as an enhanced chemiluminescent substrate.

Confocal microscopy

Optical and fluorescent images were obtained using confocal microscopy (Carl

Zeiss, Oberkochen, Baden-Württemberg; LSM710). The excitation laser had a wavelength of 488 nm, and the emission at a wavelength of 505-530 nm was used for the detection of GFP signals. All hypocotyl images were taken in the specific regions that were right above the hypocotyl-root junctions. The obtained confocal images were analyzed using the ZEN software (https://www.zeiss.com/microscopy/int/products/microscope-software/zen.html).

Endogenous production of GFP-RGA protein fusions in the p*RGA*:*GFP-RGA* transgenic seedlings was confirmed by an enhancement of fluorescence signals in the hypocotyls of PAC-treated seedlings. Seven-day-old p*RGA*:*GFP-RGA* transgenic seedlings grown on MS-agar plates at 22^{o}C under SDs were used for the detection of RGA fluorescence images from the hypocotyl cells at ZT1. To analyze alterations in the fluorescence signals of RGA proteins during the dark-to-light transitions, four-day-old dark-grown seedlings, which were allowed to germinate on MS-agar plates in the light for 6 h, were exposed to light for 1 h before taking fluorescence images. For KAR_2 treatments, a final concentration of 1 μM was included in the growth media.

Quantitation and statistical analysis

All statistical analysis were performed using the SPSS software. The two-sided Student *t*-test with *P* values of < 0.05 was employed for the determination of statistical significance between two means. The one-way analysis of variance ANOVA with *post hoc* Tukey tests ($P < 0.01$) was used for the determination of statistical significance among more than two groups.

RESULTS

GA attenuates KAR-induced suppression of hypocotyl growth

Recent studies have shown that KAR responses are intimately linked with light and hormone signaling events during plant growth and developmental processes (Nelson et al., 2009; Nelson et al., 2010; Waters et al., 2014; Wang et al., 2018). In particular, it is known that KARs play a role in hypocotyl photomorphogenesis through signaling crosstalks with light and growth hormones (Nelson et al., 2009; Nelson et al., 2010). Several growth hormones, such as auxin, GA, and brassinosteroids, are involved in hypocotyl photomorphogenesis (Szekeres et al., 1996; Achard et al., 2007; Symons et al., 2008). However, it is unexplored at the molecular level how specific growth hormones modulate the KAR-mediated hypocotyl photomorphogenesis.

On the basis of the known suppressive effects of KARs on hypocotyl growth (Nelson et al., 2010), I examined which growth hormones recover the KAR-mediated reduction of hypocotyl growth under SDs. I employed the *smax1-3* mutant that exhibits short hypocotyls due to constitutive KAR responses (Stanga et al., 2013). Treatments of the mutant seedlings with growth hormones or their precursors, such as synthetic auxin PIC, ACC, GA, and brassinolide, rescued the short hypocotyl phenotype of the mutant to variable degrees, among the chemicals tested, GA was the most effective on the recovery of hypocotyl elongation (Figure 30A). Treatments of the mutant seedlings with varying concentrations of GA revealed that the recovery of hypocotyl growth exhibited a saturated effect at 10 μM or higher (Figure 30B). To confirm the results, Col-0 seedlings were treated with varying concentrations of GA in the presence of KAR_2. Similar to what

observed with *smax1-3* mutant seedlings, I found that the repressive effects of KAR_2 on hypocotyl growth was markedly attenuated by exogenous application of GA (Figure 31). These observations suggest that GA plays a major role in the KAR-mediated repression of hypocotyl growth.

To further examine the functional linkage between GA and KAR signal transduction during hypocotyl growth, I examined the effects of PAC, a potent GA biosynthesis inhibitor, on the hypocotyl growth of KAR signaling mutants. Under SD conditions, while the *smax1-3* mutant exhibited shorter hypocotyls, the *kai2-1* and *max2-1* mutants exhibited elongated hypocotyls compared to those of Col-0 seedlings (Figure 32A). It was found that while the short hypocotyl phenotype of the *smax1-3* seedlings was further shortened in the presence of PAC, the elongated hypocotyls of the *kai2-1* and *max2-1* seedlings were significantly shortened, comparable to those of Col-0 seedlings, under identical assay conditions (Figure 32A). In addition, while hypocotyls were elongated by more than 2-fold in SMAX1-overexpressing transgenic plants, the hypocotyl phenotype was largely compromised in the presence of PAC (Figure 32B). Together, these data indicate that the KAR-mediated repression of hypocotyl growth is functionally associated with GA.

GA-DELLA module mediates the function of KARs during hypocotyl growth

It is known that KAR signals promote seed germination at least in part by inducing the transcription of GA biosynthetic genes, which has been proven to be linked with the promotion of seed germination (Nelson et al., 2009; Nelson et al., 2010). I therefore asked whether the transcriptional control of GA biosynthetic genes is also related with the KAR-mediated repression of hypocotyl growth. I found that the

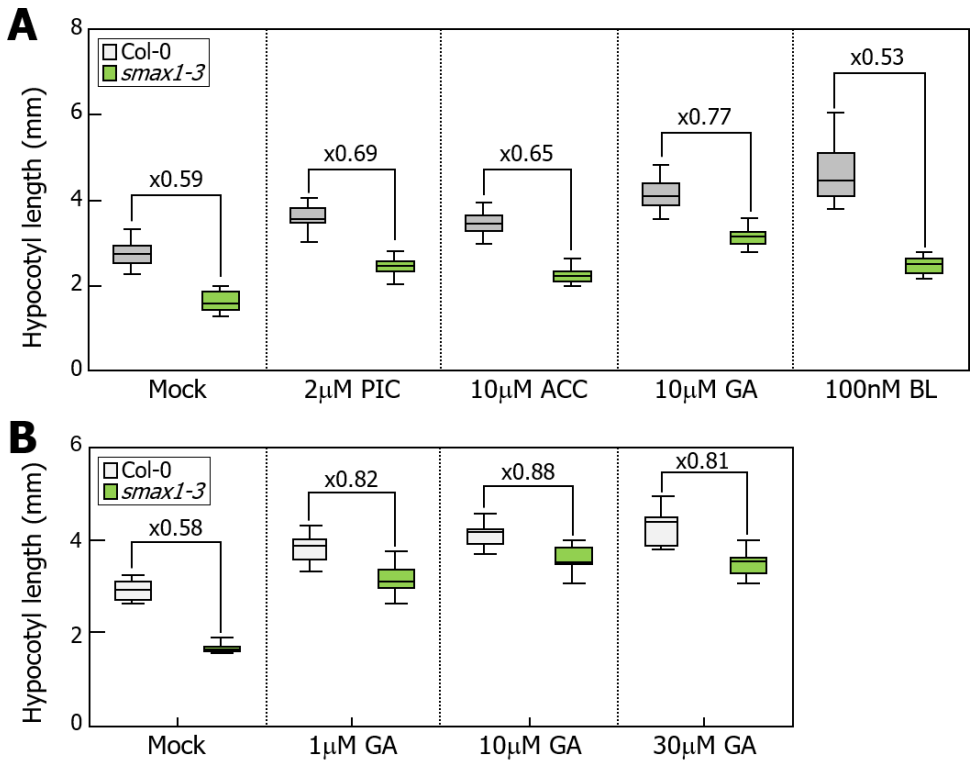

Figure 30. Effects of growth regulators on the hypocotyl growth of *smax1-3* seedlings.

Seedlings were grown on MS-agar plates at 22^{o}C for 5 d under short days (SDs, 8-h light and 16-h dark). Three independent measurements, each consisting of 15 seedlings, were statistically analyzed. PIC, picloram. ACC, 1-aminocyclopropane-1-carboxylate. GA, gibberellic acid. BL, brassinolide. Chemicals were used at the indicated concentrations. Numbers indicate the ratios of hypocotyl lengths relative to those of Col-0 seedlings.

(A) Effects of growth regulators on the hypocotyl growth of *smax1-3* mutant seedlings.

(B) Effects of varying concentrations of GA on the hypocotyl growth of *smax1-3* mutant seedlings.

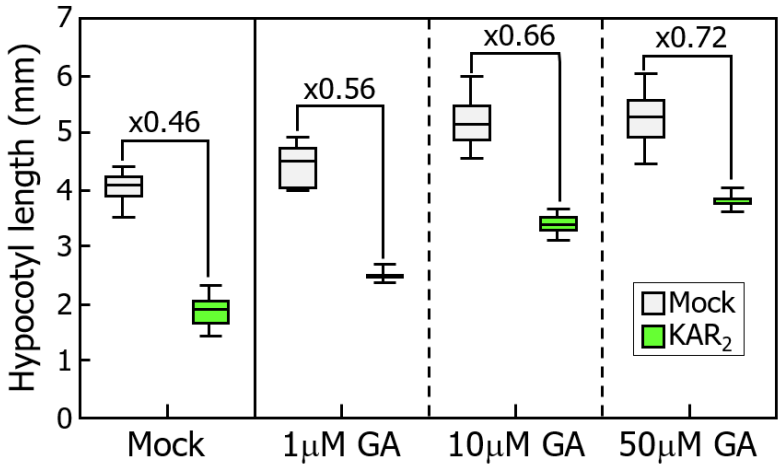

Figure 31. GA treatments counteract suppressive effects of KAR on hypocotyl growth.

Arabidopsis seedlings were grown on MS-agar plates at 22°C for 5 d under short days (SDs; 8-h light and 16-h dark). Three independent measurements, each consisting of 15 seedlings, were statistically analyzed. Karrikin 2 (KAR_2) was used at the final concentration of 1 μM. GA was used at the concentrations specified in each assay. Effects of GA on the hypocotyl growth of KAR_2-treated Col-0 seedlings. Seedlings were grown in the presence of 1 μM KAR_2 and varying concentrations of GA. Numbers indicate the ratios of hypocotyl length relative to no KAR_2 treatments.

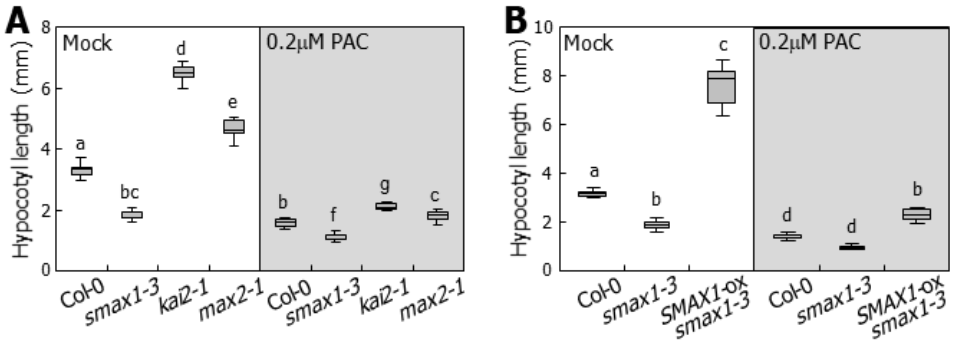

Figure 32. Application of PAC, an inhibitor of GA biosynthesis, decreased hypocotyl growth triggered by weakening of KAR/KAI2 signaling.

Arabidopsis seedlings were grown on MS-agar plates at 22°C for 5 d under short days (SDs; 8-h light and 16-h dark). Three independent measurements, each consisting of 15 seedlings, were statistically analyzed. Paclobutrazol (PAC) was used at the concentrations specified in each assay. Different letters represent significant differences ($P < 0.01$) determined by one-way analysis of variance ANOVA with *post hoc* Tukey test.

(A) Effects of PAC on the hypocotyl growth of KAR signaling mutants. SMAX1-, KAI2-, or MAX2-deficient seedlings were treated with 0.2 μM PAC.

(B) Effects of PAC on the hypocotyl growth of 35S:*SMAX1-GFP* transgenic plants. PAC treatments and seedling growth assays were performed, as described in (A).

transcription of genes encoding GA biosynthetic enzymes, such as GIBBERELLIN 3-OXIDASE 1 (GA3ox1) and GA3ox2, or that encoding a GA metabolic enzyme, GA2ox2, was not discernibly altered in the *smax1-3* and *smxl2-1* single mutants and the *smax1-3 smxl2-1* double mutant (Figure 33). The gene expression data suggest that GA biosynthesis and metabolism is not linked with the KAR-responsive hypocotyl growth.

A set of DELLA proteins plays a central role in GA signaling pathways by acting as signaling repressors, and they are degraded in response to GA stimulation (Dill et al., 2001). I examined the possibility that the GA signaling repressors DELLAs are involved in the KAR-mediated function during hypocotyl growth. It is known that among the five DELLA members, such as RGA, GAI, RGA-LIKE 1 (RGL1), RGL2, and RGL3, RGA and GAI play a major role in hypocotyl growth (Tyler et al., 2004; Penfield et al., 2006). I found that overexpression of the *RGAΔ17* transgene, a GA-resistant RGA form, attenuated the elongated hypocotyl growth of *kai2-1* and *max2-1* mutant seedlings (Figure 34A and 34B). In addition, while *RGA* overexpression barely affected hypocotyl growth in Col-0 background, it repressed the positive effects of *SMAX1* overexpression on hypocotyl growth to a degree comparable to that in Col-0 seedlings (Figure 34C). Furthermore, in accordance with the suppressive effects of *RGA* overexpression on hypocotyl growth, the short hypocotyl phenotypes of *smax1-3* mutant seedlings were somewhat rescued in the *rga-28 gai-t6* mutant background (Figure 35). In combination, these observations indicate that GA-DELLA pathways is linked with the KAR-regulated hypocotyl growth.

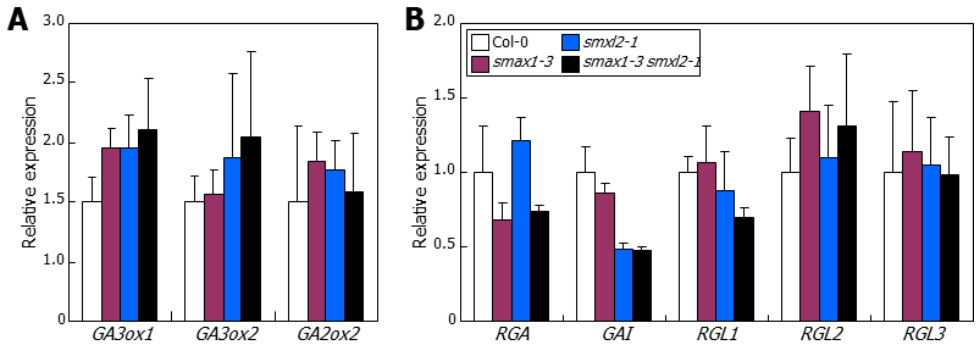

Figure 33. Transcription of GA-associated genes in SMAX1-deficient mutants.

Seedlings were grown on MS-agar plates at 22°C for 5 d under SDs. Whole seedlings were harvested for total RNA extraction. Transcript levels were analyzed by RT-qPCR. Biological triplicates, each consisting of 40 seedlings, were statistically analyzed (*t*-test, **P* < 0.05, difference from Col-0). Error bars indicate SE.

(A) Relative transcript levels of GA biosynthetic genes.

(B) Relative transcript levels of GA signaling genes.

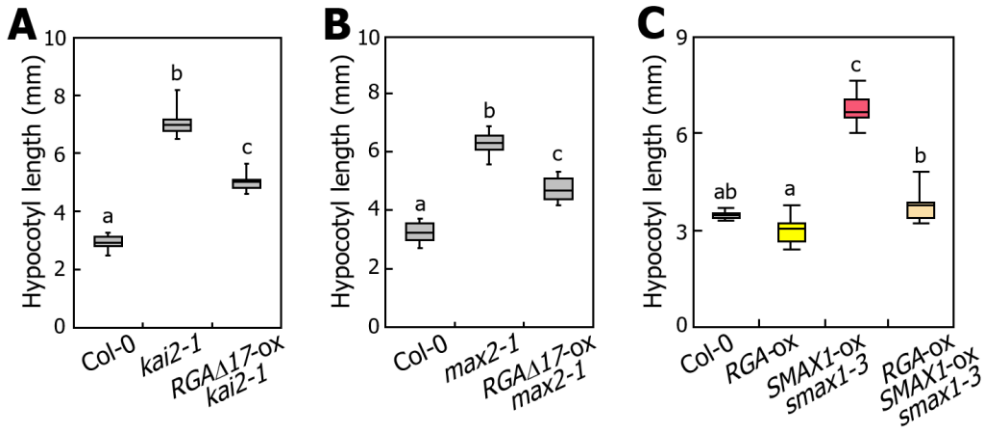

Figure 34. Overexpression of *RGA* transgene suppressed KAR-regulated seedling growth.

Seedlings were grown, as described in Figure 31. Three independent measurements, each consisting of 15 seedlings, were statistically analyzed. Different letters represent significant differences ($P < 0.01$) determined by one-way analysis of variance ANOVA with *post hoc* Tukey test.

(A and B) Hypocotyl growth phenotypes of 35S:*MYC-RGAΔ17* transgenic plants in *kai2-1* (A) and *max2-1* (B) backgrounds. The *RGAΔ17* gene sequence, encoding a GA-resistant RGA version (Dill et al., 2001), was in-frame fused to the 3' end of the MYC-coding gene sequence, and the gene fusion was overexpressed driven by the CaMV 35S promoter.

(C) Hypocotyl growth phenotypes of transgenic plants overexpressing SMAX1 and RGA. The 35S:*MYC-RGA* transgenic plants were crossed with the 35S:*SMAX1-GFP* transgenic plants in *smax1-3* mutant.

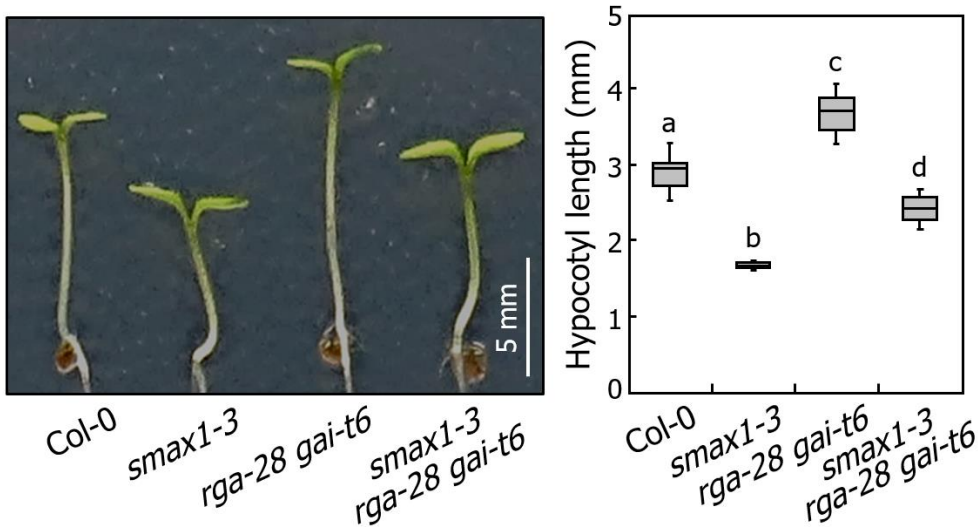

Figure 35. KAR-regulated seedling growth is functionally associated with GA-DELLA pathways.

Seedling growth was performed, as described in Figure 31. Three independent measurements, each consisting of 15 seedlings, were statistically analyzed. Different letters represent significant differences ($P < 0.01$) determined by one-way analysis of variance ANOVA with *post hoc* Tukey test. Hypocotyl growth phenotypes of a *smax1-3 rga-28 gai-t6* triple mutant. The *smax1-3* mutant was crossed with the *rga-28 gai-t6* double mutant. Representative five-day-old seedlings were photographed (left panel), statistical analysis were performed, as described above (right panel).

Interaction of SMAX1 with DELLAs is important for hypocotyl growth

A next question was how KAR signals affect the GA signaling processes in hypocotyl growth. It is known that the DELLA function is modulated mostly at the protein levels (Dill et al., 2001). Gene expression analysis revealed that the transcription of *DELLA* genes is not detectably altered in *smax1-3*, *smxl2-1*, and *smax1-3 smxl2-1* mutant seedlings (Figure 33), supporting that DELLA functions are not modulated at the gene transcriptional levels.

I then examined whether SMAX1 directly interacts with DELLA proteins. Interestingly, yeast coexpression assays revealed that SMAX1 interacts with four DELLA members, such as RGA, GAI, RGL1, and RGL3 (Figure 36A). It is notable that SMAX1 does not interact with RGL2, which is known to play a major role in seed germination (Lee et al., 2002), while other DELLA members are involved mostly in hypocotyl growth and development (Tyler et al., 2004; Penfield et al., 2006). The SMAX1-DELLA interactions were further verified by coimmunoprecipitation (coIP) assays using a MYC-RGA fusion (Figure 36B). Protein structural analysis shows that SMXL2 is the closest homologue of SMAX1 (Stanga et al., 2013). Like SMAX1, the SMXL2 protein also interacted with DELLA proteins in a similar manner (Figure 37). These observations support the notion that the KAR signaling repressors SMAX1 and SMXL2 regulate DELLA function at the protein levels during hypocotyl growth.

The SMAX1 protein consists of 5 major protein domains (Figure 38A), and putative roles of individual domains have been recently explored (Khosla et al., 2020). Among the N-terminal Double Clp-N motif (N), putative ATPase domain 1 (D1), middle region (M), and the C-terminal putative ATPase domains 2a (D2a) and D2b domains (Khosla et al., 2020), the D1 and M domains

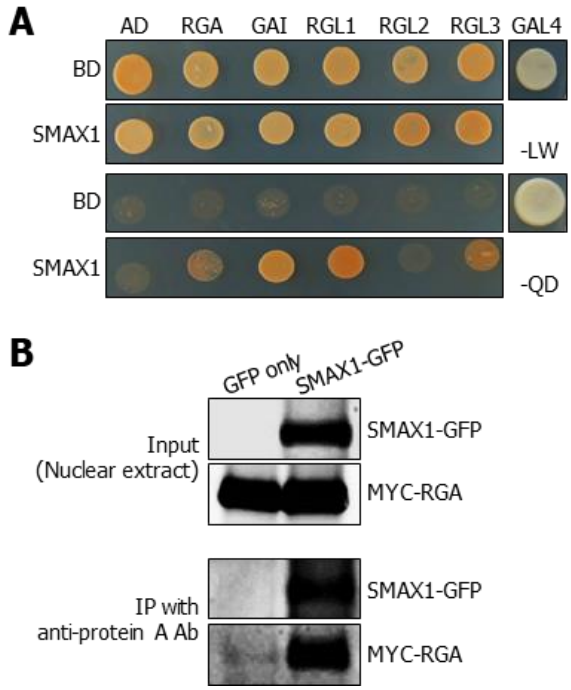

Figure 36. SMAX1 interacts with DELLA proteins.

(A) Interactions of SMAX1 with DELLA proteins in yeast cells. An exception is RGL2 that does not interacts with SMAX1 in these assay conditions. The (-LW) indicates Leu and Trp dropout plates. The (-QD) indicates Leu, Trp, His, and Ade dropout plates. AD and BD, activation domain and DNA-binding domain, respectively.

(B) Coimmunoprecipitation (CoIP) analysis on SMAX1-RGA interactions. Ten-day-old 35S:*MYC-RGA* transgenic seedlings grown at 22^{o}C under SDs were cocultured with *Agrobacterium* cells harboring either 35S:*GFP* or 35S:*SMAX1-GFP* expression vector for 36 h before harvesting whole seedlings for total protein extraction. The SMAX1 and RGA proteins were immunodetected using anti-GFP and anti-MYC antibodies, respectively.

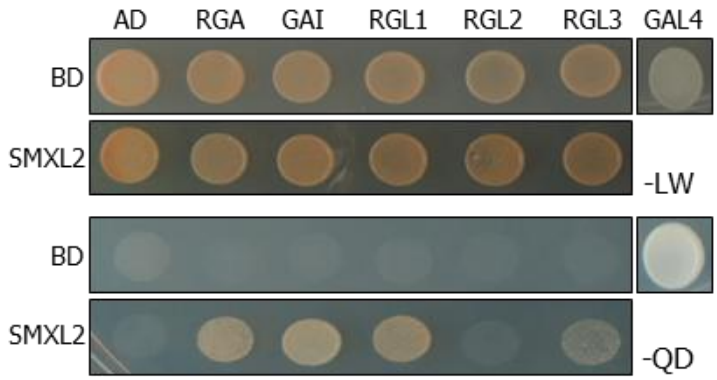

Figure 37. SMXL2 interacts with DELLA proteins.

Interactions of SMXL2 with DELLA proteins were examined by yeast two-hybrid screening. The (-LW) marks Leu and Trp dropout plates. The (-QD) marks Leu, Trp, His, and Ade dropout plates.

are important for the interaction of SMAX1 with KAI2 receptor. The D2a domain harbors a RGKT motif, which makes the SMAX1 proteins sensitive to KAR-mediated protein degradation, and a nuclear localization signal (NLS). The D2b domain enables SMAX1 and SMXL proteins to form higher order protein complexes (Khosla et al., 2020). The N domain, which has a putative Clp-N motif, has not been functionally determined yet.

To explore clues as to the potential roles of individual SMAX1 domains in the SMAX1-mediated regulation of DELLA function, I produced a set of genes encoding truncated SMAX1 forms, such as the N domain-deleted SMAX1ΔN form and the D2 domain-deleted SMAX1ΔD2 form (Figure 38A). Yeast coexpression assays revealed that while the SMAX1ΔN form did not interact with DELLA proteins, the SMAX1ΔD2 form interacted with DELLA proteins, like the full-size SMAX1 protein (Figure 38B), indicating that the N domain is important for the interaction of SMAX1 with DELLA proteins. On the other hand, overexpression of SMAX1ΔN or SMAX1ΔD2 did not complement the short hypocotyl phenotypes of *smax1-3* mutant (Figure 38C). It is known that both DELLAs and SMAX1 are localized in the nucleus (Silverstone et al., 1998; Khosla et al., 2020). The SMAX1ΔD2 form lacks NLS and thus is expected to be excluded from the nucleus. Together with the previous reports, these observations indicate that the SMAX1-DELLA interactions in the nucleus is essential for the SMAX1-regulated hypocotyl growth.

SMAX1 represses the nuclear accumulation of RGA in hypocotyl cells

A critical question was how SMAX1 regulates the DELLA functions. Western blot

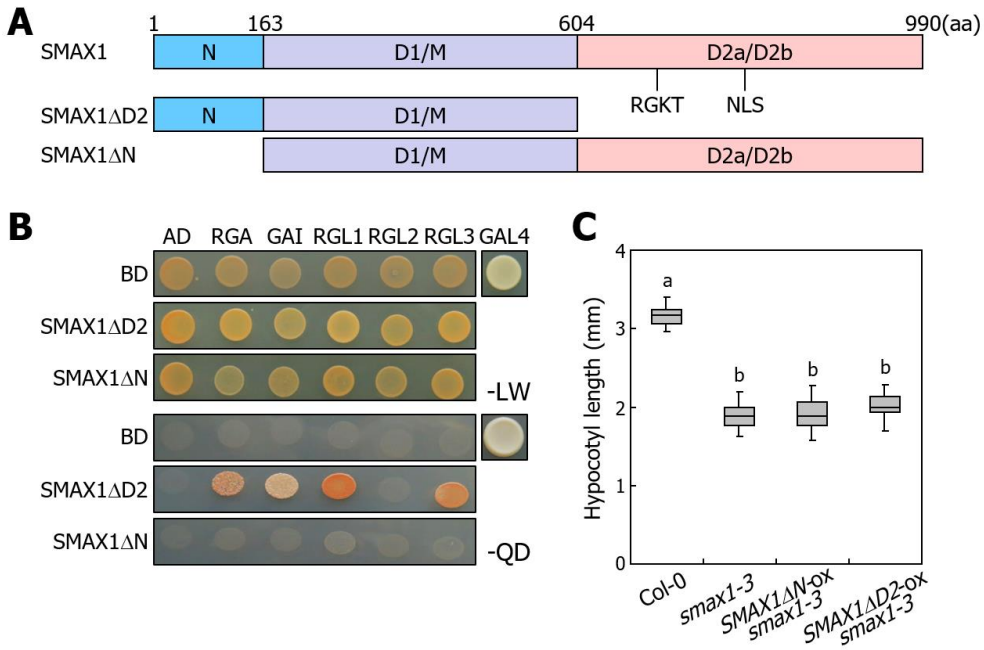

Figure 38. Interactions of SMAX1 proteins with DELLAs.

(A) SMAX1 protein constructs. Numbers indicate amino acid residue positions in the truncated SMAX1 proteins. The RGKT motif mediates the KAR-mediated degradation of SMAX1. NLS, nuclear localization signal.

(B) Interactions of SMAX1 proteins with DELLAs in yeast cells. The (-LW) indicates Leu and Trp dropout plates. The (-QD) indicates Leu, Trp, His, and Ade dropout plates. AD and BD, activation domain and DNA-binding domain, respectively.

(C) Hypocotyl growth phenotypes of transgenic plants expressing individual SMAX1 forms. The 35S:*SMAX1ΔN-GFP* and 35S:*SMAX1ΔD2-GFP* transgenic seedlings in *smax1-3* background were grown on MS-agar plates at 22^{o}C for 5 d under SDs. Different letters represent significant differences ($P < 0.01$) determined by one-way analysis of variance ANOVA with *post hoc* Tukey test.

analysis showed that RGA proteins accumulate to a higher level in *smax1-3 smxl2-1* mutant seedlings compared to that in Col-0 seedlings (Figure 39). To directly examine the effects of KARs on RGA accumulation, p*RGA*:*GFP-RGA* transgenic seedlings expressing a *GFP-RGA* gene fusion driven by an endogenous *RGA* promoter were subjected to confocal fluorescence microscopy. When PAC was included in the growth media, GFP-RGA signals were markedly elevated both in Col-0 wild-type and *smax1-3 smxl2-1* mutant seedlings (Figure 40), as has been reported previously (Silverstone et al., 2001).

I next examined the effects of KAR_2 on the intensity of fluorescent signals. It was observed that GFP-RGA signals were markedly enhanced in the hypocotyl cells, particularly in the nuclei, of the transgenic seedlings in the presence of KAR_2 (Figure 41A and 41B), which is consistent with the elevation of GFP-RGA protein levels in the *smax1-3 smxl2-1* mutant background (Figure 39). Similarly, as readily inferred from the negative effects of KARs on SMAX1 protein stability, GFP-RGA signals were significantly elevated in the *smax1-3 smxl2-1* mutant background (Figure 42A and 42B). These observations indicate that SMAX1 suppresses the nuclear accumulation of DELLA proteins in conjunction with GA signals.

SMAX1 proteins accumulate in the light

Considering that KARs are relatively rare chemicals in natural environments, it is unclear how the KAR-SMAX1 pathway is physiologically interconnected with the GA-DELLA pathway during hypocotyl photomorphogenesis. It is known that KAR signaling is closely associated with light signaling in various plant developmental and morphogenic adaptation processes, covering from seed germination to seedling photomorphogenesis (Nelson et al., 2009; Nelson et al., 2010). I therefore

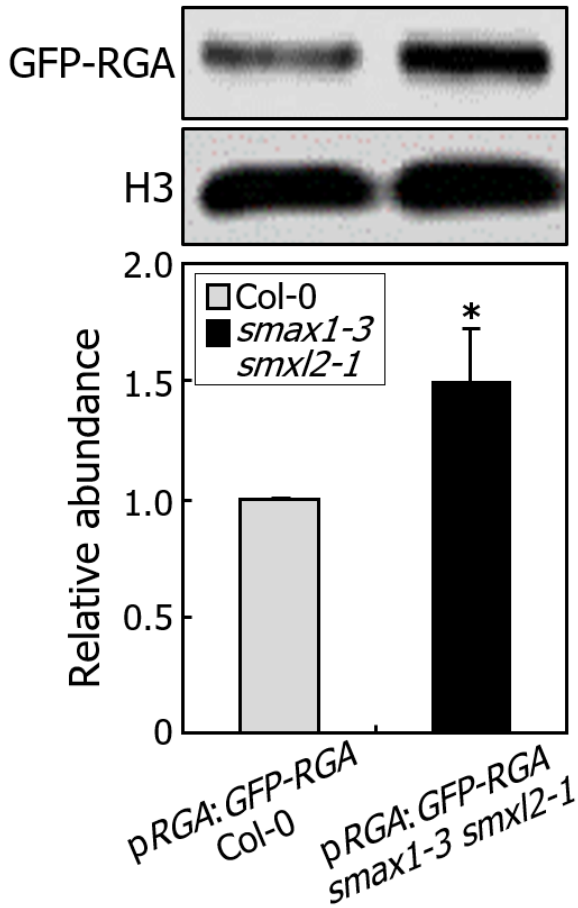

Figure 39. RGA proteins were stabilized in *smax1-3 smxl2-1* background.

RGA accumulation in *smax1-3 smxl2-1* background in plant tissues without cotyledons. Seven-day-old p*RGA:GFP-RGA* transgenic seedlings were grown on MS-agar plates at 22°C under SDs. Plant tissues without cotyledon were collected for the extraction of total proteins. GFP-RGA proteins were immunodetected using an anti-GFP antibody. Biological hexaplicates, each consisting of 40 seedlings, were averaged and statistically analyzed (*t*-test, **P* < 0.05, difference from p*RGA:GFP-RGA* in Col-0 background). H3 proteins were detected in a similar manner using an anti-H3 antibody for protein quantity control. Protein band intensities were quantitated using the ImageJ software (https://imagej.nih.gov/ij/).

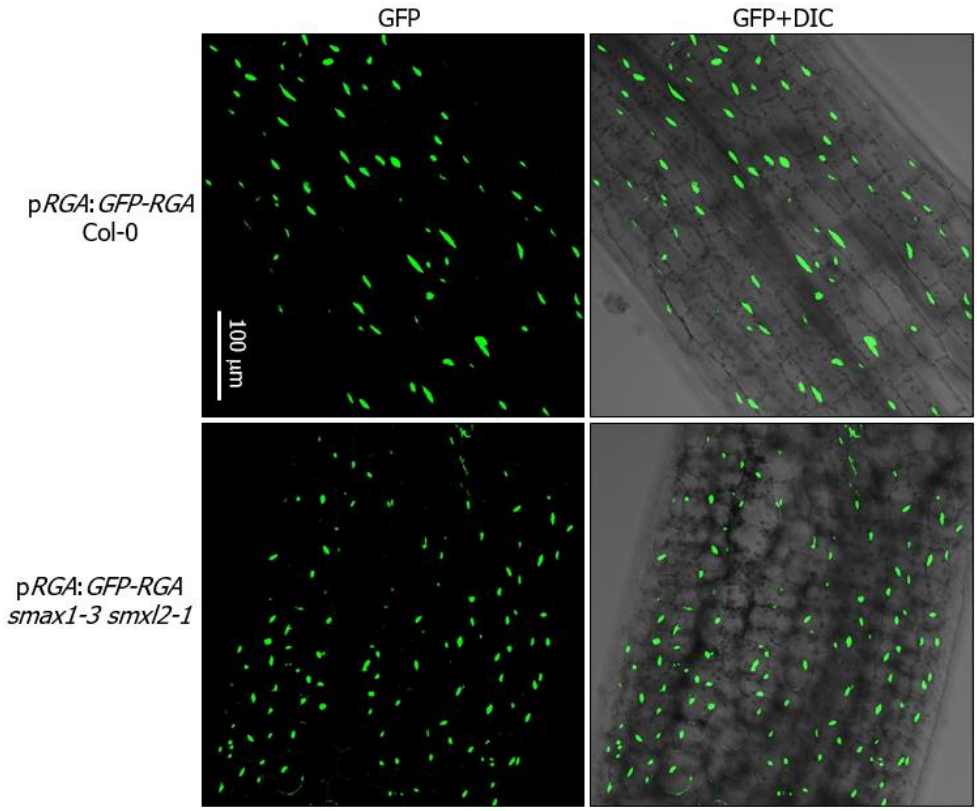

Figure 40. Confocal fluorescence images obtained from the hypocotyls of p*RGA*:*GFP-RGA* transgenic seedlings.

Confocal fluorescence images of GFP-RGA were obtained at ZT1 from the hypocotyls of seven-day-old transgenic seedlings grown on MS-agar plates supplemented with 0.2 μM PAC. Seedlings were grown under SDs at 22^{o}C. DIC, differential interference contrast.

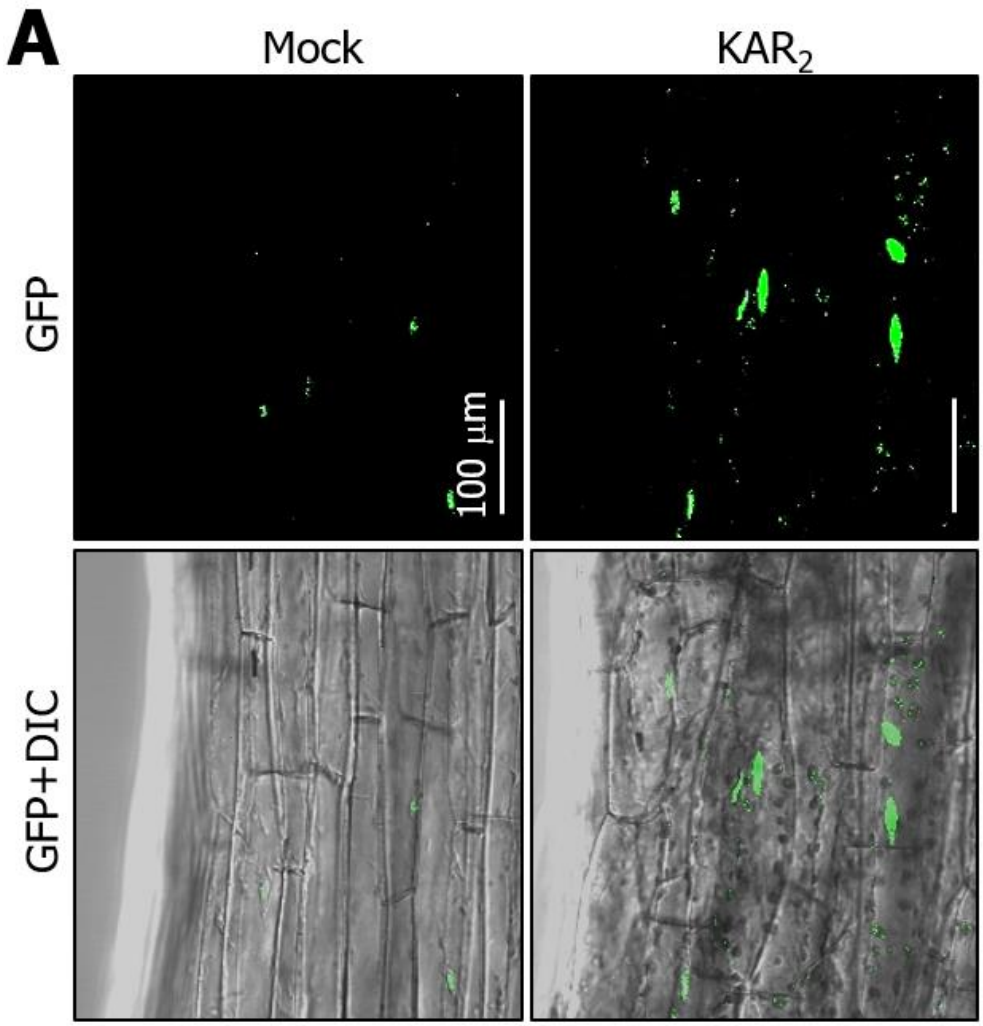

Figure 41. KAR treatments increase nuclear abundance of RGA proteins.

(A) A representative fluorescence image of GFP-RGA in hypocotyls of p*RGA*:*GFP-RGA* transgenic seedlings under KAR treatments. Seven-day-old p*RGA*:*GFP-RGA* transgenic seedlings with or without 1 μM KAR_2 treatments were harvested at ZT1 under SDs for confocal fluorescence microscopy.

(B) A full set of confocal images that include those displayed in (A).

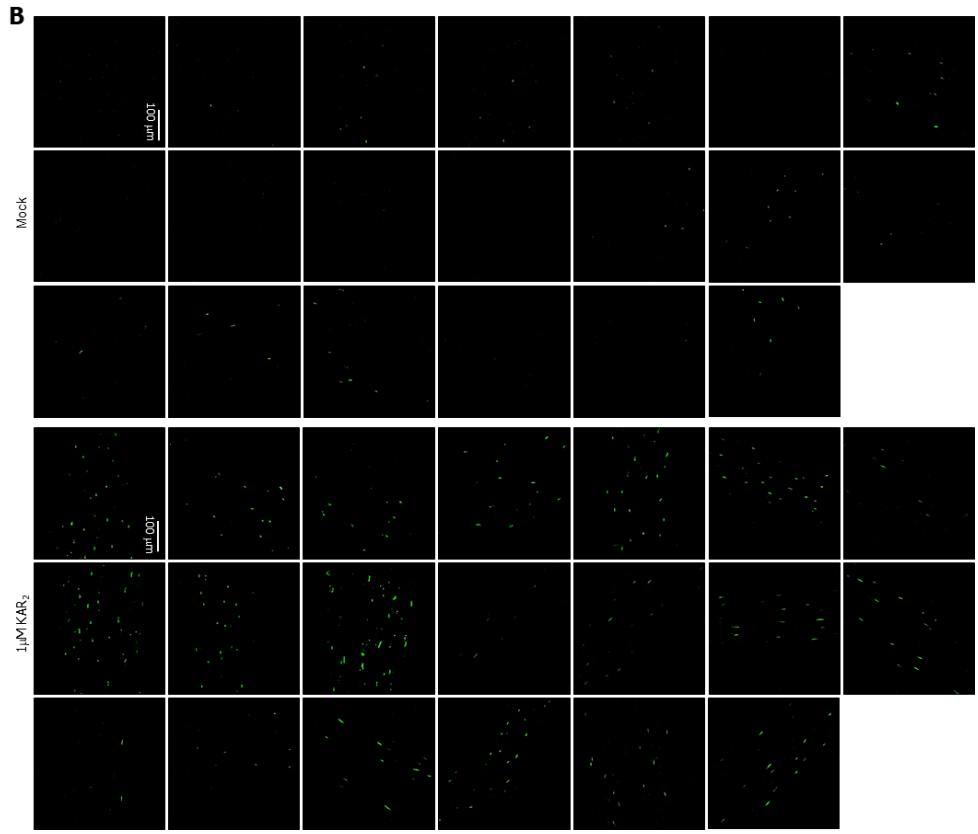

Figure 41., continued.

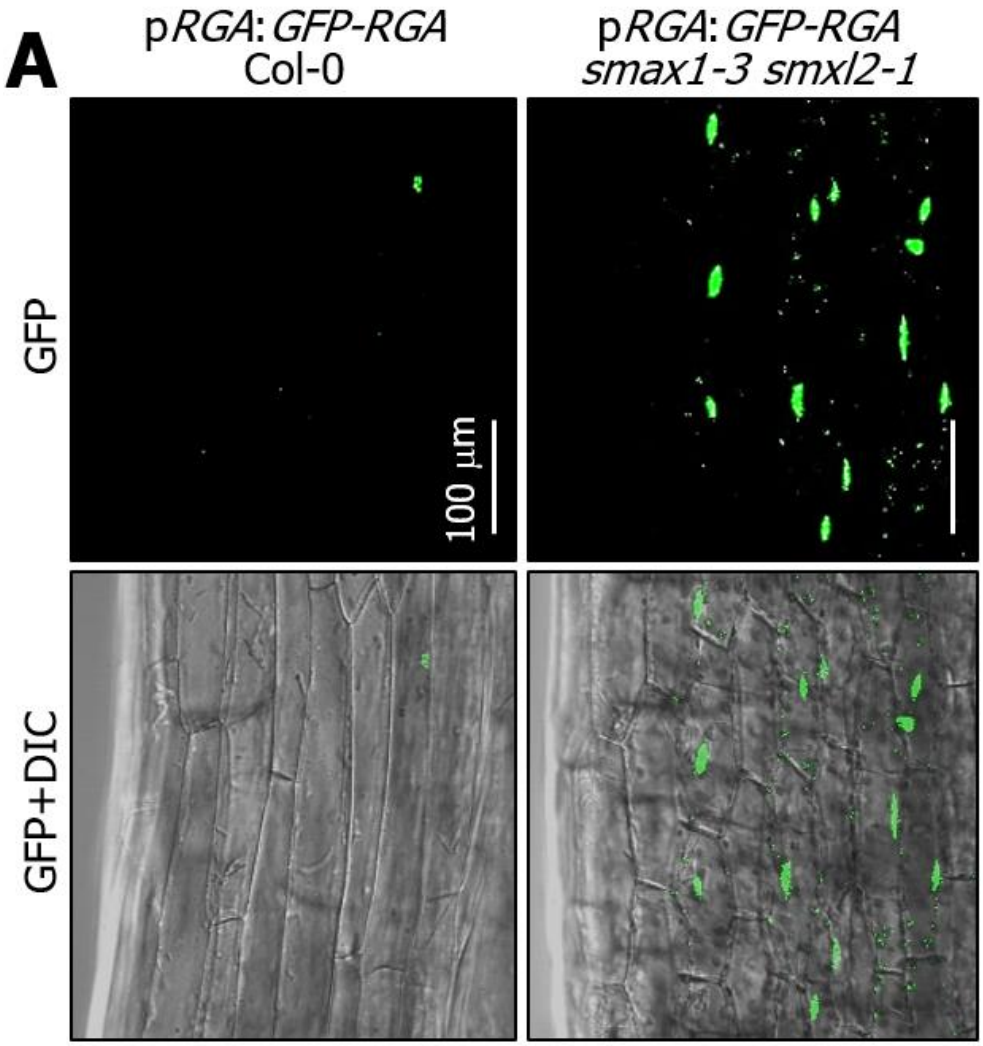

Figure 42. Nuclear accumulation of RGA proteins was evident in *smax1-3 smxl2-1* background.

(A) Nuclear accumulation of RGA proteins in hypocotyl cells of *smax1-3 smxl2-1*. Confocal images of seven-day-old seedlings were obtained at ZT1, as described in Figure 41A.

(B) A full set of confocal images that include those displayed in (A).

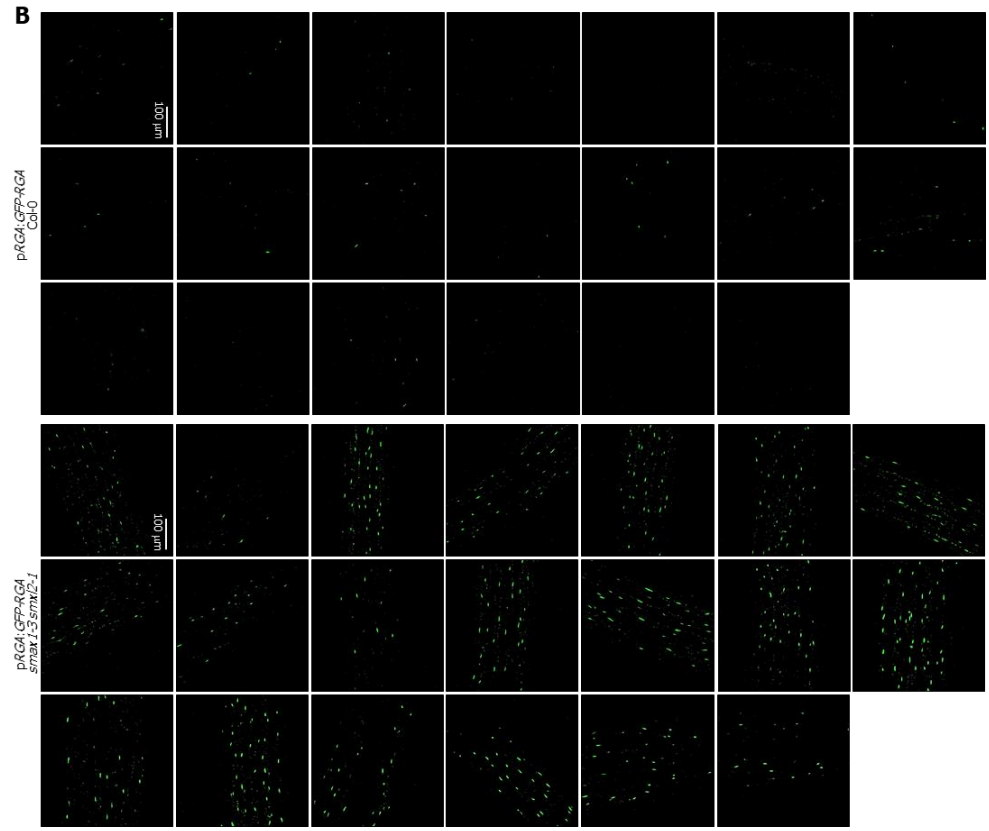

Figure 42., continued.

postulated that the functioning of KAR signaling regulators would be influenced by light environments.

I first examined the transcription patterns of KAR signaling regulator genes during the light-dark transitions. It was found that the transcription of *SMAX1* gene was not discernibly altered by light (Figure 43). Although *KAI2* transcription was marginally up-regulated in the light, this increase was not consistent with the elongated hypocotyl phenotype of the *kai2* mutant (Figure 32A). The *MAX2* transcription was also uninfluenced to a detectable level by light. These gene expression profiles indicate that the KAR signaling mediators are not regulated by light at the transcriptional level.

I next examined the effects of light on the protein accumulation of KAR signaling regulators. The endogenous levels of KAI2 and MAX2 proteins were not different in the light and dark conditions (Figure 44A and 44B). Notably, the level of SMAX1 proteins was higher by approximately 3-fold in the light compared to that in darkness (Figure 45A). The elevated accumulation of SMAX1 proteins was also evident under red light conditions. To further investigate the effects of light on the SMAX1 protein accumulation, I investigated the kinetic pattern of SMAX1 accumulation. It was found that the protein level gradually decreased following the dark transfer, reaching the ground level in 3 hours (Figure 45B). These observations indicate that SMAX1 is regulated by light at the protein level and the KAR-light signaling interactions would be mediated by SMAX1.

In the KAR-KAI2-MAX2-SMAX1 pathway, the SMAX1 proteins are degraded through a 26S ubiquitin/proteasome pathway that include the KAI2-MAX2 protein complexes in response to KAR stimulation (Khosla et al., 2020). I examined the effects of MG132, a potent 26S proteasome inhibitor, on the SMAX1

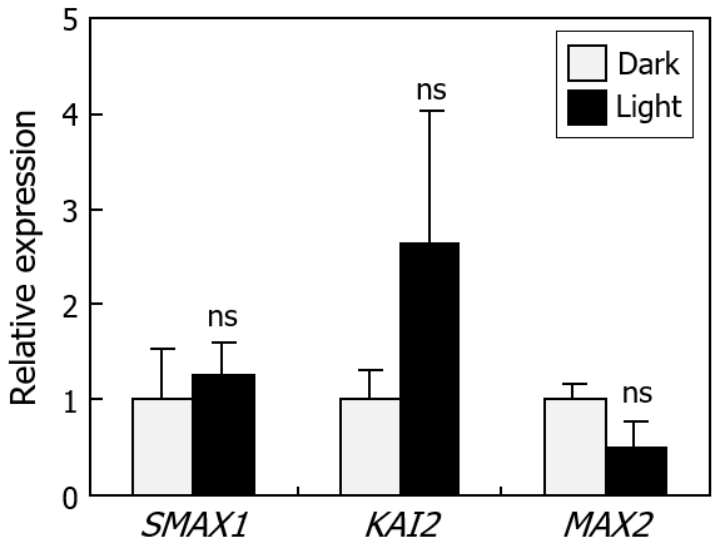

Figure 43. Relative transcript levels of KAR signaling genes during dark-to-light transition.

Transcript levels of *SMAX1*, *KAI2*, and *MAX2* genes in dark-grown and light-grown seedlings were compared. Seedlings grown on MS-agar plates at 22^{o}C for 4 d in darkness were transferred to light conditions for 12 h. Whole seedlings were harvested for total RNA extraction. Transcript levels were analyzed by RT-qPCR. Biological triplicates, each consisting of 40 seedlings, were statistically analyzed (*t*-test, **P* < 0.05, difference from dark-grown seedlings). ns, no significance.

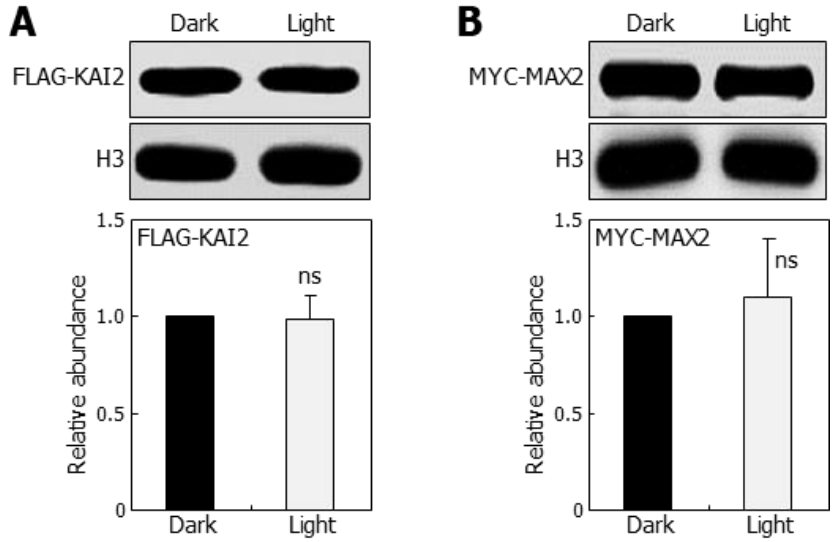

Figure 44. Abundance of KAI2 and MAX2 proteins in deetiolated seedlings.

(A) KAI2 protein abundance. Four-day-old 35S:*FLAG-KAI2* transgenic seedlings grown on MS-agar plates at 22°C in darkness were transferred to light conditions for 12 h. Biological triplicates, each consisting of 40 seedlings grown under identical conditions, were averaged and statistically analyzed (t-test, $*P < 0.05$, difference from dark). Protein band intensities were quantitated using the ImageJ software. ns, no significance.

(B) MAX2 protein abundance. Four-day-old 35S:*MYC-MAX2* transgenic seedlings grown on MS-agar plates at 22°C in darkness were transferred to light conditions for 12 h. Biological triplicates, each consisting of 40 seedlings grown under identical conditions, were averaged and statistically analyzed (t-test, $*P < 0.05$, difference from dark).

degradation in darkness. Interestingly, the reduction of SMAX1 levels in darkness still evident even in the MG132-treated seedlings (Figure 45C). These results indicate that the dark-induced degradation of SMAX1 proteins is largely independent of the KAR-induced KAI2-MAX2 ubiquitin/proteasome degradation pathway.

These data indicate that the KAR-mediated hypocotyl growth is closely associated with the GA-DELLA pathway, raising a possibility that the dark-induced degradation of SMAX1 would also be related with the GA-DELLA pathway. To test the hypothesis, I examined the protein levels of SMAX1 in seedlings grown in the presence of GA or PAC. Both GA and PAC applications did not discernibly affect the SMAX1 protein stability (Figure 46). In accordance with the lack of GA and PAC effects on the SMAX1 accumulation, I did not find any interactions of SMAX1 with DELLA-degrading enzymes (Figure 47), such as GIBBERELLIN-INSENSITIVE DWARF 1A (GID1A), GID1B, GID1C, SLEEPY1 (SLY1), and CONSTITUTIVE PHOTOMORPHOGENIC 1 (COP1) (Dill et al., 2004; Murase et al., 2008; Blanco-Touriñán et al., 2020). Together, these observations suggest that the light regulation of SMAX1 protein abundance is independent of the KAR and GA signaling pathways.

Light signals enhance SMAX1 function in DELLA-mediated seedling establishment

It has been reported that DELLA protein abundance is adjusted during deetiolation to regulate hypocotyl photomorphogenesis (Achard et al., 2007). These data show that light stabilizes SMAX1 proteins during hypocotyl growth. A question was whether the light-stabilized SMAX1 proteins affect the protein abundance of

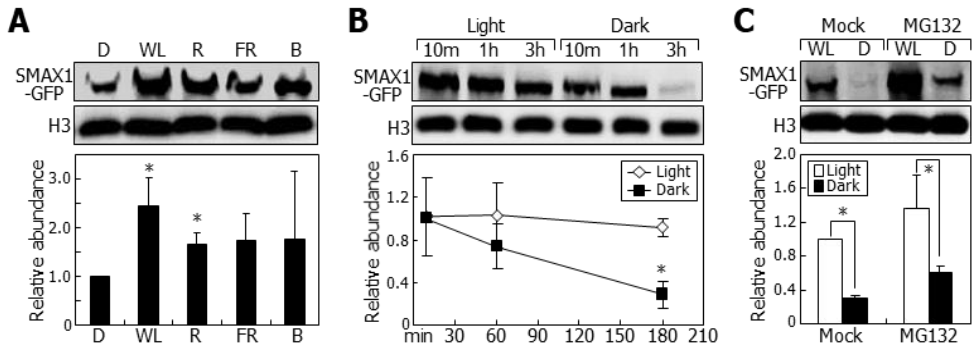

Figure 45. SMAX1 proteins accumulate in the light.

(A) SMAX1 accumulation in the dark and light. Four-day-old 35S:*SMAX1-GFP* transgenic seedlings grown on MS-agar plates at 22°C under continuous dark conditions were transferred to dark and different light environments. Whole seedlings were collected for the extraction of total proteins. SMAX1-GFP proteins were immunodetected using an anti-GFP antibody. Biological triplicates, each consisting of 40 seedlings, were averaged and statistically analyzed (*t*-test, **P* < 0.05, difference from dark). D, dark; WL, white light; R, red; FR, far-red; B, blue. H3 proteins were detected in a similar manner using an anti-H3 antibody for protein quantity control.

(B) Kinetic analysis of SMAX1 decline in the dark. Seven-day-old 35S:*SMAX1-GFP* transgenic seedlings grown on MS-agar plates at 22°C under SDs were subjected to dark conditions at ZT4 for the indicated durations before harvesting whole seedlings for the extraction of total proteins. Immunological assays were performed, as described in (A). Biological triplicates, each consisting of 40 seedlings, were averaged and statistically analyzed (*t*-test, **P* < 0.05, difference from light). m, minute; h, hour.

(C) Effects of MG132 on the SMAX1 degradation in the dark. Six-day-old 35S:*SMAX1-GFP* transgenic seedlings grown on MS-agar plates at 22^{o}C under SDs were incubated in MS liquid culture for 1 d and transferred to fresh MS liquid culture containing 5 μM MG132 for 3 h. Biological triplicates, each consisting of 40 seedlings, were averaged and statistically analyzed (*t*-test, $*P < 0.05$, difference from light).

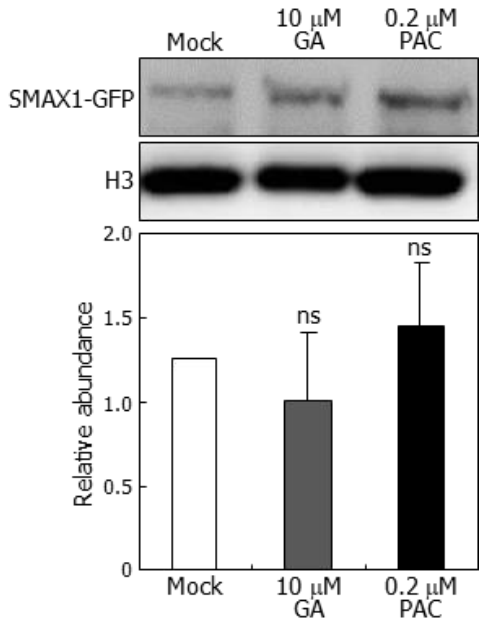

Figure 46. Effects of GA and PAC on SMAX1 protein accumulation.

Seven-day-old 35S:*SMAX1-GFP* transgenic seedlings grown on MS-agar plates containing GA or PAC at 22^{o}C under SDs were harvested for total protein extraction. Biological pentaplicates, each consisting of 40 seedlings grown under identical conditions, were averaged and statistically analyzed (t-test, $*P < 0.05$, difference from mock). Protein band intensities were quantitated using the ImageJ software. ns, no significance.

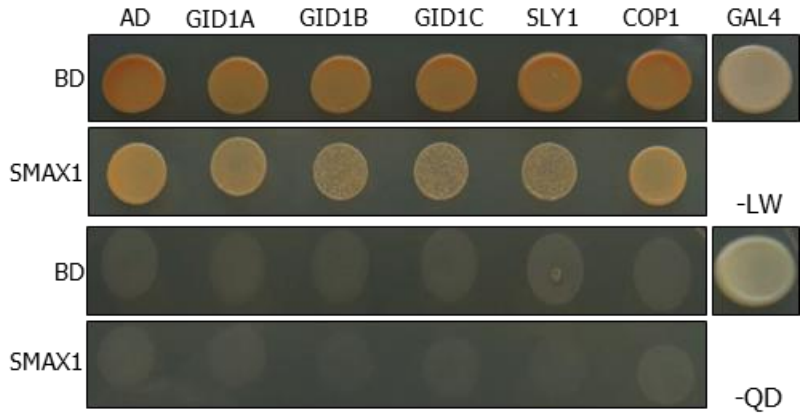

Figure 47. SMAX1 does not interact with DELLA-degrading enzymes.

Interactions of SMAX1 with GID1A, GID1B, GID1C, SLY1, and COP1 were examined in yeast cells. The (-LW) marks Leu and Trp dropout plates. The (-QD) marks Leu, Trp, His, and Ade dropout plates. AD and BD, activation domain and DNA-binding domain, respectively.

DELLAs during the dark-to-light transition.

I compared the effects of KAR_2 on hypocotyl growth in light and dark environments. In darkness, KAR_2 treatments decreased hypocotyl growth by approximately 20% (Figure 48A). In contrast, the suppressive effects of KAR_2 were more prominent with a decrease of approximately 50% in the light. Consistent with these observations, *smax1-3* and *smax1-3 smxl2-1* mutant seedlings exhibited more severe short hypocotyl phenotypes in the light than in darkness (Figure 48B), supporting that SMAX1 function is more important during hypocotyl growth in the light. In addition, while overexpression of *SMAX1* gene had no discernible effects on hypocotyl growth in darkness, the hypocotyls of the *SMAX1*-overexpressing transgenic seedlings exhibited significantly longer hypocotyls than Col-0 seedlings in the light (Figure 48B), further supporting the notion that SMAX1-mediated control of hypocotyl growth is more prominent in the light.

I next examined whether the light enforcement of SMAX1 function is attributed by SMAX1-mediated DELLA degradation during hypocotyl growth. By tracking changes in GFP-RGA signals in hypocotyl cells, I found that while KAR_2 applications caused no considerable differences on GFP-RGA signals in dark-grown seedlings (Figure 49A and 49C), the chemical treatments markedly increased GFP-RGA signals in the nuclei of hypocotyls in light-grown seedlings (Figure 49B and 49D). In addition, similar amounts of GFP-RGA signals were detected in the hypocotyl cells of etiolated Col-0 and *smax1-3 smxl2-1* seedlings (Figure 50A and 50C). In contrast, the nuclear GFP-RGA signals were detectably elevated in the hypocotyl cells of deetiolated *smax1-3 smxl2-1* seedlings compared to those in Col-0 seedlings (Figure 50B and 50D). These observations illustrate that the light-induced SMAX1 stabilization represses the nuclear accumulation of

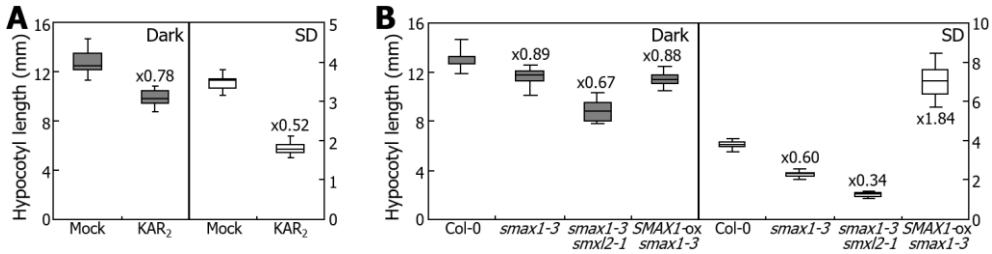

Figure 48. SMAX1 function is reinforced under light environments.

(A) Effects of KAR on hypocotyl growth in the light and darkness. Col-0 seedlings were grown on MS-agar plates at 22°C under darkness for 4 d or SDs for 7 d. KAR_2 was used at the final concentration of 1 μM. Three independent measurements, each consisting of 15 seedlings, were statistically analyzed.

(B) Hypocotyl growth phenotypes of SMAX1-deficient mutants in the light and darkness. Seedlings were grown and phenotypically analyzed, as described in (A).

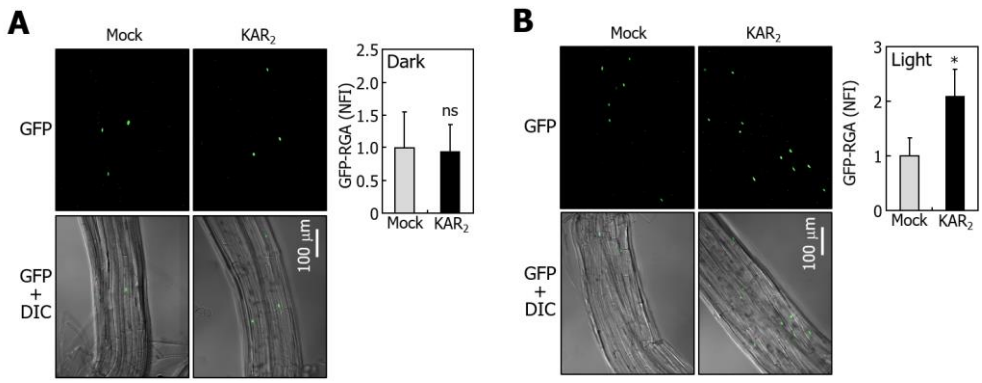

Figure 49. The KAR responses modulate DELLA-mediated hypocotyl deetiolation during seedling establishment.

(A and B) Effects of KAR on the nuclear accumulation of RGA in hypocotyl cells. Four-day-old p*RGA:GFP-RGA* transgenic seedlings germinated and grown in darkness were either left in darkness or exposed to light for 1 h prior to confocal fluorescence microscopy (A and B, respectively). A full set of confocal images are displayed in (C and D), respectively. Twenty images were statistically analyzed using Student *t*-test (*$P < 0.05$, difference from mock). Fluorescence intensities were quantitated using the ImageJ software. ns, no significance.

(C and D) A full set of confocal images that include those displayed in (A and B), respectively. Confocal fluorescence images obtained from the hypocotyls of dark-grown seedlings (C). Confocal fluorescence images obtained from the hypocotyls of seedlings following expose to light for 1 h (D).

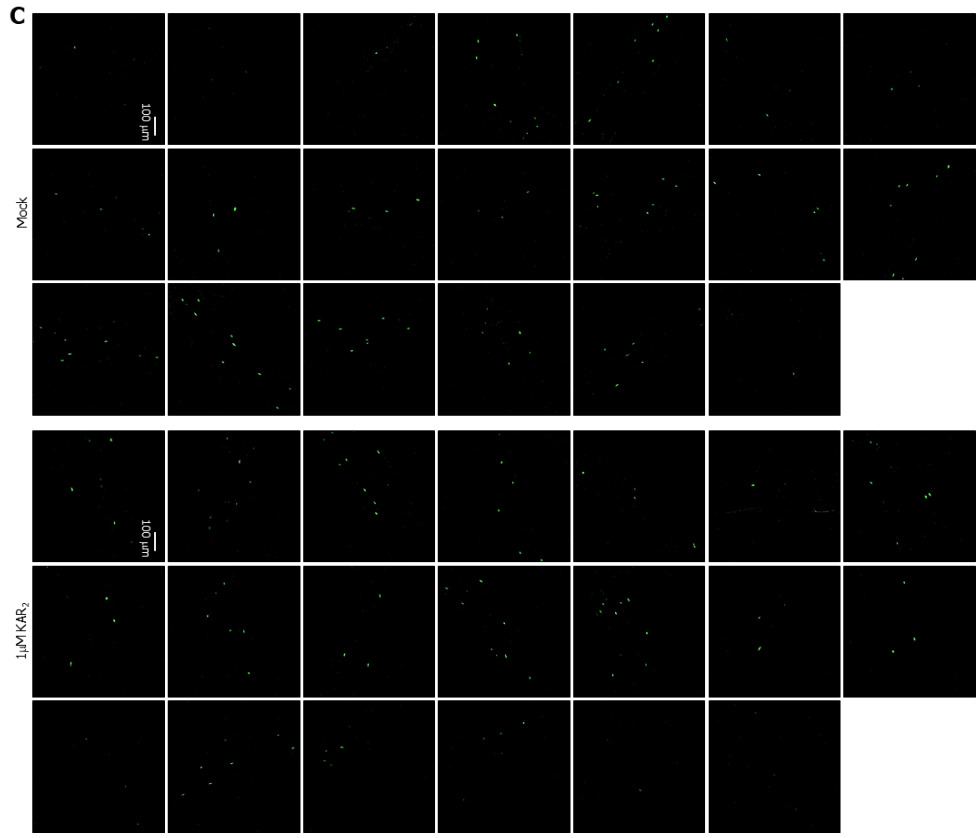

Figure 49., continued.

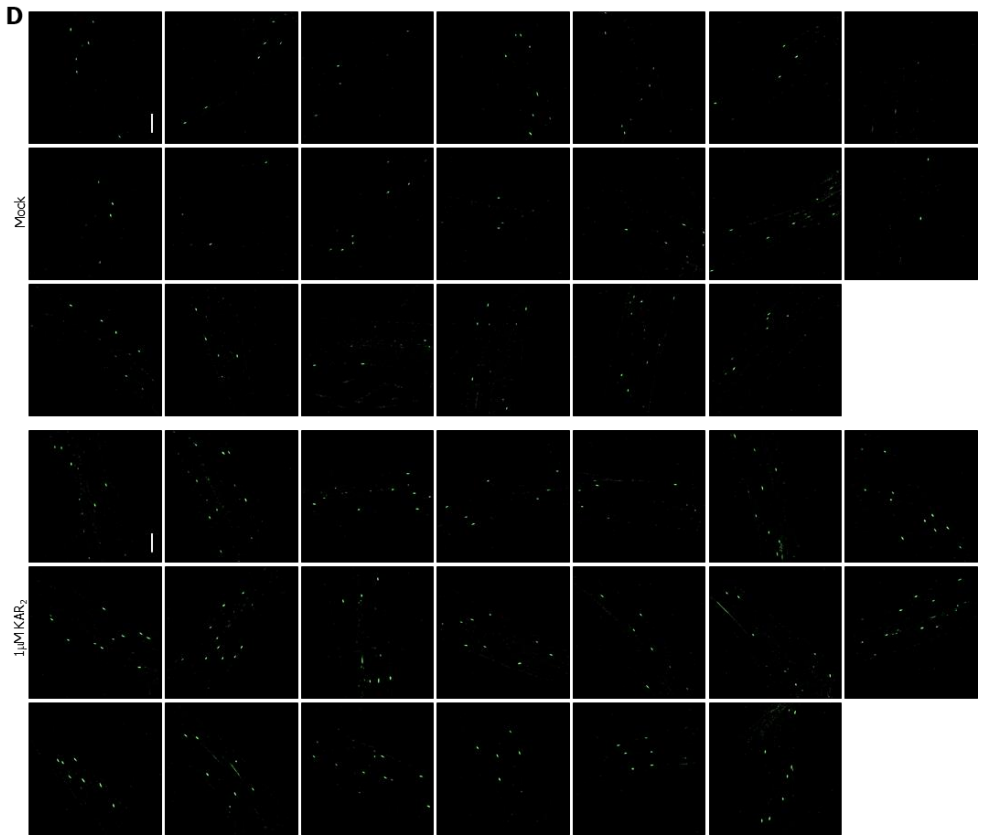

Figure 49., continued.

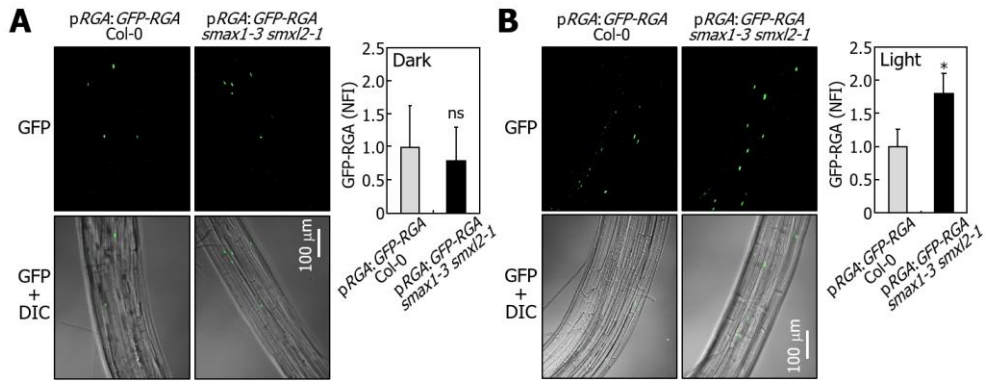

Figure 50. The KAR-SMAX1 pathway modulates hypocotyl growth during seedling establishment.

(A and B) Nuclear accumulation of RGA in hypocotyl cells of SMAX1-deficient mutants in the dark (A) and the light (B). Seedling growth and confocal fluorescence microscopic analysis were performed, as described in Figure 49. A full set of confocal images are displayed in (C and D), respectively. Twenty images were statistically analyzed using Student *t*-test (**P* < 0.05, difference from p*RGA:GFP-RGA* in Col-0). ns, no significance.

(C and D) Confocal fluorescence images obtained from the hypocotyls of dark-grown seedlings (C). Confocal fluorescence images obtained from the hypocotyls of seedlings exposed to light for 1 h (D).

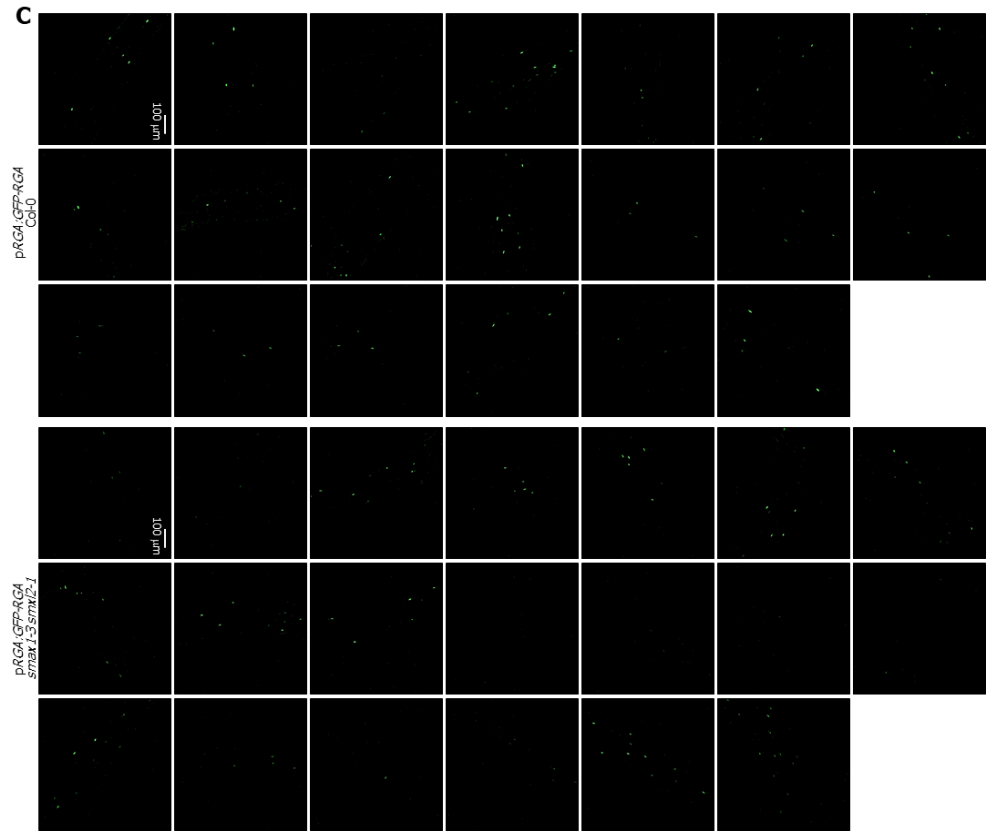

Figure 50., continued.

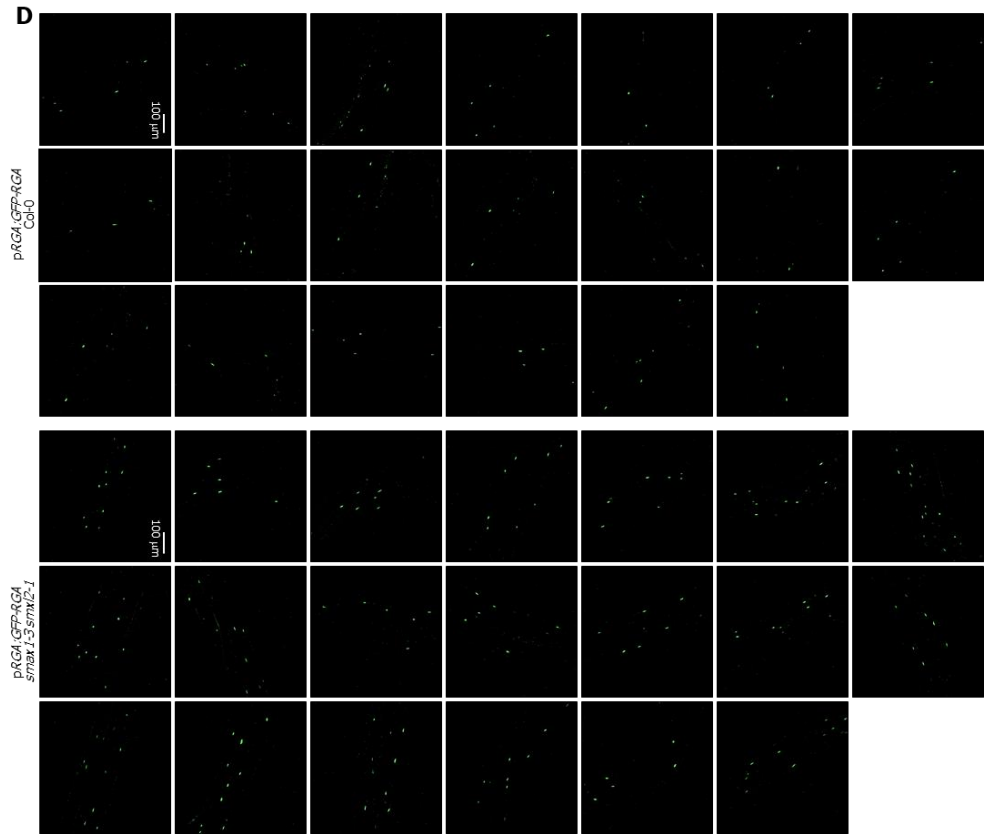

Figure 50., continued.

DELLA proteins in the hypocotyls during seedling growth.

SMAX1 integrates KAR and light signals into GA-mediated seedling establishment

A last question was as to the physiological relevance of the light stabilization of SMAX1, which acts as a negative regulator of KAR responses, during hypocotyl growth. It is known that KAR signals trigger the degradation of SMAX1 proteins by forming KAI2-MAX2-SMAX1 protein complexes (Khosla et al., 2020). I found that SMAX1 is stabilized in the light and attenuates the nuclear accumulation of DELLA proteins. A most plausible working scenario would be that SMAX1 serves as a signaling hub that integrates KAR and light signals into the GA-DELLA pathway during hypocotyl photomorphogenesis (Figure 51), which is a critical step towards successful seedling establishment.

The light-KAR signaling interaction illustrates that in the absence of KAR stimulation, the combined mode of two functionally contrasting pathways, the promotive GA-DELLA pathway and the suppressible SMAX1-DELLA pathway, on DELLA protein stability maintains hypocotyl photomorphogenesis in a way that its growth is compatible with surrounding plants. On the other hand, when KAR signals prevail in surrounding environments, as encountered following wildfires, KAR signals promote SMAX1 degradation, leading to an elevation of DELLA abundance and thus a maximization of hypocotyl photomorphogenesis (Figure 51). I believe that the SMAX1-meditaed integration of KAR and light signals into GA-DELLA pathways helps growing young plants to achieve optimized establishment to KAR-prevailing environments.

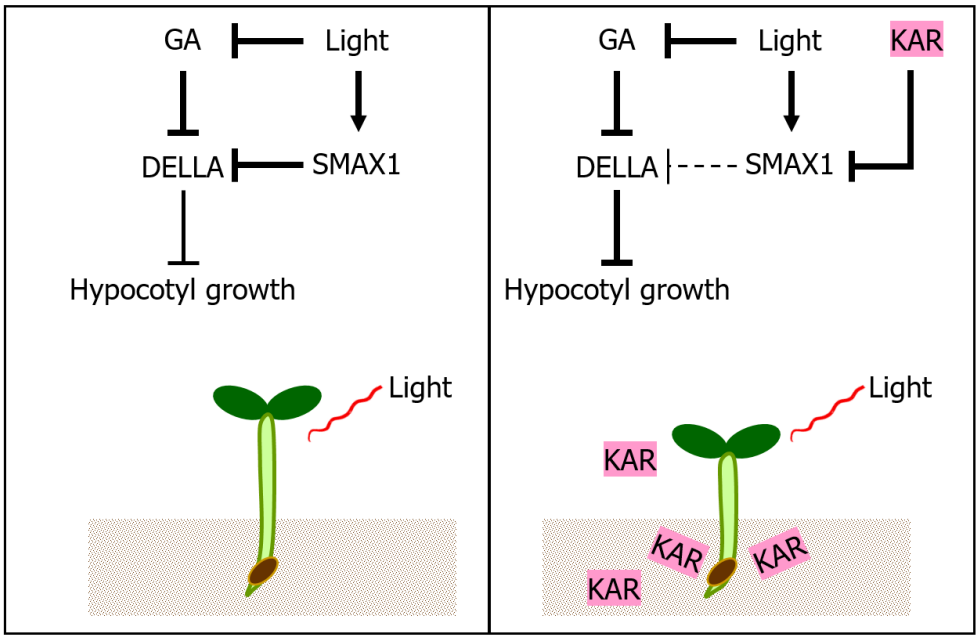

Figure 51. SMAX1 integrates KAR and light signals to facilitate seedling establishment.

Under an environment lacking KAR stimuli, while light triggers the accumulation of DELLAs by suppressing GA responses, the light-stabilized SMAX1 suppresses the DELLA accumulation (left panel). On the other hand, when KARs are present in the environment, as occurred during wildfires, KAR signals destabilize SMAX1, eliminating its suppressive effects in DELLA accumulation. As a result, photomorphogenesis is optimized to enhance seedling establishment.

DISCUSSION

These findings provide a distinct molecular mechanism by which the KAR-SMAX1 signaling pathway contributes to successful seedling establishment under relative open environments, such as those occurring following wildfires. In this signaling scheme, the SMAX1 negative regulator of KAR signaling integrates light signals into the GA-DELLA pathway that regulates hypocotyl photomorphogenesis.

Light exposure of developing seedlings during the deetiolation process brings about a reorganization of endogenous molecular systems to deal with fluctuations in neighboring environments (McNellis and Deng 1995). In nature, thriving habitats often are accompanied with crowded plants, which impose adaptive difficulties on pursuing seedling photomorphogenesis (Casal 2012). In this regard, the SMAX1-mediated DELLA degradation pathway, which is activated by light stimulation, would help emerging seedlings to avoid unfavorable photomorphogenic conditions by escaping from plant canopy. On the other hand, when the limited light conditions are relieved by wildfires that eliminates neighboring competitors, KAR signals would contribute to optimizing seedling photomorphogenic growth by attenuating the SMAX1 signaling pathway.

The attenuation of SMAX1 actions during photomorphogenic hypocotyl growth is similar to plant responses during shade avoidance syndrome (SAS). SAS includes a set of phenotypic traits that helps plants to dodge shaded conditions, such as elongated hypocotyl growth, apical dominance, accelerated flowering, and upward leaf movement (Casal 2012). It has been reported that DELLA degradation is induced by an elevation of GA biosynthesis or through the COP1-mediated 26S proteasome pathway, resulting in the derepression of PIF function (Djakovic-

Petrovic et al., 2007; De Lucas et al., 2008; Feng et al., 2008; Blanco-Touriñán et al., 2020). The DELLA degradation also promotes plant avoiding responses from canopy shade. These findings that SMAX1 stability is enhanced by light to promote DELLA degradation suggest that SMAX1 would also function in plant responses to shade conditions. It will be interesting to investigate the potential roles of SMAX1 in SAS and its functional relationships with shade avoidance regulators, such as PIFs (Lorrain et al., 2008).

Light signals often regulate the protein stability of light signaling mediators through the photoreceptor-associated ubiquitin/proteasome-dependent mechanisms (Ito et al., 2012; Podolec and Ulm 2018). A well-known example is the phyB-mediated regulation of PIF protein stability. The phyB photoreceptor induces various growth and developmental traits by triggering the protein degradation of PIF transcription factors, such as induction of seed germination, chloroplast development, and photomorphogenic seedling growth (Oh et al., 2007; Shen et al., 2008; Shin et al., 2009; Liu et al., 2013). I found that SMAX1 proteins are light-stabilized, thus suppressing DELLA function in regulating hypocotyl growth. It is currently unclear whether the protein stability of SMAX1 is associated with any specific photoreceptors. It is known that SMAX1 proteins are degraded through the canonical KAR signaling pathway, which is mediated by a KAI2-MAX2-associated ubiquitin/proteasome pathway (Khosla et al., 2020). Meanwhile, a recent study has shown that SMAX1 is also degraded through a KAI2/MAX2-independent pathway (Khosla et al., 2020). Similarly, I found that the dark-induced degradation of SMAX1 is independent of the KAR-KAI2-MAX2 pathway and the GA-DELLA pathway. It is possible that the protein stability of SMAX1 is modulated through multiple mechanisms that are either dependent or independent

of KARs and photoreceptors in various signaling pathways.

These data show that the SMAX1-mediated hypocotyl growth is facilitated by promoting the degradation of DELLA proteins. It is unclear how SMAX1 induces the destabilization of DELLAs. It is interesting that KAR and GA signaling modules are biochemically similar to each other. In both cases, the receptor proteins are proven or suggested to be α/β-hydrolases (Shimada et al., 2008; Guo et al., 2013). In addition, the F-box proteins MAX2 and SLY1 are required for the degradation of their signaling repressors in KAR and GA signaling processes, respectively (Dill et al., 2004; Khosla et al., 2020). These biochemical similarities raise a possibility that GA signaling modules would promote SMAX1-mediated DELLA degradation. However, these observations that DELLA-degrading enzymes do not directly interact with SMAX1 do not support the above-mentioned hypothesis. Meanwhile, it has been reported that a rice DELLA protein SLR1 interacts with a strigolactone (SL) receptor DWARF14 (D14), a close homologue of KAI2 (Nakamura et al., 2013), supporting a potential signaling linkage between KAR-KAI2 signaling and GA-DELLA modules.

While these data indicate that SMAX1 directly interacts with DELLAs, it is currently unknown how SMAX1 triggers the degradation of DELLA proteins. The SMAX1 protein does not harbor any protein domains that mediate protein degradation. Since SMAX1 does not interact with DELLA-degrading enzymes, it is unlikely that the GA-GID1-DELLA module is involved in the SMAX1-mediated degradation of DELLA proteins. Considering that endogenous levels of SMAX1 proteins are thought to be extremely low (Khosla et al., 2020), a possibility would be that SMAX1 inhibits the accumulation of DELLA proteins by a suicidal codegradation of both the interacting partners, as has been observed in plants (Zhu

and Huq 2014).

One distinction of this study is that SMAX1 interacts with DELLA proteins except for RGL2 (Figure 36A). It is known that DELLA-mediated regulation of seed germination and hypocotyl growth is facilitated by unequal functional redundancy among the five DELLA members in *Arabidopsis*. While DELLA proteins function in repressing both seed germination and hypocotyl growth, RGL2 plays a major role in inhibiting seed germination (Lee et al., 2002). In contrast, RGA and GAI are mostly involved in the suppression of hypocotyl growth (Tyler et al., 2004; Penfield et al., 2006). I found that SMAX1 and SMXL2 do not directly interact with RGL2 but efficiently interact with other DELLA members. It is likely that SMAX1 provides a discrete GA signaling pathway that is functionally distinct from other GA signaling pathways through differential interactions of SMAX1 with different DELLA members.

ACKNOWLEDGMENTS

I thank Giltsu Choi for providing the *rga-28 gai-t6* double mutant and Ottoline Leyser and Mark Waters for providing the *kai2-1* mutant in Col-0 background.

REFERENCES

Achard, P., Liao, L., Jiang, C., Desnos, T., Bartlett, J., Fu, X., and Harberd, N.P. (2007). DELLAs contribute to plant photomorphogenesis. Plant Physiol. 143:1163.

Alabadí, D., Gallego-Bartolomé, J., Orlando, L., García-Cárcel, L., Rubio, V., Martínez, C., Frigerio, M., Iglesias-Pedraz, J.M., Espinosa, A., Deng, X.W., et al. (2008). Gibberellins modulate light signaling pathways to prevent *Arabidopsis* seedling de-etiolation in darkness. Plant J. 53:324-335.

Arsovski, A.A., Galstyan, A., Guseman, J.M., and Nemhauser, J.L. (2012). Photomorphogenesis. Arabidopsis Book 10:e0147.

Blanco-Touriñán, N., Legris, M., Minguet, E.G., Costigliolo-Rojas, C., Nohales, M.A., Iniesto, E., García-León, M., Pacín, M., Heucken, N., Blomeier, T., et al. (2020). COP1 destabilizes DELLA proteins in *Arabidopsis*. Proc. Natl. Acad. Sci. U S A 117:13792-13799.

Botton, A. and Ruperti, B. (2019). The yes and no of the ethylene involvement in abscission. Plants 8:187.

Bursch, K., Niemann, E.T., Nelson, D.C., and Johansson, H. (2021). Karrikins control seedling photomorphogenesis and anthocyanin biosynthesis through a HY5-BBX transcriptional module. Plant J. 107:1346-1362.

Casal, J.J. (2012). Shade avoidance. Arabidopsis Book 10:e0157.

Casal, J.J. and Balasubramanian, S. (2019). Thermomorphogenesis. Annu. Rev. Plant Biol. 70:321-346.

Cheminant, S., Wild, M., Bouvier, F., Pelletier, S., Renou, J.P., Erhardt, M., Hayes, S., Terry, M.J., Genschik, P., and Achard, P. (2011). DELLAs regulate

chlorophyll and carotenoid biosynthesis to prevent photooxidative damage during seedling deetiolation in *Arabidopsis*. Plant Cell 23:1849-1860.

Chen, Y.F., Etheridge, G.E. and Schaller, G.E. (2005). Ethylene signal transduction. Ann. Bot. (Lond.) 95:901-915.

Chen, Y.F., Randlett, M.D., Findell, J.L. and Schaller, G.E. (2002). Localization of the ethylene receptor ETR1 to the endoplasmic reticulum of *Arabidopsis*. J. Biol. Chem. 277:19861-19866.

Chory, J., Chatterjee, M., Cook, R.K., Elich, T., Fankhauser, C., Li, J., Nagpal, P., Neff, M., Pepper, A., Poole, D., et al. (1996). From seed germination to flowering, light controls plant development via the pigment phytochrome. Proc. Natl. Acad. Sci. U S A 93:12066-12071.

Cortleven, A., and Schmülling, T. (2015). Regulation of chloroplast development and function by cytokinin. J. Exp. Bot. 66:4999-5013.

Crawford, A.J., McLachlan, D.H., Hetherington, A.M. and Franklin, K.A. (2012). High temperature exposure increases plant cooling capacity. Curr. Biol. 22:R396-R397.

De Lucas, M., Daviere, J.M., Rodríguez-Falcón, M., Pontin, M., Iglesias-Pedraz, J.M., Lorrain, S., Fankhauser, C., Blázquez, M.A., Titarenko, E., and Prat, S. (2008). A molecular framework for light and gibberellin control of cell elongation. Nature 451:480-484.

De Simone, S., Oka, Y. and Inoue, Y. (2000). Effect of light on root hair formation in *Arabidopsis thaliana* phytochrome-deficient mutants. J. Plant Res. 113:63-69.

Dharmasiri, N., Dharmasiri, S. and Estelle, M. (2005). The F-box protein TIR1 is an auxin receptor. Nature 435:441-445.

Dill, A., Jung, H.S., and Sun, T.P. (2001). The DELLA motif is essential for

gibberellin-induced degradation of RGA. Proc. Natl. Acad. Sci. U S A 98:14162-14167.

Dill, A., Thomas, S.G., Hu, J., Steber, C.M., and Sun, T.P. (2004). The *Arabidopsis* F-box protein SLEEPY1 targets gibberellin signaling repressors for gibberellin-induced degradation. Plant Cell 16:1392-1405.

Djakovic-Petrovic, T., Wit, M.D., Voesenek, L.A., and Pierik, R. (2007). DELLA protein function in growth responses to canopy signals. Plant J. 51:117-126.

Feng, Y., Xu, P., Li, B., Li, P., Wen, X., An, F., et al. (2017). Ethylene promotes root hair growth through coordinated EIN3/EIL1 and RHD6/RSL1 activity in *Arabidopsis*. Proc. Natl. Acad. Sci. U S A 114:13834-13839.

Flematti, G.R., Ghisalberti, E.L., Dixon, K.W., and Trengove, R.D. (2004). A compound from smoke that promotes seed germination. Science 305:977.

Franklin, K.A., Lee, S.H., Patel, D., Kumar, S.V., Spartz, A.K., Gu, C., Ye, S., Yu, P., Breen, G., Cohen, J.D., et al. (2011). PHYTOCHROME-INTERACTING FACTOR 4 (PIF4) regulates auxin biosynthesis at high temperature. Proc. Natl. Acad. Sci. U S A 108:20231-20235.

Gray, W.M., Ostin, A., Sandberg, G., Romano, C.P. and Estelle, M. (1998). High temperature promotes auxin-mediated hypocotyl elongation in *Arabidopsis*. Proc. Natl. Acad. Sci. U S A 95:7197-7202.

Grbić, V. and Bleecker, A.B. (1995). Ethylene regulates the timing of leaf senescence in *Arabidopsis*. Plant J. 8:595-602.

Grégory, A.V., Jean-François, B. and Catherine, C. (2003). Dual regulation of the *Arabidopsis* high-affinity root iron uptake system by local and long-distance signals. Plant Physiol. 132:796-804.

Guo, Y., Zheng, Z., La Clair, J.J., Chory, J., and Noel, J.P. (2013). Smoke-derived

karrikin perception by the α/β-hydrolase KAI2 from *Arabidopsis*. Proc. Natl. Acad. Sci. U S A 110:8284-8289.

Guzman, P. and Ecker, J.R. (1990). Exploiting the triple response of *Arabidopsis* to identify ethylene-related mutants. Plant Cell 2:513-523.

Halliday, K.J., Martínez-García, J.F., and Josse, E.M. (2009). Integration of light and auxin signaling. Cold Spring Harb. Perspect. 1:a001586.

Han, X., Yu, H., Yuan, R., Yang, Y., An, F. and Qin, G. (2019). *Arabidopsis* transcription factor TCP5 controls plant thermomorphogenesis by positively regulating PIF4 activity. iScience 15:611-622.

Hatfield, J.L. and Prueger, J.H. (2015). Temperature extremes: Effect on plant growth and development. Weather Clim. Extrem. 10:4-10.

Ito, S., Song, Y.H., and Imaizumi, T. (2012). LOV domain-containing F-box proteins: light-dependent protein degradation modules in *Arabidopsis*. Mol. Plant 5:573-582.

Jin, H., Pang, L., Fang, S., Chu, J., Li, R. and Zhu, Z. (2018). High ambient temperature antagonizes ethylene-induced exaggerated apical hook formation in etiolated *Arabidopsis* seedlings. Plant Cell Environ. 41:2858-2868.

Jung, J.H., Domijan, M., Klose, C., Biswas, S., Ezer, D., Gao M., Khattak, A.K., Box, M.S., Charoensawan, V., Cortijo, S., et al. (2016). Phytochromes function as thermosensors in *Arabidopsis*. Science 354:886-889.

Khosla, A., Morffy, N., Li, Q., Faure, L., Chang, S.H., Yao, J., Zheng, J., Cai, M.L., Stanga, J., Flematti, G.R., et al. (2020). Structure-function analysis of SMAX1 reveals domains that mediate its karrikin-induced proteolysis and interaction with the receptor KAI2. Plant Cell 32:2639-2659.

Kieber, J.J., Rothenburg, M., Roman, G., Feldmann, K.A. and Ecker, J.R. (1993).

CTR1, a negative regulator of the ethylene response pathway in *Arabidopsis* encodes a member of the Raf family of protein kinases. Cell 72:427-441.

Kim, N.Y., Jang, Y.J. and Park, O.K. (2018). AP2/ERF family transcription factors ORA59 and RAP2.3 interact in the nucleus and function together in ethylene responses. Front. Plant Sci. 9:1675.

Kim, J.Y., Park, Y.J., Lee, J.H. and Park, C.M. (2019). Developmental polarity shapes thermo-induced nastic movements in plants. Plant Signal. Behav. 14:1617609.

Lee, H.J., Jung, J.H., Llorca, L.C., Kim, S.G., Lee, S., Baldwin, I.T., Park, C.M. (2014). FCA mediates thermal adaptation of stem growth by attenuating auxin action in *Arabidopsis*. Nat. Commun. 5:5473.

Lee, O.R., Kim, S.J., Kim, H.J., Hong J.K., Ryu, S.B., Lee, S.H., Ganguly, A., Cho, H.T. (2010). Phospholipase A_2 is required for PIN-FORMED protein trafficking to the plasma membrane in the *Arabidopsis* root. Plant Cell 22:1812-1825.

Lee, S., Cheng, H., King, K.E., Wang, W., He, Y., Hussain, A., Lo, J., Harberd, N.P., and Peng, J. (2002). Gibberellin regulates *Arabidopsis* seed germination via RGL2, a GAI/RGA-like gene whose expression is up-regulated following imbibition. Genes Dev. 16:646-658.

Legris, M., Klose, C., Burgie, E.S., Rojas, C.C., Neme, M., Hiltbrunner, A., Wigge, P.A., Schäfer, E., Vierstra, R.D., Casal, J.J. (2016). Phytochrome B integrates light and temperature signals in *Arabidopsis*. Science 354:897-900.

Li, J.F., Park, E., von Arnim, A.G., and Nebenführ, A. (2009). The FAST technique: a simplified *Agrobacterium*-based transformation method for transient gene expression analysis in seedlings of *Arabidopsis* and other plant species. Plant Methods 5:1-15.

Li, W., Nguyen, K.H., Chu, H.D., Ha, C.V., Watanabe, Y., Osakabe, Y., Leyva-González, M.A., Sato, M., Toyooka, K., Voges, L., et al. (2017). The karrikin receptor KAI2 promotes drought resistance in *Arabidopsis thaliana*. PLoS Genet. 13:e1007076.

Liu, M., Pirrello, J., Chervin, C., Roustan, J.P. and Bouzayen, M. (2015). Ethylene control of fruit ripening: revisiting the complex network of transcriptional regulation. Plant Physiol. 169:2380-2390.

Liu, X., Chen, C.Y., Wang, K.C., Luo, M., Tai, R., Yuan, L., Zhao, M., Yang, S., Tian, G., Cui, Y., et al. (2013). PHYTOCHROME-INTERACTING FACTOR 3 associates with the histone deacetylase HDA15 in repression of chlorophyll biosynthesis and photosynthesis in etiolated *Arabidopsis* seedlings. Plant Cell 25:1258-1273.

Liu, X., Li, Y., and Zhong, S. (2017). Interplay between light and plant hormones in the control of *Arabidopsis* seedling chlorophyll biosynthesis. Front. Plant Sci. 8:1433.

Lorrain, S., Allen, T., Duek, P.D., Whitelam, G.C. and Fankhauser, C. (2008). Phytochrome-mediated inhibition of shade avoidance involves degradation of growth-promoting bHLH transcription factors. Plant J. 53:312-323.

Ma, Q., Wang, X., Sun, J. and Mao, T. (2018). Coordinated regulation of hypocotyl cell elongation by light and ethylene through a microtubule destabilizing protein. Plant Physiol. 176:678-690.

McNellis, T.W. and Deng, X.W. (1995). Light control of seedling morphogenetic pattern. Plant Cell 7:1749.

Møller, J.V., Juul, B. and le Maire, M. (1996). Structural organization, ion transport, and energy transduction of P-type ATPases. Biochim. Biophys. Acta, 1286:1-51.

Morffy, N., Faure, L., and Nelson, D.C. (2016). Smoke and hormone mirrors: action and evolution of karrikin and strigolactone signaling. Trends Genet. 32:176-188.

Morgan, P.W. and Drew, M.C. (1997). Ethylene and plant responses to stress. Physiol. Plant. 100:620-630.

Munns, R., Day, D.A., Fricke, W., Watt, M., Arsova, B., Barkla, B.J., Bose, J., Byrt, C.S., Chen, Z.H., Foster, K.J., et al. (2020). Energy costs of salt tolerance in crop plants. New Phytol. 225:1072-1090.

Murase, K., Hirano, Y., Sun, T.P., and Hakoshima, T. (2008). Gibberellin-induced DELLA recognition by the gibberellin receptor GID1. Nature 456:459-463.

Nakamura, H., Xue, Y.L., Miyakawa, T., Hou, F., Qin, H.M., Fukui, K., Shi, X., Ito, E., Ito, S., Park, S.H., et al. (2013). Molecular mechanism of strigolactone perception by DWARF14. Nat. Commun. 4:1-10.

Nelson, D.C., Riseborough, J.A., Flematti, G.R., Stevens, J., Ghisalberti, E.L., Dixon, K.W., and Smith, S.M. (2009). Karrikins discovered in smoke trigger *Arabidopsis* seed germination by a mechanism requiring gibberellic acid synthesis and light. Plant Physiol. 149:863-873.

Nelson, D.C., Flematti, G.R., Riseborough, J.A., Ghisalberti, E.L., Dixon, K.W., and Smith, S.M. (2010). Karrikins enhance light responses during germination and seedling development in *Arabidopsis thaliana*. Proc. Natl. Acad. Sci. U S A 107:7095-7100.

Nelson, D.C., Scaffidi, A., Dun, E.A., Waters, M.T., Flematti, G.R., Dixon, K.W., Beveridge, C.A., Ghisalberti, E.L., and Smith, S.M. (2011). F-box protein MAX2 has dual roles in karrikin and strigolactone signaling in *Arabidopsis thaliana*. Proc. Natl. Acad. Sci. U S A 108:8897-8902.

Nelson, D.C., Flematti, G.R., Ghisalberti, E.L., Dixon, K.W., and Smith, S.M. (2012). Regulation of seed germination and seedling growth by chemical signals from burning vegetation. Annu. Rev. Plant Biol. 63:107-130.

Nusinow, D.A., Helfer, A., Hamilton, E.E., King, J.J., Imaizumi, T., Schultz, T.F., Farré, E.M., Kay, S.A. (2011). The ELF4-ELF3-LUX complex links the circadian clock to diurnal control of hypocotyl growth. Nature 475:398-402.

Ogawara, T., Higashi, K., Kamada, H. and Ezura, H. (2003) Ethylene advances the transition from vegetative growth to flowering in *Arabidopsis thaliana*. *J. Plant Physiol.* 160: 1335-1340.

Oh, E., Yamaguchi, S., Hu, J., Yusuke, J., Jung, B., Paik, I., Lee, H.S., Sun, T.P., Kamiya, Y., and Choi, G. (2007). PIL5, a phytochrome-interacting bHLH protein, regulates gibberellin responsiveness by binding directly to the GAI and RGA promoters in *Arabidopsis* seeds. Plant Cell 19:1192-1208.

Park, Y.J., Lee, H.J., Gil, K.E., Kim, J.Y., Lee, J.H., Lee, H., Cho, H.T., Vu, L.D., Smet, I.D., Park, C.M. (2019). Developmental programming of thermonastic leaf movement. Plant Physiol. 180:1185-1197.

Park, Y.J., Lee, H.J., Ha, J.H., Kim, J.Y. and Park, C.M. (2017). COP1 conveys warm temperature information to hypocotyl thermomorphogenesis. New Phytol. 215:269-280.

Penfield, S., Gilday, A.D., Halliday, K.J., and Graham, I.A. (2006). DELLA-mediated cotyledon expansion breaks coat-imposed seed dormancy. Curr. Biol. 16:2366-2370.

Podolec, R., and Ulm, R. (2018). Photoreceptor-mediated regulation of the COP1/SPA E3 ubiquitin ligase. Curr. Opin. Plant Biol. 45:18-25.

Potuschak, T., Lechner, E., Parmentier, Y., Yanagisawa, S., Grava, S., Koncz, C.,

Genschik, P. (2003). EIN3-dependent regulation of plant ethylene hormone signaling by two *Arabidopsis* F box proteins: EBF1 and EBF2. Cell 115:679-689.

Quint, M., Delker, C., Franklin, K.A., Wigge, P.A., Halliday, K.J. and van Zanten, M. (2017). Molecular and genetic control of plant thermomorphogenesis. Nat. Plants 2:15190.

Sasidharan, R. and Voesenek, L.A. (2015). Ethylene-mediated acclimations to flooding stress. Plant Physiol. 169:3-12.

Schweighofer, A., Hirt, H. and Meskiene I. (2004). Plant PP2C phosphatases: emerging functions in stress signaling. Trends Plant Sci. 9:236-243.

Shah, F.A., Ni, J., Yao, Y., Hu, H., Wei, R., and Wu, L. (2021). Overexpression of karrikins receptor gene *Sapium sebiferum* KAI2 promotes the cold stress tolerance via regulating the redox homeostasis in *Arabidopsis thaliana*. Front. Plant Sci. 12:657960.

Shen, H., Zhu, L., Castillon, A., Majee, M., Downie, B., and Huq, E. (2008). Light-induced phosphorylation and degradation of the negative regulator PHYTOCHROME-INTERACTING FACTOR 1 from *Arabidopsis* depend upon its direct physical interactions with photoactivated phytochromes. Plant Cell 20:1586-1602.

Shen, H., Zhu, L., Bu, Q.Y., and Huq, E. (2012). MAX2 affects multiple hormones to promote photomorphogenesis. Mol. Plant 5:750-762.

Shi, H., Liu, R., Xue, C., Shen, X., Wei, N., Deng, X.W., Zhong, S. (2016). Seedlings transduce the depth and mechanical pressure of covering soil using COP1 and ethylene to regulate EBF1/EBF2 for soil emergence. Curr. Biol. 26:139-149.

Shimada, A., Ueguchi-Tanaka, M., Nakatsu, T., Nakajima, M., Naoe, Y., Ohmiya, H., Kato, H., and Matsuoka, M. (2008). Structural basis for gibberellin recognition by its receptor GID1. Nature 456:520-523.

Shin, J., Kim, K., Kang, H., Zulfugarov, I.S., Bae, G., Lee, C.H., Lee, D., and Choi, G. (2009). Phytochromes promote seedling light responses by inhibiting four negatively-acting phytochrome-interacting factors. Proc. Natl. Acad. Sci. U S A 106:7660-7665.

Silverstone, A.L., Ciampaglio, C.N., and Sun, T.P. (1998). The *Arabidopsis* RGA gene encodes a transcriptional regulator repressing the gibberellin signal transduction pathway. Plant Cell 10:155-169.

Song, Y.H., Ito, S. and Imaizumi, T. (2013). Flowering time regulation: photoperiod- and temperature-sensing in leaves. Trends Plant Sci. 18:575-583.

Soundappan, I., Bennett, T., Morffy, N., Liang, Y., Stanga, J.P., Abbas, A., Leyser, O., and Nelson, D.C. (2015). SMAX1-LIKE/D53 family members enable distinct MAX2-dependent responses to strigolactones and karrikins in *Arabidopsis*. Plant Cell 27:3143-3159.

Spartz, A.K., Ren, H., Park, M.Y., Grandt, K.N., Lee, S.H., Murphy, A.S., Sussman, M.R., Overvoorde, P.J., Gray, W.M. (2014). SAUR inhibition of PP2C-D phosphatases activates plasma membrane H^+-ATPases to promote cell expansion in *Arabidopsis*. Plant Cell 26:2129-2142.

Stanga, J.P., Smith, S.M., Briggs, W.R., and Nelson, D.C. (2013). SUPPRESSOR OF MORE AXILLARY GROWTH2 1 controls seed germination and seedling development in *Arabidopsis*. Plant Physiol. 163:318-330.

Sun, J., Ma, Q. and Mao, T. (2015). Ethylene regulates the *Arabidopsis* microtubule-associated protein WAVE-DAMPENED2-LIKE5 in etiolated

hypocotyl elongation. Plant Physiol. 169:325-337.

Symons, G.M., Smith, J.J., Nomura, T., Davies, N.W., Yokota, T., and Reid, J.B. (2008). The hormonal regulation of de-etiolation. Planta 227:1115-1125.

Szekeres, M., Németh, K., Koncz-Kálmán, Z., Mathur, J., Kauschmann, A., Altmann, T., Rédei, G.P., Nagy, F., Schell, J., and Koncz, C. (1996). Brassinosteroids rescue the deficiency of CYP90, a cytochrome P450, controlling cell elongation and de-etiolation in *Arabidopsis*. Cell 85:171-182.

Takahashi, K., Hayashi, K. and Kinoshita, T. (2012). Auxin activates the plasma membrane H^+-ATPase by phosphorylation during hypocotyl elongation in *Arabidopsis*. Plant Physiol. 159:632-641.

Tyler, L., Thomas, S.G., Hu, J., Dill, A., Alonso, J.M., Ecker, J.R., and Sun, T.P. (2004). DELLA proteins and gibberellin-regulated seed germination and floral development in *Arabidopsis*. Plant Physiol. 135:1008-1019.

Villaécija-Aguilar, J.A., Hamon-Josse, M., Carbonnel, S., Kretschmar, A., Schmidt, C., Dawid, C., Bennett, T., and Gutjahr, C. (2019). SMAX1/SMXL2 regulate root and root hair development downstream of KAI2-mediated signalling in *Arabidopsis*. PLoS Genet. 15:e1008327.

Wang, L., Waters, M.T., and Smith, S.M. (2018). Karrikin-KAI2 signalling provides *Arabidopsis* seeds with tolerance to abiotic stress and inhibits germination under conditions unfavourable to seedling establishment. New Phytol. 219:605-618.

Waters, M.T., Scaffidi, A., Sun, Y.K., Flematti, G.R., and Smith, S.M. (2014). The karrikin response system of *Arabidopsis*. Plant J. 79:623-631.

Yan, Y., Li, C., Dong, X., Li, H., Zhang, D., Zhou, Y., Jiang, B., Peng, J., Qin, X., Cheng, J., Wang, X., et al. (2020). MYB30 is a key negative regulator of

Arabidopsis photomorphogenic development that promotes PIF4 and PIF5 protein accumulation in the light. Plant Cell 32:2196-2215.

Yoo, S.D., Cho, Y.H., Tena, G., Xiong, Y. and Sheen, J. (2008). Dual control of nuclear EIN3 by bifurcate MAPK cascades in C_2H_4 signalling. Nature 451:789-795.

Zhang, B., Holmlund, M., Lorrain, S., Norberg, M., Bakó, L., Fankhauser, C., Nilsson, O. (2017). BLADE-ON-PETIOLE proteins act in an E3 ubiquitin ligase complex to regulate PHYTOCHROME INTERACTING FACTOR 4 abundance. eLife 6:6.

Zhong, S., Shi, H., Xue, C., Wang, L., Xi, Y., Li, J., Quail, P.H., Deng, X.W., Guo, H. (2012). A molecular framework of light-controlled phytohormone action in *Arabidopsis*. Curr. Biol. 22:1530-1535.

Zhong, S., Shi, H., Xue, C., Wei, N., Guo, H. and Deng, X.W. (2014). Ethylene-orchestrated circuitry coordinates a seedling's response to soil cover and etiolated growth. Proc. Natl. Acad. Sci. U S A 111:3913-3920.

Zhu, L., and Huq, E. (2014). Suicidal co-degradation of the PHYTOCHROME-INTERACTING FACTOR 3 and phytochrome B in response to light. Mol. Plant 7:1709-1711.

PUBLICATION LIST

*equal contribution.

1. Lee JH, Park YJ, **Kim JY**, Park CM. (2021) Phytochrome B conveys low ambient temperature cures to the ethylene-mediated leaf senescence in *Arabidopsis*. *Plant Cell Physiol.* pcab178.
2. Han SH, **Kim JY**, Lee JH, Park CM. (2021) Safeguarding genome integrity under heat stress in plants. *J. Exp. Bot.* 72:7421-7435.
3. **Kim JY**, Lee JH, Park CM. (2021) A multifaceted action of phytochrome B in plant environmental adaptation. *Front. Plant Sci.* 12:659712.
4. **Kim JY**, Park CM. (2021) A dual mode of ethylene actions contributes to the optimization of hypocotyl growth under fluctuating temperature environments. *Plant Signal. Behav.* 16:e1926131.
5. Park YJ, **Kim JY**, Lee JH, Han SH, Park CM. (2021) External and internal reshaping of plant thermomorphogenesis. *Trends Plant Sci*. 26:810-821.
6. **Kim JY**, Park YJ, Lee JH, Kim ZH, Park CM. (2021) EIN3-mediated ethylene signaling attenuates auxin response during hypocotyl thermomorphogenesis. *Plant Cell Physiol*. 62:708-720.
7. Park YJ, Lee JH, **Kim JY**, Park CM. (2020) Synchronization of photoperiod and temperature signals during plant thermomorphogenesis. *Plant Signal*. *Behav*. 15:e1739842.
8. Park YJ*, **Kim JY***, Lee JH, Lee BD, Paek NC, Park CM. (2020) GIGANTEA shapes the photoperiodic rhythms of thermomorphogenic

growth in *Arabidopsis*. *Mol. Plant* 13:459-470.

9. Lee JH*, **Kim JY***, Kim JI, Park YJ, Park CM. (2020) Plant thermomorphogenic adaptation to global warming. *J. Plant. Biol*. 63:1-9.
10. Park YJ, Lee JH, **Kim JY**, Park CM. (2019) Alternative RNA splicing expands the developmental plasticity of flowering transition. *Front. Plant Sci*. 10:606.
11. **Kim JY***, Park YJ*, Lee JH, Park CM. (2019) Developmental polarity shapes thermo-induced nastic movements in plants. *Plant Signal. Behav*. 14:e1617609.
12. Park YJ, Lee HJ, Gil KE, **Kim JY**, Lee JH, Ha JH, Lee H, Cho HT, Dai Vu L, De Smet I, Park CM. (2019) Developmental programming of thermonastic leaf movement. *Plant Physiol*. 180:1185-1197.
13. Park YJ, Lee HJ, Ha JH, **Kim JY**, Park CM. (2017) COP1 conveys warm temperature information to hypocotyl thermomorphogenesis. *New Phytol*. 215:269-280.

ABSTRACT IN KOREAN

새싹돋움에서부터 새싹확립까지의 초기 발달 단계에 있는 식물들은 극심한 주변 환경 변화를 겪게 된다. 새싹들은 빛과 온도와 같은 환경 자극의 작은 변화에도 민감하게 반응하고 기관의 형태적 변화를 통해서 그 환경에 유리한 건강한 식물체를 얻고자 한다. 이런 식물체의 변화들은 외부 환경 신호들과 식물체 내의 신호전달경로들의 조직적 및 통합적인 조절 과정으로 인해 만들어지게 된다. 그러므로, 내•외부 신호전달 경로 간의 신호교차들을 연구하는 것은 환경변화에 대한 식물 새싹의 생리적인 반응들을 이해하는 데 필수적이다. 하지만, 아직까지 연구되지 않은 내•외부 신호전달 경로 간 분자적 유전자적 연결점이 여전히 존재한다. 본 연구에서는 변화하는 빛과 온도 환경 하에서, 내부적인 신호전달경로들에 의해 조절되는 새싹 줄기의 형태적 적응에 대한 분자적•유전자적 기작을 연구하였다.

제 1장에서는 빛이 있는 환경에서의 새싹 줄기 온도형태형성에 대한 식물호르몬 에틸렌의 작용에 대해 연구하였다. 기체 상태의 식물호르몬 에틸렌은 과일숙성, 새싹확립, 물리적 자극에 대한 스트레스 저항력, 그리고 잠수탈출과 같은 다양한 발달적•환경적 적응 과정에 중요한 역할을 한다. 또한, 빛이 있는 환경에서, 에틸렌은 PHYTOCHROME-INTERACTING FACTOR 3 (PIF3) 전사인자의 발현량을 증가시켜 새싹의 줄기 세포의 미소관의 재조립을 통해 새싹의 줄기 생장을 촉진한다고 알려져 있다. 특히, 최근에 식물의 온도

반응성에 대한 에틸렌이 연관되어 있음이 밝혀지고 있었다. 그러나, 아직까지는 어떻게 에틸렌 신호가 새싹 줄기의 온도형태형성을 조절하는지에 대한 분자적인 수준에서 연구된 바 없다. 본 연구에서는, ETHYLENE-INSENSITIVE 3 (EIN3) 에 의한 에틸렌 신호가 또 다른 식물호르몬인 오옥신 (auxin) 의 반응성을 억제함으로써 새싹 줄기 온도형태형성을 약화시킨다는 것을 밝혔다. 온도형태형성을 촉진하는 PIF4 전사인자가 활성화되는 비교적 따뜻한 온도에서는, 에틸렌에 의해 활성화된 EIN3 전사인자가 직접적으로 원형질막의 H^+-ATPase 양성자펌프를 불활성화하는 단백질 탈인산화효소가 코드화되어 있는 *ARABIDOPSIS PP2C CLADE D7* (*APD7*) 유전자의 전사를 유도한다. 기존에 알려진 H^+-ATPase의 세포 생장을 촉진하는 역할과 더불어, 본 연구에서 밝힌 EIN3에 의한 *APD7* 유전자의 전사 유도가 오옥신에 의한 세포 생장을 억제하는 것과 연관되어 제한된 새싹 줄기의 온도형태형성에 기인할 것이라 생각된다. 이에 따라, APD7은 새싹 줄기 온도형태형성에서 에틸렌과 오옥신 신호들을 통합하는 분자적인 중추라고 정리할 수 있다. EIN3-APD7 모듈에 의해 에틸렌-오옥신 신호 전달 경로 간의 교차가 일어나는 것은 여러 환경자극들이 복잡한 방법으로 종종 변하는 자연적인 환경에서 새싹 줄기 온도형태형성을 세밀하게 조정하기 위함이라 생각된다.

제 2장에서는 탈황화과정 (deetiolation process) 에서 새싹의 줄기 안에서 일어나는 카리킨 (KAR) 과 지베렐린산 (gibberellic acid) /DELLA 신호 전달 경로들 간의 교차에 대한 연구를 기술하였다. 빛

자극에 대한 어린 새싹들의 형태적인 적응은 흙 안을 벗어난 후의 생존과 번영을 보장하는 중요한 발달 과정이다. 빛형태형성적 반응들은 오옥신과 지베렐린산과 같은 생장호르몬들과 빛 신호들의 네트워크에 의해 조절된다. 들불에 의해 불타는 식물체에서 생성되는 작은 뷰테놀라이드계 화합물들 중의 일부분인 카리킨은 불에 약한 식물종들의 씨앗 발아를 촉진한다고 알려져 있다. 흥미롭게도, 최근 연구에 따르면, 카리킨은 새싹확립을 용이하게 해준다고 알려져 있다. 하지만 그에 대한 분자적인 기작에 대해서는 아직 알려진 바 없다. 본 연구에서는 카리킨 신호 전달의 음성조절자인 SUPPRESSOR OF MAX2 1 (SMAX1) 이 빛과 카리킨 신호들을 새싹 빛형태형성과 확립 과정 중 새싹 줄기 생장을 조절하는 지베렐린산-DELLA 신호전달경로에 통합시킨다는 것을 밝혔다. SMAX1이 결여된 애기장대 (*Arabidopsis thaliana*) 돌연변이체들은 짧은 새싹 줄기 표현형을 보여주고, 그 짧은 표현형은 외부적인 지베렐린산 첨가와 *REPRESSOR OF ga1-3* (*RGA*) 과 *GIBBERELLIC ACID INSENSITIVE* (*GAI*) 과 같은 DELLA 유전자들을 돌연변이 시킴으로써 회복되는 것을 보여주었다. 이와 일관되게, 빛 조건 하에서 새싹 줄기 내의 SMAX1이 DELLA 단백질들의 분해를 용이하게 해준다는 것을 발견하였다. 흥미롭게도, 빛 자극은 SMAX1 단백질의 축적을 유도하고 SMAX1에 의한 DELLA 단백질의 분해 과정은 빛 환경으로 전환될 때 더 촉진된다. 본 연구에서는 SMAX1에 의해 지베렐린산 신호전달경로로 빛과 카리킨 신호들이 통합되는 것이 새싹확립 과정을 세밀히 조절하는 것을 밝혔다.

이를 통해, 자연적으로 발생하여 주변을 태워 깨끗이 정리하는 들불에 의해 생성되는 카리킨이 주는 최적의 생장 환경이 있다는 지시 신호에 따라 SMAX1은 빛형태형성의 최적화를 보장하는 보호 장치로서 작용한다 생각된다.

주요어 : EIN3, 에틸렌, 새싹 줄기 온도형태형성, SMAX1, 카리킨, 새싹 확립

학번 : 2018-21999